WARWICK
THE UNIVERSITY OF WARWICK

Analysis of Neuroimaging with Big Data to Understand Brain Systems Involved in Emotion

by

Zhuo Wan

A thesis submitted in fulfilment of the requirements for the degree of

Doctor of Philosophy

The University of Warwick, Department of Computer Science

October 2021

Key Words:

Machine learning

Elastic net

Support vector machine

Resting-state fMRI

Functional connectivity

Effective connectivity

Granger causality

Impulsivity

Sensation-seeking

Risk-taking

Childhood traumatic events

Depression

Anxiety

Addiction

Orbitofrontal cortex

Anterior cingulate cortex

Precuneus

Table of Contents

List of Tables

Table **Page**

List of figures

Figure **Page**

List of Appendices

Acknowledgements

I am deeply indebted and would like to express deep gratitude to my advisor, Prof Jianfeng Feng, for his fundamental role in my doctoral work. I appreciate all his contributions of time, ideas, guidance and funding to make my PhD experience productive and stimulating. He provides constructive guidance and counselling in overcoming various bottlenecks during the study. He has taught me how computational methods should be applied to neuroimaging data, how important it is to strengthen the basic theory and new research advances.

I am very appreciative to my co-advisor, Prof Edmund Thomson Rolls, who has taught me a lot throughout my PhD studies. He is very kind and provides careful and detailed suggestions at different stages of this research program. His help and assistance in the overall research made the biological explanation of this thesis comprehensive. As a respected neuroscientist, his dedication and passion for scientific research were admirable. I appreciate his continuous encouragement.

My gratitude is also due to Dr Wei Cheng, young principal investigator, Institute of Science and Technology for Brain-Inspired Intelligence, Fudan University, for his extraordinary support to the whole process of this research project. I was immensely benefited from his continuous assistance in methodology, imaging preprocessing, and other technical guidance.

I would like to thank my friends in the computer science department at Warwick for all the great times we have shared. I am particularly thankful to Ruiqing Feng, Peng Jiang, and Yujing Chang, excellent friends and roommates, for their company and for always be supportive during this very special period of my life.

Lastly, my heartiest thanks to my family for their love, support, and sacrifices. Without them, this thesis would never have been written. For my parents who raised me with love, give me the freedom to chase my dream and support me unconditionally. For my grandfather who trusts me, support me and being proud of me all the time. Thank you.

Zhuo Wan

University of Warwick

October 2021

Declaration

This thesis is submitted to the University of Warwick in support of my application for the degree of Doctor of Philosophy. It has been composed by myself and has not been submitted in any previous application for any degree. The work including data analysis, texts, and figures presented was carried out by the author with advice from my two supervisors Prof. JianFeng Feng, Prof. Edmund Rolls, and Dr Wei Cheng from Fudan University.

Three chapters of this thesis have been published or submitted for publication by the author, as listed:

1. Wan, Z., Rolls, E. T., Cheng,W. and Feng, J. (2020) Sensation-seeking is related to functional connectivities of the medial orbitofrontal cortex with the anterior cingulate cortex. NeuroImage 215: 116845. (Chapter 4)
2. Rolls, E. T., Wan, Z., Cheng,W. and Feng, J. (2022) Risk-taking in humans and the medial orbitofrontal cortex reward system. Neuroimage 249: 118893. (Chapter 6)
3. Wan, Z., Rolls, E. T., Cheng,W. and Feng, J. (2022) Brain functional connectivities that mediate the association between childhood traumatic events, and adult mental health and cognition. EBioMedicine (Minor revision). (Chapter 7)

Abstract

The development of neuroimaging technologies and open-access large-scale datasets provides the opportunity to explore biological big data, by developing computational models for the brain network, aiming to find biomarkers for mental disorders and investigate brain mechanisms. Due to the high dimensionality and massive sample size of neuroimaging data, exploring new computational methods and modelling approaches for neuroimaging data with various behavioural patterns is of great importance. This will lead to more stable and reliable models to understand the pattern of human behaviours and the underlying brain mechanism.

The research interest of this thesis is to explore new data analysis methods and novel modelling approaches of the brain network related to mental disorders including addiction, anxiety and depression, and brain functions related to emotion, personality, and cognitive performance with large scale neuroimaging data.

First, a novel prediction model was developed based on the elastic net regression of the sensation-seeking personality from brain functional connectivity in a large-scale study (Wan et al., 2020). This provides a novel way to investigate the relationship between behavioural measures and brain functional connectivity, replacing the usual correlation analysis with a prediction model. Furthermore, the prediction model examines groups of functional connectivity links, instead of an individual link, which is usual in correlation analysis; this indicates the relationship between behaviour measures and a group of links as community. Biologically, the sensation-seeking score was found to be optimally predicted from the functional connectivity mostly between the medial orbitofrontal cortex and the anterior cingulate cortex brain areas. This discovery helps to show how this group of links in part of the medial orbitofrontal cortex reward system plays a role in sensation-seeking.

Second, the relationship between risk-taking and worrier/anxious feeling was investigated in an advanced approach with over 30,000 participants from a massive open-access dataset, the UK Biobank (Rolls et al., 2022). Instead of performing the traditional correlation between behaviour scores, the association pattern of behaviour measures with functional connectivity was analysed. In this project, the significantly associated functional connectivity links between risk-taking and anxiety involved similar regions of the brain, including the medial orbitofrontal cortex, VMPFC, and the parahippocampal gyrus, but in the opposite direction ($p<0.001$, FDR corrected). This investigation revealed, to my knowledge for the first time, that risk-taking individuals were not normally worriers, and the medial orbitofrontal cortex, which is a key area of the reward system, was associated positively with risk-taking, and negatively with anxiety.

In addition, childhood traumatic events in relation to cognitive performance, various psychological disorders, including anxiety, depression and addiction in adulthood was investigated with the UK Biobank dataset. This investigation focused on

the long-lasting relationship of childhood trauma with other behaviours over 30 years later, while most childhood trauma studies are limited to childhood or early adolescence. Moreover, with the massive datasets of various behaviour measures available, the relationships were investigated with nine mental health measures and three cognitive measures in adults, and the associated patterns of functional connectivity. These findings highlight the long-lasting relationship between childhood traumatic events and a wide range of mental health problems and cognition in later life. They also provide insights into the neural mechanisms of the long-lasting relationship, including brain areas involved in executive function, emotion, face processing, and memory.

By exploring novel computational methods and modelling approaches to large-scale neuroimaging data, efficient models were developed in different cases. Moreover, significant progress has been made in understanding the brain mechanism of human behaviours and mental disorders, including impulsivity (sensation-seeking in Chapter 4, risk-taking in Chapter 6), verbal intelligence (Chapter 5), and childhood trauma with mental health problems and cognitive performances (Chapter 7).

List of Abbreviations

fMRI functional Magnetic Resonance Imaging

DTI Diffusion Tensor Imaging

HCP Human Connectome Project

NKI-RS/NKI enhanced Nathan Kline Institute-Rockland Sample

RBF Radial Basis Function

FC Functional Connectivity

GC Granger Causality

EC Effective Connectivity

SSRT Stop-Signal Reaction Time

HSS High Sensation Seeker

LSS Low Sensation Seeker

NAc Nucleus Accumbens

OFC Orbitofrontal Cortex

ACC Anterior Cingulate Cortex

VMPFC Ventral Medial Prefrontal Cortex

LPFC Lateral Prefrontal Cortex

BOLD Blood Oxygenation Level-Dependent

GSReg Global Signal Regression

DCM Dynamic Causal Modelling

OLSR Ordinary Least Squares Regression

LSVR Linear Support Vector Regression

FDR False Discovery Rate

DOSPERT Domain-Specific Risk-Taking Scale

ASR Adult Self-Report Questionnaire

BA Brodmann Area

MAE Mean Absolute Error

SD Standard Deviation

CLPM Cross-Lagged Panel Model

SEM Structural Equation Modelling

CFI Comparative Fit Index

RMSEA Root Mean Square Error of Approximation

Chapter 1
Introduction

1.1 Background

The rapid development of non-invasive neuroimaging technologies, including functional magnetic resonance imaging (fMRI), diffusion tensor imaging (DTI) and positron emission tomography (PET), have boosted a large amount of studies exploring and applying modern computational and biostatistical methods on neuroimaging in animal and human brains in recent years (Smitha et al., 2017; Kim, 2018; Yaple and Arsalidou, 2018; Eickhoff et al., 2020). With available high dimensional extensive sample size neuroimaging data, these studies have contributed to understanding human mental health, cognitive performances, and the underlying brain mechanism (Linhartova et al., 2019; Perosa et al., 2020; Zovetti et al., 2020). However, due to the high dimension of neuro features, large sample sizes and potential underlying multicollinear relationships between pairs of neuro features, exploring novel modelling approaches, especially suitable for neuroimaging data with large scale datasets, is of great importance. The research interest is to develop novel modelling approaches for the large-scale and high dimensional neuroimaging data (resting-state fMRI data in this thesis) and explore the brain mechanism of various behavioural measures including impulsivity and cognitive performances, and mental disorders including addiction, anxiety, and depression.

Impulsivity describes a tendency for taking quick but usually hasty acts without adequate foresight which can be associated with risky dangerous behaviours and addictions (Evenden, 1999). Recent studies suggested a more detailed breakdown of component behavioural processes and their underlying brain mechanism (Kruschwitz et al., 2012; Cai et al., 2014; Rae et al., 2015). Many researchers have discovered the neurological and psychological factors underlying impulsivity, although the results may vary in different studies. More explorations of the fractionation of impulsivity and their neuron system are needed with large scale data and novel approaches to get reliable findings. *Sensation seeking* is a multifaceted personality trait with components that include experience-seeking, thrill and adventure seeking, disinhibition, and susceptibility to boredom, which is highly associated with impulsivity (Zuckerman, 1994). In Chapter 4, a novel prediction model on the sensation-seeking from the brain

functional neuroimaging data was developed to explore the mechanism of sensation-seeking, which is highly associated with impulsivity with 414 participants included. Besides, the concept was advanced that one type of impulsivity, which is related to sensation-seeking, is related to increased functional connectivity of a reward-related cortical region, the medial orbitofrontal cortex.

In addition, the risk taking is also highly associated with impulsivity and sensation-seeking. In Chapter 6, research on risk-taking and the underlying brain mechanism with a large-scale dataset including around 20,000 participants was developed to further explore the impulsive behaviour and the neuron systems. *Risk-taking* is used to describe the tendency of taking certain risks when people were making decisions or aiming for higher targets (Green and Myerson, 2013), which was reported to be associated with risky drug use, alcohol use, and gambling problems. In this project, the risk-taking was found related to the medial orbitofrontal cortex, which is involved in the functions of reward system, and associated with impulsivity and alcohol/drug use. This supports the hypothesis that one type of reward-driven impulsivity is related to the medial orbitofrontal cortex of the brain, as proposed in the previous sensation-seeking project (Chapter 4).

Brain *functional connectivity* is defined as the correlation of the BOLD signal averaged across time between pairs of brain regions or voxels (Biswal et al., 1995), which is widely used in MRI studies and in Chapter 4, 6, and 7. The functional connectivity describes un-directional relationship between pairs of brain regions, which gives no clue of how one brain region influents the other. Although the functional connectivity has been widely used and inspirited large amount of literature, the *directional connectivity* which gives the direction and causality of how one brain regions have the effects on the other will help to understand the asymmetries of how these brain regions work hierarchically underlying certain processes, such as sensory information processing in the brain. In Chapter 5, two directional connectivity methods including the effectivity connectivity (Gilson et al., 2018) and the Granger causality (Granger, 1969) was investigated. The efficiency of these two methods was examined by applying machine learning prediction models involving the whole brain connectome.

In Chapter 7, the long-lasting relationship between childhood traumatic events and mental health problems, and the underlying neuron system were investigated with around 20,000 participants. *Childhood traumatic events* are an established risk factor for psychopathology including depression (Copeland et al., 2018). Children who had

sexual, physical, or emotional abuse, or physical and emotional neglect experiences may feel overwhelmed, and this can be associated with lasting mental and physical differences. Despite a large amount of literature on childhood traumatic events with mental health problems, the association of an individual's childhood traumatic events and psychopathology, and how brain function related to that, is still an important topic and needs more findings with large sample sizes (Susser and Widom, 2012; Teicher and Samson, 2016; Baldwin et al., 2019). In Chapter 7, with a large scale of participants, the relationship between the childhood traumatic events and a wide range of mental health problems was investigated including addiction, anxiety, cannabis use, depression, mania, mental distress, unusual and psychotic experiences, self-harm, and wellbeing. A brief introduction for the mental health problems involved in this chapter. *Addiction* is a condition characterized by compulsive engagement in a behaviour or unable to stop using a substance despite adverse consequences, for example, addiction to tobacco, alcohol, or other drugs (Koob and Volkow, 2010). *Anxiety* describes a feeling of fear, uneasiness, and dread, which will cause sweat, feel restless and tense, and might have a rapid heartbeat (Julian, 2011). For the anxiety disorder, the anxiety does not go away and can get worse over time, which can interfere with daily activities such as schoolwork, job performance, and relationships. Anxiety was usually found to have high association with *depression,* which will cause a persistent feeling of sadness and loss of interest for nearly every day, for at least two weeks (Hammen, 2005). At its worst, depression can lead to suicide. *Mania* is a psychological condition which will cause unreasonable euphoria, hyperactivity, delusions, and very intense moods (Fink, 1999). People with mania may not sleep or eat, engage in risky behaviours, and harm themselves. *Mental distress* is used to describe a wide variety of symptoms and experiences of a person's internal life that are commonly to be confusing, troubling, or out of the ordinary (Bhui and Bhugra, 2002). The measurements of these mental health problems may vary depending on how the dataset collects these symptoms. Detailed information of the symptom scores will be described in the method section of each chapter while the measures are used in the analyses.

The underlying brain function involving different personality measures, mental health problems, and cognitive measures was investigated with the functional MRI data. The parcellation of brain regions used in this thesis including two types: the AAL2 atlas in Chapter 4, 5, and 6 and the Shen atlas in Chapter 7. The *Automated-Anatomical-Labelling Atlas 2 (AAL2)* parcellate the brain into 94 regions (excluding the cerebellum),

which include clear subdivisions of the orbitofrontal cortex, which is the area of interest related to emotion (Rolls et al., 2015). The names of the brain areas are shown in Appendix-1. The *Shen atlas* parcellate the brain into 228 regions (excluding the cerebellum), was developed based on functional connectivity, which can help the explanations with functional connectivity results. This has been validated in different resting-state fMRI investigations (Finn et al., 2015; Rosenberg et al., 2016). The mapping of Shen atlas areas to AAL2 atlas areas is presented in Appendix-3 and adopted the AAL2 area names when referring to brain regions and the related functional connectivities because the Shen atlas areas do not have region names

In recent years, more and more online available massive datasets with a range of behavioural measures, brain imaging data, and genetic data are open-accessed to researchers, such as the enhanced Nathan Kline Institute-Rockland sample (NKI-RS) (Nooner et al., 2012), the Human Connectome Project (HCP) (Van Essen et al., 2012; Van Essen et al., 2013), and the UK Biobank dataset (http://biobank.ctsu.ox.ac.uk/crystal/refer.cgi?id=2367). The availability of these big datasets motivated more research on exploring human mental health problems, including anxiety, depression, and addictions, whose diagnoses and underlying brain mechanisms are still unclear, which urging for efficient computational models and useful statistical measures to produce reliable and stable result. For example, with different datasets, by performing the same analysis approaches on the same behavioural measures and brain measures, different conclusions may be leaded to. This may be due to the sample size is too small to deduce reliable result, which requires useful statistical measures to define significant results more efficiently. Besides, this un-consistent result may be leaded due to the analysis method is too sensitivity to data variation, i.e., easily affected by the data noise. This requires for exploring novel modelling approaches which can deal with the noisy neuroimaging data to conduce consistent results.

1.2 Research question and objective

The research interest of this thesis is to explore new data analysis methods and novel modelling approaches of the neuroimaging data, mainly resting-state fMRI data, related to behavioural measures of mental disorders including addiction, anxiety and depression, emotion, personality, and cognitive performance. By exploring novel modelling approaches on various behavioural measures with neuroimaging big data,

the aim is to produce efficient models fitting the high dimension, large sample size and noisy neuroimaging data. The biological emphasis is to find biomarkers for mental disorders, and the underlying brain mechanism related to emotion, personality, and cognitive performance.

1.3 Scope of the research

Following my research interest, I developed my researches on exploring new modelling methods on neuroimaging data related to personality, cognitive performances, and mental health measures with different large datasets. Besides, biostatistical methods and validations with independent datasets were performed to examine the significance of the findings. Instead of exploring the dataset with specific mental health patients, the emphasis was on large-scale databases which record various behaviour measures, cognitive performances, mental health measures, physical assessments, medical history, and the well-being of a large number of volunteers, such as the NKI dataset, HCP and UK Biobank dataset. These huge datasets provide more opportunities to explore novel methods for neuroimaging data related to different behaviour measures. Biologically, investigating the relationship of personality, cognitive performances, and other behavioural measures with mental health problems benefits the early diagnosis of mental health problems and help to reduce the risk of psychiatric disorders. There are four projects covered in my PhD research, and details are described as follows.

The first project developed a novel prediction model based on the elastic net regression of the sensation-seeking personality from brain functional connectivity were developed in a large-scale study with 414 participants (Chapter 4). A paper on this project has been published on NeuroImage (Wan et al., 2020). In this project, elastic net regression was selected over a support vector machine, as it can deal with the multicollinear brain functional connectivity features to model the whole-brain functional connectivity network. This provides a novel way to investigate the relationship between behavioural measures and brain functional connectivity with a prediction model instead of ordinary correlation analysis. Besides, the prediction model examines groups of functional connectivity links instead of the individual link in correlation analysis, which indicates the relationship between a group of links as a community and behaviour measures. The sensation-seeking score was found optimally

predicted from the functional connectivity mostly between the medial orbitofrontal cortex and the anterior cingulate cortex brain areas with correlation r=0.34 ($p=7.3x10^{-13}$) between the predicted and actual sensation-seeking score across all participants. Besides, significant associations between drug use, alcohol use, risk-taking and sensation-seeking were identified. Based on these findings, we propose that sensation-seeking reflects a strong effect of reward, which is implicated by the medial OFC areas, on promoting actions to obtain rewards, which is involved by the ACC areas.

The second project investigated the relationship between risk-taking and worrier/anxious feeling in an advanced approach with over 30,000 participants from the UK Biobank dataset (Chapter 6). Instead of performing the traditional correlation between behaviour scores, the association pattern of behaviour measures with functional connectivity was analysed, which enables the analyses of behaviour differences together with brain functional connectivity differences. In this project, the association pattern of the risk-taking with functional connectivity and association pattern of the worrier/anxious feelings with functional connectivity in the whole brain was found of significant correlation ($r=-0.66$, $p<1x10^{-20}$) (Rolls et al., 2022). Interestingly, the significantly associated functional connectivity links with risk-taking and with anxious feeling were involving similar brain regions including the medial orbitofrontal cortex, VMPFC, and the parahippocampal, but in the opposite direction ($p<0.001$, FDR corrected). In addition, the significant correlation between risk-taking, which is a kind of reward-driven impulsive behaviour, and the medial orbitofrontal cortex is consistent with the finding of sensation-seeking with the NKI dataset described in Chapter 4. This investigation reveals, to my knowledge, the first time that the risk-taking participants normally is not worrier, and the medial orbitofrontal cortex, which is a key area of the reward system, was associated with risk-taking positively, and with worrier negatively.

A comparison of traditional Granger causality (GC) and the newly developed brain's effective connectivity method (EC) on measuring the whole-brain connectivity network was conducted in the third project by performing different machine learning prediction models (Chapter 5). The functional connectivity of the brain, which was widely used in many studies, can only give an undirected correlation between pairs of brain regions. This project explored directional connectivity measures on the brain and compared two connectivity measures by performing prediction models of behaviours from these connectivities. The Granger causality modelling and effective connectivity

modelling were used to measure the directional connectivity of the whole brain. The effects of these two directional connectivity methods on measuring the brain were examined by performing predictions on behaviour data (verbal intelligence used in this study) with five different machine learning regression algorithms. Besides, the prediction efficiency of these machine learning methods with varying sizes of the sample was investigated. Generally, the GC feature provided slightly better prediction accuracy than the EC feature, indicating that the GC feature model the directional connectivity of the brain better than the EC based on this study. Additionally, by comparing the efficiency of these five commonly used prediction models, the elastic net regression provided better prediction accuracy than the other four algorithms in both EC and GC based models.

In the fourth project, the long-lasting relationships between childhood traumatic events (such as child abuse and neglect) and mental health problems, and cognitive performance in adulthood were investigated with 19,535 participants from the UK Biobank dataset. This investigation focused on the long-lasting relationship of childhood trauma with other behaviour performances after over 30 years later, while most of the childhood trauma studies stuck on only the childhood or early adolescents. Besides, with the massive datasets with various behaviour measures available, the long-lasting relationships between nine mental health measures, three cognitive measures in adults, and childhood trauma, and the association patterns with functional connectivity, were investigated. In a mediation analysis, the functional connectivity links, which were significantly associated with childhood trauma ($p<0.01$, FDR corrected), significantly mediated the association between childhood traumatic events and addiction, anxiety, depression, and well-being ($p<1.0\times10^{-3}$), and cognitive performance. These findings highlight the long-lasting relationship between childhood traumatic events and a wide range of mental health problems and cognition in later life and provide insights into the neural mechanisms of the long-lasting relationship, including brain areas involved in executive function, emotion, face processing, and memory.

1.4 Significance and contributions

By exploring novel computational methods and modelling approaches on large scale neuroimaging data for analyses of the brain function and various behaviour measures, efficient models for neuroimaging data were developed in different cases to

investigate the underlying mechanism of personality and mental disorders on massive datasets. This provides insights into the underlying mechanism of many behaviours, including impulsive, verbal intelligence, and how childhood trauma may affect mental health and cognitive performance.

In the sensation-seeking study, the first prediction model from the functional connectivity links on the sensation-seeking personality with four hundred and fourteen participants was developed. The finding on this project has been written up and published in NeuroImage (Wan et al., 2020). The prediction accuracy was high with $r=0.34$, $p<1\times10^{-10}$. Furthermore, associations between sensation-seeking and functional connectivities of the medial OFC were found, which suggested a reward-driven kind of impulsivity.

Following the research interest on impulsivity, investigation on risk-taking, which is highly associated with impulsivity and sensation-seeking, was developed with the UK Biobank dataset with over 30,000 participants included. Functional connectivities of the medial orbitofrontal cortex, VMPFC, and the parahippocampal areas were significantly higher in the risk-taking group ($p<0.001$, FDR corrected). In addition, risk-taking was significantly associated with alcohol drinking amount, cannabis use, and anxious feelings. The result is consistent with the finding in the sensation-seeking project. The implication is that a brain system involved in reward value (medial orbitofrontal cortex) may be one way in which risk-taking/sensation-seeking, as highly associated with impulsivity, is driven by reward systems that are different in the brains of different individuals (published in NeuroImage (Rolls et al., 2022)).

In the childhood trauma study, the long-lasting relationship of childhood trauma with other behaviour performances after over 30 years later was investigated, while most of the childhood trauma studies stuck on only the childhood or early adolescents. Childhood traumatic events were found strongly associated with adult mental health problems and cognitive performances. Furthermore, these behaviour associations were mediated by brain functional connectivities that were significantly correlated with childhood traumatic events. These findings highlight the long-lasting relationship between childhood traumatic events and mental health problems in later life and provide insights into the neural mechanisms of the long-lasting relationship. A paper on this project is in revision at eBioMedicine , as it provided significant results and is the first study, to our knowledge, investigating the relationship of brain functional connectivity with childhood traumatic events on a large dataset.

In conclusion, by exploring novel computational methods and modelling approaches on large scale neuroimaging data, significant progress has been made in understanding the brain mechanism of human behaviour and mental disorders in different projects, including impulsivity (sensation-seeking in Chapter 4, risk-taking in Chapter 6), and childhood trauma with mental health problems and cognitive performances (in Chapter 7). The study of the sensation-seeking project as described in Chapter 4 has been published in NeuroImage (Wan et al., 2020). A paper based on the findings of risk-taking investigation (Chapter 6) has also been published (Rolls et al., 2022). A paper on the childhood traumatic events in Chapter 7 is in revision at eBioMedicine.

Chapter 2

Literature Review

The literature review section mainly includes three parts: application of machine learning methods to neuroimaging data, literature on impulsivity including sensation-seeking and risk-taking, and literature on childhood traumatic events. The first part is a general literature review of the implements of computational methods, and machine learning approaches on neuroimaging data and the performances of these approaches on improving the process and analysis of neuroimaging data. General computational methods on neuroimaging data are used in the whole thesis, including all chapters stated in this thesis. The machine learning methods, particularly prediction models, are of particular interest in Chapters 4 and 5. The second part is literature on impulsivity with brain imaging data, especially interested in sensation-seeking and risk-taking, which is more specifically related to the project described in Chapters 4 and 6. Finally, the third part reviews current literature on childhood traumatic events with the brain and other behaviours, which is of interest in Chapter 7.

2.1 Application of computational methods on neuroimaging

Computational algorithms have been applied in the analysis of brain functions to process and analyse neuroimage data, which includes imaging techniques (Strother, 2006; Caballero-Gaudes and Reynolds, 2017), dimensionality reduction (Kandel et al., 2015; Kafashan et al., 2018), brain network modelling (Park and Friston, 2013; Smitha et al., 2017) and analysing the neuroimaging data with other modal data (e.g. clinical data, genetic data and behavioural data) (Cheng et al., 2019b; Luo et al., 2019). Besides, many available toolboxes have been developed for neuroimaging data analysis (Penny et al., 2011; Schrouff et al., 2013). Among all these studies applying various computational algorithms, machine learning methods to neuroimaging data contributed to enormous progress because of the ability to deal with high dimensional data (Orru et al., 2012; Arbabshirani et al., 2017). Primary applications of machine learning method to neuroimaging data include classification of the patients with mental disorders (Wang et al., 2017; de Vos et al., 2018) and clustering of potential subtyping disease and behavioural patterns (Yokota et al., 2015; Drysdale et al., 2017), and regression approaches to predict behavioural measures including personality and cognitive

performances (continuous variables) of individuals (Cui and Gong, 2018; Feng et al., 2018).

Wang et al. (2017) developed a different method to construct the functional brain network by applying a sparse low-rank model, which removes weak relationships and retains the functional brain network's modular structure. In this reported classification model of identifying depression patients and healthy people, a leave-one-out cross-validated linear support vector machine classifier was applied, and the accuracy was very high, which achieved 95%. Compared with the linear support vector machine classifier, Wang et al. (2017) also constructed classification models with a support vector machine with radial basis function (RBF) kernel, naïve Bayes model, and linear discriminant analysis in their study. The linear support vector machine had the best performance in classifying depression patients and healthy people in their research. This study provided a different way to construct a functional brain network and compared the prediction performances of several commonly used classification approaches, which offers valuable experiences for other researchers to apply classification models to neuroimaging studies, especially research on mental health diseases. However, only 60 participants were included in this study. Considering the high dimension of functional connectivity in the brain, such small number of samples included was not reliable. Comparison of the performances of different machine learning algorithms on neuroimaging data is valuable, which suggests further research can be developed with large sample size.

A study on the classification of patients who have Alzheimer's disease was developed by de Vos et al. (2018), with 250 participants included. In this study, different resting-state fMRI measures, including FC matrices (Koch et al., 2012), FC dynamics (Wee et al., 2016) and the amplitude of low-frequency fluctuations (Dai et al., 2012) were used as predictors separately and combined to examine the performances of these measures on predicting the Alzheimer's disease. A logistic regression based on the elastic net model was applied as a classifier in this study. The best classification performance was achieved by predicting from the combination of all these three resting-state measures (AUC=0.85). The elastic net regression is particularly helpful when the predictors outnumber subjects by using regularization to abandon some of the predictors to enter the prediction model (Zou and Hastie, 2005; Friedman et al., 2010). Due to the high dimension of brain connectivities, the elastic net model is more helpful in neuroimaging data than other prediction models in general. Besides, a

nested cross-validation approach (Krstajic et al., 2014) was applied to avoid overfitting issues. The hyperparameters were tuned in the inner loop, and the outer loop was used to fit and test the performances of the regression model.

Clustering was also widely used in neuroimaging studies to identify potential subtypes of diseases or behaviour patterns (Franco and Vivo, 2019). For example, a study developed by Yokota et al. (2015) applied a k-means cluster on 277 developing children to investigate possible sub patterns of cognitive development relating to brain structures. Six subtypes of cognitive patterns were obtained, and significant grey matter volume differences among different subtypes were also reported in this study. One subtype identified in this study is participants who generally had lower cognitive scores than average, and they showed larger volume in the middle temporal gyrus. The application of the k-means cluster provides a way to investigate the cognitive pattern related to brain structure. However, clustering is an unsupervised method that cannot be validated and can produce biased and unstable results based on different data groups. For example, in this study, although a group of participants with a relatively low cognitive score was identified, no group with higher cognitive performance was found. Therefore, analyses should be performed with large sample sizes, and validations are needed with dependent datasets in future studies when applying the clustering methods for subtyping in neuroimaging data.

Apart from classification and clustering, regression models were applied to predict continuous variables (e.g., behavioural characteristics, personality, and cognitive ability) in neuroimaging studies widely (Norman et al., 2006; Dosenbach et al., 2010; Haynes, 2015; Siegel et al., 2016; Liu et al., 2018a).

Feng et al. (2018) developed a study on a prediction mode of narcissism from functional connectivity with 155 participants by performing a linear regression model. A feature selection was conducted before the prediction model to select the most associated brain features with narcissism instead of using the whole-brain FCs. A leave-one-out cross-validation was applied in this model. The prediction accuracy was indicated by the correlation between the actual narcissism score and the predicted narcissism score ($r=0.24$, $p<0.005$). Besides, different cross-validation schemes such as two-fold, five-fold, and ten-fold validation were also performed to validate the prediction model further. In this prediction model, key brain areas contributing highly to the prediction model, including the prefrontal cortex, the amygdala, and the ACC areas, were identified. In summary, this study conducted a feature selection step before

the prediction, which helped to reduce the high dimensional feature numbers to match the sample size. However, the prediction accuracy was not very significant, and an ordinary linear regression model without any penalty of overfitting will provide product models with low generalization fitting for other datasets.

A comparison of the prediction performance of several commonly used machine learning methods on resting-state fMRI data was performed by Cui and Gong (2018). Six different machine learning algorithms, including ordinary least squares regression, ridge regression, LASSO regression, linear support vector regression, relevance vector regression, and elastic net regression were performed to predict behavioural measures with continuous variables from the brain functional connectivities. Apart from comparing the prediction accuracy and computation efficiency of these prediction models on the HCP dataset (Van Essen et al., 2012), the effect on the prediction performance with different sample sizes was also tested in this study. The LASSO regression showed relatively low accuracy, while the other algorithms showed similar performances in general with varying sizes of samples. The accuracy and stability of all these prediction models grown higher with the increasing sample size regardless of the regression models. This study conducted a comprehensive comparison of the commonly used prediction models and tested the influence of sample size, which provides a good reference for potential prediction model selection.

2.2 Brain reward system, impulsivity fractionation, sensation-seeking and risk-taking

A *reward* is a stimulus or event that one works to obtain, such as food, and a punisher is what one works to escape from or avoid (or which suppresses an action on which its delivery is contingent), such as a painful stimulus or the sight of an object associated with a painful stimulus (Rolls, 2018b). A *positive reinforcer* (such as food) increases the probability of emission of a response on which it is contingent, the process is termed positive reinforcement, and the outcome is a reward (such as food). The *brain reward system* is a collection of brain structures and neural pathways that responsible for reward-related cognition, including incentive salience (i.e., "wanting"; desire or craving for a reward and motivation), associative learning (primarily positive reinforcement and classical conditioning), and positively-valanced emotions, particularly emotions that involve pleasure (e.g., joy, euphoria and ecstasy) (Berridge

and Kringelbach, 2015; Schultz, 2015). The orbitofrontal cortex plays a key role in the reward system. It receives information from the last stages for each sensory modality including visceral information from the anterior insular cortex, visual information from the inferior temporal visual cortex, olfactory information from the primary olfactory, and auditory information from the superior temporal cortex; and send outputs directly to the anterior cingulate cortex for action-outcome learning, to striatum for stimulus-response habit learning, and to gateways to hippocampal memory systems. The hypothesis is that the orbitofrontal cortex is involved in representing reward value and rapidly updating these representations, which has been investigated in different studies(Rolls, 2017a; Rolls, 2018b). Following the hypothesis of the orbitofrontal cortex involving in the brain reward system, these are two investigations developed together with behavioural measures including sensation-seeking in Chapter 4 and risk-taking in Chapter 6.

Impulsivity is a multidimensional trait found in humans and other mammalian animals. It is defined as a tendency for taking quick but frequently hasty acts without adequate foresight. (Evenden, 1999). Recent advances in the neuroscientific study of impulsivity have inspirited a more detailed breakdown of component behavioural processes and their underlying brain mechanism (Kruschwitz et al., 2012; Cai et al., 2014; Rae et al., 2015). Impulsivity is described as a tendency of taking rapid actions, often with insufficient forethought or consideration of potential consequences. Many researchers have discovered the neurological and psychological factors underlying impulsivity, although the results may vary in different studies. In a review of the neural and biochemical finding of impulsivity by Dalley and Robbins (2017), fractionation of impulsive behaviour was proposed, which suggested that impulsivity may have many subtypes, and these subtypes depend on distinct neuron systems. It can indicate either a lack of information processing or a lack of control over response output. Besides, a fractionation of impulsive behaviour was proposed, which suggested that impulsivity may have many subtypes, and these subtypes depend on distinct neuron systems. Three subtypes were described in this paper, including: ‘waiting impulsivity’, ‘stopping impulsivity’, and ‘risky impulsivity’.

The *waiting impulsivity* refers to self-restraint to delay rewards, usually measured by the temporal discounting and the premature-response tests (Ainslie, 1975; Robbins, 2002). The waiting impulsivity is associated with the ventral striatum, the prefrontal cortex (both dorsolateral and ventrolateral parts), and the parietal cortices, which are

areas involving the delayed reward (Voon et al., 2014; Morris et al., 2016). Alternatively, another theory of waiting impulsivity has been suggested that the delay might be conducted with the lateral prefrontal cortex and the parietal circuit, while the reward magnitude was involved with the ventral striatum and medial prefrontal cortex (Ballard and Knutson, 2009).

Stopping impulsivity is characterized by a lack of response inhibition, which is typically assessed using the stop-signal reaction time (SSRT) task (Logan et al., 2014). When action outpaces thought, it is functional and adaptive to be able to terminate a response after it has started. The brain circuits governing performance on the SSRT task have been well-defined, with components of the ACC, the right inferior frontal cortex, the pre-supplementary cortex, and the premotor areas (Bari and Robbins, 2013). The volume of grey matter loss in the right inferior frontal sulcus in patients with frontal brain injury was linked most strongly with the SSRT measure (Aron and Poldrack, 2006). Another fMRI research revealed the association between the right inferior frontal cortex and the premotor areas and striatal circuitry by investigating the same task (Whelan et al., 2012). In a review of over seventy fMRI literature by Cai et al. (2014), two clusters of activation in the right inferior lateral frontal cortex and the right insula were identified with distinct functional properties. To be more specific, the inferior frontal cluster was functionally connected to the parietal cortex. In contrast, the insula cluster was more tightly coupled with the ACC and has greater activations on the failure of SSRT trials. The dorsomedial prefrontal cortex was related to individual differences and was more activated on successful SSRT trials than unsuccessful attempts. These findings suggest that the inferior frontal cluster is more critical for response inhibition than monitoring task outcomes (Rae et al., 2015) but does not rule out the potential that this cluster has other functions, for example, executive attention (Dodds et al., 2011).

Risky impulsivity is about risky decision making and is associated with sensation-seeking (Green and Myerson, 2013). The neural mechanisms underlying risky impulsivity include the lateral prefrontal cortex involving a tendency for ambiguity with unpredictable probabilities of outcomes and the posterior parietal cortex involving the tendency for risk with known probabilities (Huettel et al., 2006). Risky behaviour is typically related to impulsivity (‘risky impulsivity') due to the relevance of value and the uncertainty of the outcome of responding. The probability discounting paradigm illustrates this risky behaviour (Green and Myerson, 2013), in which risky options (for

example, a 50% chance of a high reward vs a 100% chance of a lower return) are favoured. Besides, there's always a possibility of being penalized in exchange for a higher reward. Sensation-seeking is frequently associated with the willingness to engage in risky behaviour (MacPherson et al., 2010; Ruedl et al., 2012).

Sensation-seeking is a multidimensional personality trait that includes experience-seeking, thrill and adventure seeking, susceptibility to boredom, and disinhibition (Zuckerman, 1994). High sensation seekers (HSS) are more prone to substance use (Bardo et al., 1996), reckless driving (Jonah, 1997), unprotected sexual activities (Hoyle et al., 2000), physical risk sports (Ruedl et al., 2012), and problem gambling (Harris et al., 2015) compared to low sensation seekers (LSS). The mechanisms that predispose persons with a high level of sensation seeking to engage in such dangerous behaviours is a crucial issue. Therefore, prevention strategies targeted at decreasing the occurrence of sensation-seeking behaviours (Sargent et al., 2010) and the development of risk-taking models is of great importance (Schonberg et al., 2011).

The earliest stage of sensation-seeking research only relied on clinical data, with no examination of the specific neural systems underlying the reported behaviours. The high sensation-seeking group had higher neurobiological responses to strong and unexpected stimuli than the low sensation-seeking group. In humans, for instance, the high sensation-seeking group has a greater orienting response to novel stimuli and higher cortical arousal in response to strong visual or auditory stimuli than the low sensation-seeking group. The low sensation-seeking group, on the other hand, exhibits cortical inhibition in response to strong stimuli, especially at the highest levels of stimulus intensity (Zuckerman and Kuhlman, 2000). Skin conductance reactions to sexually explicit and violent stimuli are also stronger in the high sensation-seeking group (Smith et al., 1990). In conclusion, the research implied that the high sensation-seeking group were hypersensitive to strong and new stimuli. However, it is unclear whether the observed behavioural changes related to sensation-seeking may be related to specific brain systems that regulate approach and avoidance.

Investigations on neuroimaging data together with behavioural data help to look into the neural systems underlying the behavioural difference. Abler et al. (2006) developed the first study to investigate the underlying neural system related to sensation-seeking with fMRI data. This study found that the nucleus accumbens (NAc), which is part of the ventral striatum, was positively associated with the sensation-seeking score across all eleven participants included. The ventral striatum works as an

essential part of the reward system, which receives a strong emotional response output from the OFC, the ACC, and amygdala (Gregorios-Pippas et al., 2009; Rolls, 2014a). This investigation applied a monetary incentive task, which is suitable for studying reward sensitivity but less well adapted to studying strong reactivity to intense stimuli (Zuckerman, 1994) and preference for arousal (Zuckerman and Como, 1983). The study of Abler suggests the potential relation between sensation-seeking behaviour and the brain reward system. In a study by Joseph et al. (2009) on the neural system with sensation-seeking, the emotion-induction task was adopted, which is more suitable for examining strong reactivity to intense stimuli and preference for arousal (Bradley et al., 2001). The result in Joseph's study was consistent with the framework developed by the clinical data, which showed that HSSs responded to high-arousal stimuli more strongly than LSSs. Besides, brain regions, including the insula and the medial OFC, were found associated with arousal and reinforcement during sensation-seeking related tasks. In summary, these two studies suggested that HSSs showed stronger activation of intense stimuli in the brain areas, which function in the reward system.

Apart from the brain regions with the brain reward system, brain regions including the insula, prefrontal cortex, and superior frontal gyrus were also commonly reported in sensation-seeking studies. Kruschwitz et al. (2012) developed an analysis exploring the neural underpinnings of sensation-seeking behaviour (mainly interested in adventure-seeking and thrill-seeking) using fMRI data. By performing a gambling task, high sensation-seeking individuals were found to show an enhanced reward sensitivity in the superior frontal gyrus, the insula, and the precuneus than the low sensation-seeking group. The enhanced reward sensitivity in the nucleus accumbens was consistent with previous reviews. Besides, there were studies of sensation-seeking to focus on a specific group of people, for example, adolescents. A study using fMRI data of adolescent sample only was developed to examine differences in brain activity that included 27 high sensation seekers and 27 low sensation seekers (Cservenka et al., 2013). A wheel-of-fortune task was conducted during the scanning, and the HSSs had a stronger response in the bilateral insula and prefrontal cortex on Win vs No Win than LSS. However, in the study of Collins et al. (2012), the typically described sensation-seeking related regions, including the insula, the lateral prefrontal, the cingulate cortex, and the motor areas, exhibited no difference activation in high sensation seekers. In Zheng et al. (2017), the activation of the prefrontal cortex was lower in the HSS than in LSS.

In summary, the brain regions with the brain reward system, including the medial OFC areas and the ventral striatum, showed enhanced activation in the high sensation seeking group than the low sensation-seeking group as reported in many studies(Abler et al., 2006; Joseph et al., 2009; Kruschwitz et al., 2012). The other brain regions reported in different studies, including the insula, the prefrontal cortex, and the cingulate cortex, were found to behave differently, even opposite in some of these reviewed studies(Collins et al., 2012; Kruschwitz et al., 2012; Cservenka et al., 2013; Zheng et al., 2017).In the study of Kruschwitz et al. (2012) and Zheng et al. (2017), the tasks used for the subjects were both monetary reward-related (gambling task and monetary reward-based decision-making task). The insula was correlated with the expected value and the uncertainty of the magnitude of the reward obtained in a neuro-economics study (Rolls et al., 2008). Hence, the interpretation might be that the insula was significant in these two studies because it was related to only the monetary reward task instead of the main focus of sensation-seeking behaviour. In the study of Joseph et al. (2009), the insula, the medial OFC and the ACC areas were picked out. The role of the anterior insula in emotion is that it receives input from the ACC and the OFC areas, which were involved in the fundamental computations for emotion. In addition, the insula is involving in producing autonomic responses (Rolls, 2014a). Hence, the essential brain regions picked up in this study might be medial OFC areas and the anterior cingulate cortex.

Although some studies tried to find the underlying brain mechanism of sensation-seeking, most of these studies used task-related fMRI data. Task-related studies can be related to different task trials instead of sensation-seeking behaviour, which will produce a not robust result. Besides, the sample size in these studies was small, which might lead to different results in different studies and less reliability, leading to poor understanding and controversy in sensation seeking. Taking together, investigations on sensation-seeking with big dataset and ideally with resting-state fMRI data which lead to robust results are needed. In Chapter 4, a large-scale resting-state study on sensation-seeking with prediction models is described, and the relationship between sensation-seeking and the brain reward system is indicated.

Risk-taking is used to describe the tendency of taking certain risks when people were making decisions or aiming for higher targets. Risky behaviour was defined as riskier behaviour in a lab-based risky decision making, high score in the personality measures, for example, sensation-seeking, or risky behaviours in drug or alcohol usage

(Steinberg, 2008). People have different preferences on whether to act in behaviours that have a higher possibility of risks and a higher chance of more rewards. The critical hypothesis was that the heightened reward sensitivity, sensation-seeking, preferences for risky behaviours were related, and together with a risky-impulsivity (Dalley and Robbins, 2017). To better understand human behaviour, neuroimaging research has attempted to decode the brain underpinnings of these risk attitudes. To help the understanding of typical and abnormal decision-making procedures, neural associations of risky decision-making have been used as a neural system biomarker of treatment outcomes (Macoveanu et al., 2014), analysed as a potential heritable trait (Rao et al., 2018), and investigated along with the development (Qu et al., 2015).

Individual differences in risk-taking behaviours have been linked to several brain areas, as reported in different studies. For example, the ventral striatum was positively correlated with a higher tendency in pursuing rewards and a higher likelihood of seeking fun (Braams et al., 2016). In another study with 136 adolescent participants, increased risky behaviour was associated with perceptions of more deviant peer norms for participants with high ventral striatum sensitivity. In contrast, participants with low ventral striatum sensitivity showed common risk-taking preferences and are relatively resilient to deviant peer norms (Telzer et al., 2021).

The ventral medial prefrontal cortex (VMPFC), which were in the function of the reward system, is related to reward sensitivity and seeking rewards. In the study of Blankenstein et al. (2017), greater risk preferences were found related to higher activation of the ventral medial prefrontal areas. Furthermore, decreased activation in the lateral prefrontal cortex, which is a critical region involved in self-control (Dixon, 2015), was linked to increased risk-taking in young adults (Gianotti et al., 2009). In contrast, in a longitudinal analysis by Qu et al. (2015), the association between the lateral prefrontal cortex activation and reductions in the frequency of risky behaviours (such as getting drunk or getting high at parties) was rejected. In a study with 244 pairs of twins on brain activation with genetic contributions, risk-taking behaviours were found related to the left insula and right striatum in the balloon analogue risk task (Rao et al., 2018). Risk-taking was reported to be associated with drug use, alcohol use, and gambling problems. A positive correlation between the frequencies of drug use, a large number of drinking problems, and sexual risky behaviours and the ventral striatum were found in different studies (Bjork and Pardini, 2015; Braams et al., 2016). Risk-taking behaviours in the financial domain have also drawn lots of attention. In a study by

Raggetti et al. (2017), with around 20 financial decision events were collected for each participant, the ventrolateral and dorsolateral prefrontal cortex and the posterior parietal cortex had stronger activation in the risk-seeking group comparing to the risk-averse group. The ventrolateral prefrontal cortex was involved with strategic planning, which is shown to be associated with the financial trades with long experiences (Levy and Wagner, 2011). The dorsolateral prefrontal cortex, which involves the cognitive action control, was found associated with the response latency (Cieslik et al., 2013).

In a literature review on risk-taking with the brain activations of more than 20 studies, no brain region was consistently related to risk-taking behaviour. This limited convergence and conflicting findings, as the review above, may be disappointing and can be caused by relatively small sample sizes in many of these studies. On the other hand, the limited convergence can indicate that the risk-taking behaviour can be related to activations across the brain with many regions instead of localized in a few ones. Besides, many of these studies are task related. Therefore, different tasks can affect the result quite much, which may not be the risk-taking behaviour but varies with varying tasks and how the precise was defined in various tasks. Hence, we posit that more investigations on risk-taking should be developed to enrich the literature and contribute to a comprehensive understanding of the neural mechanism of risk-taking with brain activations. More importantly, according to current literature, studies with relatively large sample sizes, analysing the whole-brain activations with risk-taking instead of focusing on only a few regions with resting-state fMRI data will be helpful and provide a novel contribution to the study of risky impulsivity behaviours. Therefore, an investigation on risk-taking with around 20,000 participants from the UK Biobank dataset was developed, aiming to understand risk-taking, worrier/anxious feelings, and the related brain functional connectivity on the whole brain. The *worrier/anxious feelings* describe people who spend a lot of time thinking about problems that they have or unpleasant things that might happen. In the UK Biobank, this is a psychosocial factor question, which indicates whether the participants are a worrier with binary answer. Different with the mental health diagnosis, this question measures a personality and tendency of normal participants.

2.3 Childhood traumatic events and underlying brain mechanism

Childhood traumatic event is an established risk factor for psychopathology. To be specific, Children who went through sexual, physical, or emotional abuse, physical and emotional neglect may feel overwhelmed and often results in lasting mental and physical effects. Despite the century-old debate on the origins of this risk, the association and causality between the psychopathology and an individual's experience of childhood traumatic events, and how the brain alterations related to that, is still a hot topic and need more findings with a large sample size to convergence (Susser and Widom, 2012; Teicher and Samson, 2016; Baldwin et al., 2019).

Childhood traumatic events are suggested to be related to the risk of psychotic symptoms and diseases. In a systematic review of the literature of 20 studies on childhood traumatic events, 17 of these studies suggested positive correlations between psychotic disorders with different types of childhood traumatic events (Trotta et al., 2015). However, in a further meta-analysis of nine studies, the heterogeneity of studies was high, indicating that more methodologically reliable studies are needed. Besides, the associations between many mental disorders, including anxiety, depression, and post-traumatic stress disorder, and childhood traumatic events, were reported in the literature. Four types of childhood traumatic events, including neglect, parent psychopathology, physical and sexual abuse, were all related to a higher risk of post-traumatic stress disorder compared to those who did not have childhood traumatic events, with over 20,000 participants included collected by the World Mental Health Surveys (McLaughlin et al., 2017). Furthermore, childhood, adolescence and early middle adulthood had stronger associations than later adulthood. In a longitudinal study that assessed traumatic events in childhood eight times and follow-up four more times in adulthood with over 1000 participants, childhood traumatic event was related to greater risks of psychotic diseases and lower functional outcomes in adulthood, including substantial impacts that suggest a significantly delayed transition to adulthood (e.g., failure to hold a job and social isolation) (Copeland et al., 2018). Higher childhood traumatic events scores were associated with hospital diagnosed depression in a meta-analysis on childhood traumatic events and depression, including 68,830 participants from 192 independent datasets (Humphreys et al., 2020). Especially the emotional abuse and neglect were more significantly associated with depression than other types of childhood traumatic events. Apart from mental disorders, a review by

Suglia et al. (2018) found considerable evidence of a relationship between childhood traumatic events and cardiometabolic consequences throughout the lifetime. In a meta-analysis involving 16 unique research, the relationship between prospective and retrospective assessments of childhood traumatic events was investigated. (Baldwin et al., 2019). This study suggested that the prospectively identified childhood traumatic events can have a different relationship with mental disorders compared to the retrospectively self-reported childhood traumatic events. When developing analyses on childhood traumatic events and designing interventions, researchers and public health experts should be aware of these variations of prospective and retrospective childhood trauma. 'Time does not heal all wounds': a growing number of studies have shown that various types of childhood traumatic events were linked to an increased risk of personality disorders and increased odds of negative mental health impacts, such as anxiety and depression (Raposo et al., 2014). These findings highlight the necessity to avert childhood traumatic events and intervene afterwards if they occur to prevent long-term impacts on mental health.

In addition to the behaviour level association, studies emphasizing mechanisms, resiliency, and vulnerability aspects will increase the knowledge further and give more comprehensive and helpful information aiming for effective interventions. The relationship between childhood traumatic events and the brain structural and functional alterations have been examined in different studies (Teicher and Samson, 2016). An increasing number of studies suggested that childhood traumatic events have long-term impacts on the brain circuitry function on stress-susceptible (Marusak et al., 2016). In a review of the neuroimaging studies by Bolsinger et al. (2018), the history of childhood traumatic events is associated with functional and volume changes of the prefrontal cortex and limbic regions. Longitudinal behavioural studies provided more evidence, showing that a smaller volume of the prefrontal cortex after childhood traumatic events was associated with low cognitive performances (Raymond et al., 2018) and diagnosis of depression (Lu et al., 2019) in later life. McLaughlin et al. (2014), Sheridan and McLaughlin (2014) show that childhood traumatic events are likely to have a significant impact on brain systems involving threat perception and learning, as well as emotion control and salience processing, which includes the limbic or frontal-amygdala system (Tottenham, 2015), involving the amygdala, medial prefrontal cortex and the hippocampus. In a study on participants with depression symptoms on brain resting-state network, childhood traumatic event was related to a

multivariate pattern of different connectivity networks involving the dorsal attention network, the frontoparietal network, the cingulo-opercular network subcortical regions, ventral attention network, and the salience network (Yu et al., 2019). This study focused on the association between depression and childhood traumatic events, in which adults retrospectively report childhood traumatic events with current mental illness. Comparing to what was registered with the prospective childhood traumatic events, more brain regions were identified in this study. This may indicate the difference between the retrospective and prospective childhood traumatic events as supporting the idea reported in Baldwin et al. (2019). However, this may also be more related to depression, as this study works on the depression patients' group, not healthy people. In another study on the retrospective childhood traumatic events with a large size dataset (over 6,000 participants), participants who had experienced emotional abuse in early life were found to have smaller volumes of the cerebellar and the ventral striatum areas compared to the group who had not experienced childhood emotional abuse (Gheorghe et al., 2021). This study focused on retrospective childhood maltreatment and the long-term effects on the brain alterations in old adults with a large dataset, which supported that childhood traumatic events may impact the brain structure into old age.

However, the exact underlying pathways of which childhood traumatic events impact brain development and behaviour are still unclear, and more studies are needed to achieve a coverage conclusion. Furthermore, significant variations in effect sizes were observed in different studies. These variations might be explained by methodological difficulties, including small sample size, cross-site data, differences in how childhood traumatic events and mental health symptoms were measured, and the level of confounding adjustment.

In summary, it is not clear if the relationship between childhood traumatic events and psychotic experiences is causal and reliable and how the underlying biological pathways are related. Besides, the difference between retrospective and prospective childhood traumatic events has been reported in studies. Therefore, researchers and public health experts should be aware of these variations of prospective and retrospective childhood trauma in future investigations. Finally, the long-lasting impact of childhood traumatic events on the brain and mental disorders in old age adults should be emphasized.

Chapter 3
Methodology

3.1 Measurements of the resting-state brain connectivity

3.1.1 Functional connectivity

The human brain includes 100 billion neurons linked together by nerve fibers to form a highly complex structure. To comprehend how the neurons work together in the brain, connectivities between neural systems and how the brain functions were conducted within and between these networks is of great importance. Therefore, it is critical to examine the anatomy of distinct brain regions as well as functional connectivity to unravel the brain's mystery. However, researchers do not focus on the integration of brain function in the early stages of brain functional magnetic resonance investigations. Instead, they concentrate on the distinction of brain functions, i.e., different brain areas are responsible for different types of recognition. The study of Biswal et al. (1995) on the spontaneous low-frequency oscillatory signal of the brain led to the definition of resting-state functional connectivity. The phenomenon of functional connectivity describes the high consistency of activations of different brain regions when they have a large spatial distance. After Biswal et al. (1995) revealed the synchronization between low-frequency signals, studies have found that the blood oxygenation level-dependent (BOLD) signals between the brain areas whose functional systems have a high level of synchronization in the resting state activations. Functional connectivity is defined simply, and the Pearson correlation is the most often utilized method. Specifically, the functional connectivity between two brain areas (i.e. Pearson correlation) is calculated using the time series $x(t)$ of a brain region as follows:

$$r_{ij} = \frac{\sum_{t=1}^{T}[x_i(t) - \bar{x_i}]\left[x_j(t) - \bar{x_j}\right]}{\sqrt{\sum_{t=1}^{T}[x_i(t) - \bar{x_i}]^2} \cdot \sqrt{\sum_{t=1}^{T}\left[x_j(t) - \bar{x_j}\right]^2}}$$

Where $x_i(t)$ and $x_j(t)$ $(t = 1,2, \dots, T)$ denotes the time courses of brain regions i and j.

Whether to apply global signal regression (GSReg), which includes regressing out signal averaged over the whole brain, is a crucial point in neuroimaging data analysis (Fox et al., 2009). This will cause resting-state correlations to vary drastically, affecting correlation patterns and, as a result, inferences concerning brain functional connectivity

(Saad et al., 2012). The global signal regression is usually not applied in neuroimaging studies. The reasons are as described as follows (Cheng et al., 2016).

The impacts are introduced with the help of an intuitive example. Consider the fact that only visible portions rise for a short time. With the mean global signal set to zero, the signal in brain areas that have nothing to do with the visual areas will be compelled to reflect negative 'signal' values during this time. As a result, there will be negative correlations between the visual and other brain areas even if there is no functional connectivity between them. As a result, negative associations may be spurious and difficult to evaluate. Moreover, GSReg has the potential to profoundly alter inter-regional correlations within a group of people, as well as disparities between groups (Saad et al., 2012). This may propagate underlying group differences to brain areas where functional connectivity variations may never have existed.

Furthermore, rather than just modifying the mean or range of correlation values between pairs of brain regions, GSReg consistently affects the rank ordering of results and introduces negative values in functional connectivity research in autism spectrum disorder. In comparison to previous pre-processing procedures, this results in a reversal of group correlation differences, with a higher occurrence of both long-range and local correlation differences favouring the patient group. In addition, findings in locations that indicate group differences no longer correspond with the associations with behavioural symptoms (Gotts et al., 2013). Furthermore, greater cortical power and variance were found in schizophrenia in research, an effect that was predictive of symptoms but was hidden by GSReg (Yang et al., 2014). In bipolar patients, the finding was not present, indicating diagnostic specificity (Yang et al., 2014). As a result, in resting-state functional connectivity datasets, GSReg may hide other information of potential interest. Furthermore, it was demonstrated in a study of macaques that the global signal could reflect some underlying neurophysiological effects of importance, such as those related to gamma frequencies in the local field potential measured in even remote cortical regions (Scholvinck et al., 2010). Hence, there are solid reasons to leave the global mean signal un-regressed.

In summary, after the functional connectivity was defined by Biswal et al. (1995), it became the most widely used brain connectivity measure with large amounts of literature and studies. In this thesis, most of these investigations used the functional connectivity measure as the first step to produce the brain connectivity matrix, and then

further modelling methods were followed, including the sensation-seeking study in Chapter 4, risk-taking study in Chapter 6, and childhood traumatic events in Chapter 7.

3.1.2 Directional connectivity

3.1.2.1 Effective connectivity

Effective connectivity assesses the efficacy of each existing link between two brain regions, i.e., how much one brain region influences the other. It focuses on transitions between different fMRI "activity states" throughout time (Mitra et al., 2015). The investigation into asymmetric connectivity is of great meaning in neuroscience, as it happens a lot in the communication of neurons in the brain. Based on a large body of evidence in rich literature, forward connections between any pair of cortical areas are assumed to be stronger than backward connections within a cortical hierarchy of connectivity. These asymmetries are fundamental in understanding how these brain regions work hierarchically underlying certain processes, such as sensory information processing in the brain. In a sensory hierarchy, forward connectivity from layer 2-3 pyramidal cells to layers 4, of the following cortical areas was found to be stronger than the backward connection from layer 5, which is a deeper layer of the cerebral cortex, and project back to layer 1 of the antecedent cortical regions (Markov et al., 2014; Rolls, 2016). The top-down or back projection is weaker than the forward connection, which is also essential for attention and memory recall. Attentional bias and memory recall do not dominate the bottom-up forward input (Turova and Rolls, 2019). Due to the asymmetries of the connectivities between different brain areas are functionally essential and usually have an anatomical basis, the directional connections, especially with anatomical prior selections of the links, are crucial to investigate.

Dynamic causal modelling (DCM) is a classical approach to measuring effective connectivity (Friston, 2009). It is often applied in conjunction with a circuit composed of brain areas that were prior selected to test hypotheses on the interactions between the regions considered. It involves the Balloon model, a very detailed modelling method that is low in computational efficiency (Friston et al., 2000). A new effective connectivity modelling method that applies a simpler model to limits the degrees of freedom for individual brain areas was proposed by Gilson et al. (2016). In addition, the structural connectivity information from DTI is used to reduce the number of possible connections in the model. In comparison to the DCM, this method enables the calculation of maximum likelihood effective connectivity estimates for a large number

of nodes on the whole-brain level, individually for large datasets, in a very efficient way. By performing this method, analyses can be applied on the whole-brain level and target significant effective connectivity differences for all existing connections that characterize the behaviour or mental health problems without preliminary knowledge.

The EC method efficiently calculates maximum-likelihood effective connectivity estimates for many brain regions (Gilson et al., 2016). The approach takes into account known anatomical connections and exploits transitions of fMRI data over successive repeat intervals. The resting-state analysis described here can be thought of as probing the connectivities between brain areas by assessing the impact of noise produced by random spiking times of neurons on the system. This model uses the covariances with nonzero temporal shifts to capture and exploit this information. The criteria of optimization of this model for the EC and the local input variance in a parameter Σ is to reproduce statistics of the observed fMRI signals most accurately. Detailed descriptions of the EC model are as follows, example code of calculating the EC is attached in Appendix-7, and a complete illustration of the EC method can be referred to in (Gilson et al., 2016).

The estimated effective connectivity assesses the intensity of causal linkages from one brain area to another using BOLD fluctuations as a proxy: it generates a single value that combines the impacts of synapse strength, neurotransmitter release, and other factors. A network model is iteratively optimized using the estimate process. It replicates empirical cross-covariances between brain regions, which are canonically connected to cross-spectral density, which has been exploited in recent investigations (Friston et al., 2014; Razi et al., 2017). This model discards very slow-frequency fluctuations and employs an exponential estimate of BOLD autocovariance (locally across a few TRs). The effective connectivity was simplified by using an adiabatic approximation. Because broadband (slow) fluctuations in neural signals were studied, the observed signals were considered as a direct reflection of underlying neuronal activity. Finally, following known neuroanatomy and earlier modelling research, positive restrictions were imposed on extrinsic or between-node connections.

Empirical covariances

For each session of the resting-state fMRI scanning, the BOLD time series is denoted by x_i^t for brain area $1 \leq i \leq N$ of time point $1 \leq t \leq T$, T denote the duration time of the whole scanning session. The mean signal is indicated by: $\bar{x}_i =$

$\frac{1}{T}\sum_t x_i^t$ for all brain regions. As consistent with Gilson et al. (2016), the empirical functional connectivity consists of BOLD covariances with zero-lag and one-lag are calculated as follows:

$$\hat{Q}_{ij}^0 = \frac{1}{T-2} \sum_{1 \le t \le T-1} (x_i^t - \overline{x_\iota})(x_j^t - \overline{x_J})$$

$$\hat{Q}_{ij}^1 = \frac{1}{T-2} \sum_{1 \le t \le T-1} (x_i^t - \overline{x_\iota})(x_j^{t+1} - \overline{x_J})$$

The time constant τ_x associated with the exponential decay of the autocovariance averaged across all brain areas using time shifts from zero-lag to one-lag was evaluated for each participant:

$$\tau_x = \frac{N}{\sum_i \log(\hat{Q}_{ii}^0) - \log(\hat{Q}_{ii}^1)}$$

Dynamic cortical model

The activity x_i of each region is governed by a multivariate Ornstein-Uhlenbeck process. The activity variable x_i of node i changes exponentially with the time constant τ_x and depends on the activities of other populations to evolve:

$$dx_i = \left(\frac{-x_i}{\tau_x} + \sum_{j \neq i} C_{\mathrm{ij}} x_j \right) dt + dB_i$$

Here, dB_i represents the white Gaussian noise with covariance matrix Σ, where the input variances are on the diagonal and are zero elsewhere. A matrix C embodies these input fluctuations propagate by effective connectivity. The mathematical mapping between Q^0 , Q^1, and matrices C, is given by Lyapunov equation:

$$J\mathrm{Q}^0 + Q^0 J^T + \Sigma = 0$$

Where $\tau = 0$ and $Q^1 = Q^0 \mathrm{expm}(J^T)$ where $\tau > 0$. The *expm* denotes the matrix exponential, and the superscript T denotes the matrix transpose. J is the Jacobian of dynamical systems, which depends on the time constant τ_x and the network EC:

$$J_{\mathrm{ij}} = -\frac{\delta_{ij}}{\tau_x} + C_{\mathrm{ij}}$$

Here, δ_{ij} is the Kronecker delta. Without modelling the network, these consistency equations allow for rapid calculation of the predicted FC matrices.

Parameter estimation

Considering the noise matrix Σ to be known, for now, the network parameters C were optimized in this step to minimize the model error, which is defined by a Lyapunov function as a sum of two matrix distances:

$$V(C) = \sum_{i,j}(Q_{ij}^0 - \hat{Q}_{ij}^0)^2 + \sum_{i,j}(Q_{ij}^1 - \hat{Q}_{ij}^1)^2$$

The Jacobian J is computed from the current value of C at the first step. Secondly, the model FC matrices Q^0 and Q^1 are then computed from the consistency equations, with the Lyapunov equation solved using the Bartels-Stewart algorithm. The target of the Jacobian update is to reduce the FC error between empirical and model FC, as calculated by the Lyapunov function $V(C)$. The optimized parameters were obtained when the model error was minimized in 1000 optimization iterations, and the local minima was addressed by the replication with subsets of subjects. Finally, the connectivity update is $\delta C_{ij} = \eta_C \delta J_{ij}$ for existing connections. The input variance is tuned according to $\delta\Sigma_{ij} = -\eta_\Sigma(J\delta Q_{ii}^0 + \delta Q_{ii}^0 J^T)$. $\eta_\Sigma = 0.1$ and $\eta_C = 0.0001$ were applied here.

Model estimates normalization

The effective connectivity was normalized by applying a z-score transform over the matrix elements within each participant:

$$score(V_{ij}) = \frac{V_{ij} - mean(V_{ij})}{std(V_{ij})}$$

Where the V is either C or Σ, this normalization was implemented to enable that the effective connectivity of each participant contributes similarly to the statistics.

This effective connectivity method has been performed on a study of rest and movie viewing and successfully identified differences in cortical coordination (Gilson et al., 2018) and also mental disorder analyses (Rolls et al., 2020b).

3.1.2.2 Granger causality

The concept of cross prediction was the base of the Granger causality. To be specific, if including the previous values of time series X enhances the future forecast of time series Y, X is defined to have a causal effect on Y (Granger, 1969). The efficacy of cross-prediction could be deduced from the residual error after the prediction (Roebroeck et al., 2005) or the magnitude of the predictor coefficients (Blinowska et al., 2004) in any two time-series X and Y. Both of these two approaches are identical,

and the detailed analyses on the relationship of these two methods are given by Granger (1969). The model order was typically determined by the Akaike information criterion (AIC) (Akaike, 1974). In describing brain effective connectivity, the Granger causality was applied to compute the temporal effects of the fMRI signal of one brain region on another brain region.

As the number of regions of interest grows, the computational complexity can become intractable, and the numerical procedure can become unreliable for traditional methods like DCM. These drawbacks can be mitigated significantly using approaches based on cross-prediction between two time courses, i.e. Granger causality (Granger, 1969). The Granger causality analysis has been applied in many studies on neuroimaging works related to mental disorders and other behaviours (Hamilton et al., 2011; Luo et al., 2013; Wang et al., 2016; Shi et al., 2019).

Bivariate Granger causality

The bivariate linear autoregressive model of the time course Y with previous values in Y and another time course X is as follows:

$$Y_t = \sum_{i=1}^{p} A_i X(t-i) + \sum_{i=1}^{p} B_i Y(t-i) + CZ_t + \varepsilon_t$$

When ignoring the directional causality from X_t to Y_t in the Y_t, the time-variant process Y will become:

$$Y_t = \sum_{i=1}^{p} B_i Y(t-i) + CZ_t + \widetilde{\varepsilon_t}$$

Here the parameter p represents the time lag in this model. A_i and B_i are autoregression coefficient, ε_t is residual, and Z_t is covariant included, for example, global trend, head motion, and physiological noise.

If the A_i is significantly smaller or larger than zero, the time series X_t is said to Granger causes the time series Y_t. Similarly, the Granger causality from Y_t to X_t can be inferred in the same way. The Akaike Information Criterion is typically used to calculate the optimal lag parameter (Akaike, 1974). To enhance the temporal resolution of estimates of neural effect, the time-directed prediction between the BOLD time series was usually estimated across a lag of one TR.

Following the concept of Granger causality (Granger, 1969), the value of one time course X at one time point has a causal impact on another time course Y after a certain temporal lags p can be inferred if the value of X in previous time point can contribute to the prediction of the value in the time course Y to achieve better prediction accuracy

than considering only information in the past of Y itself. The Granger causality from X to Y is computed by cumulating the residual square errors as estimated by:

$$F_{X\to Y} = \log\left[\frac{\sum_{t=1}^{T} var(\widetilde{\varepsilon_t})}{\sum_{t=1}^{T} var(\varepsilon_t)}\right]$$

Multivariate Granger causality

The bivariate Granger causality formulation can be extended to multivariate conditions as the multivariate autoregressive model shown below.:

$$Y_{1t} = \sum_{i=1}^{p} A_{11}^{i} Y_1(t-i) + \cdots + \sum_{i=1}^{p} A_{1n}^{i} Y_n(t-i) + C_1 Z_t + \varepsilon_t$$

…

$$Y_{nt} = \sum_{i=1}^{p} A_{n1}^{i} Y_1(t-i) + \cdots + \sum_{i=1}^{p} A_{nn}^{i} Y_n(t-i) + C_n Z_t + \varepsilon_t$$

The multivariate Granger causality model is used for identifying an identical, temporal prediction among diverse time-varying signals in a multivariate autoregressive procedure. In the multivariate GC analysis, multiple time series were included in the prediction instead of pairs of time series, enabling a more comprehensive analysis of the whole system. However, compared to the bivariate, the computational cost of the multivariate model is higher and less efficient.

Statistical significance testing

To assess whether the result detected by Granger causality is significant, surrogate data (Kus et al., 2004) was employed to build an empirical null distribution, i.e. a permutation test was performed. To be specific, the original time series were converted to the frequency domain, and the phase was randomized to form a uniform distribution over (-pi, pi) (Kus et al., 2004). The signal was then converted back to the time domain to produce the surrogate data. The surrogate data had the same spectrum as the original data, but the causal phase relations were destroyed by this approach. To calculate the p value, the actual Granger causality value was compared to the corresponding null distribution for each connectivity. Then, the p values from individual participants were merged by the Fisher's method (Fisher, 1992) to create a single p value for group significance inference. No permutation test was performed in this step to test the group significance, following prediction analysis and statistical methods using the Granger causality coefficients are described in Chapter 5.

In the investigation described in Chapter 5, the Granger causality modelling (Hamilton et al., 2011) and effective connectivity modelling (Gilson et al., 2018) were

performed to measure the directional connectivity of the brain. In addition, the effects of these two directional connectivity methods on measuring the brain were examined by performing predictions on the behavioural measure (verbal intelligence) with five different machine learning regression algorithms.

3.2 Machine learning regression algorithm

The existing research in neuroimaging field consists of five widely used machine learning linear regression methods: ordinary least squares regression (OLSR), linear support vector regression (LSVR), ridge regression, LASSO regression, and elastic net regression. Here, the basic algorithms of these five methods are described. In Chapter 4, a novel prediction approach of sensation-seeking based on elastic net regression was developed, and the schematic overview of this approach is shown in Fig. 4.1 (details described in Chapter 4). In Chapter 5, to compare the prediction efficiency of the effective connectivity and the Granger causality, nested-5-fold cross validation prediction models were developed with these five regression models. The inner 5F-CV was used to determine the optimal parameters of the correlation regression algorithm (Lasso, ridge λ, elastic net λ, α and LSVR C). The parameters and the formula are described next in this section. The schematic overview of this approach is shown in Fig. 5.1 (details described in Chapter 5). Besides, the prediction accuracy of these five models was investigated with different sample sizes.

Considering a model with *n* explanatory variables, the regression model has the form:

$$\hat{Y} = \sum_{j=1}^{n} \hat{\beta}_j X_j + \hat{\beta}_0$$

Where $\hat{Y} = (\hat{y}_1,...,\hat{y}_n)^T$, and $\hat{y}_i (i = 1,...,n)$ represents the predicted value for the *j-th* subject, $X_j = (x_{1,j},...,x_{n,j})^T$ and $x_{i,j}$ represents the *j-th* subject's value of the *j-th* feature, and $\hat{\beta}_j$ represents the regression coefficient of the *j-th* feature. Given training data $((x_1, y_1),...,(x_N, y_N))$, the N denotes the training sample size, *Xj* represents a vector of high dimensional features.

3.2.1 Ordinary least squares regression

Ordinary least squares regression (OLSR) is more commonly called a simple or multiple linear regression model depending on the number of explanatory variables. To minimize the residual (the sample estimate of the error for each observation) sum of squares differences between actual values y_i in the training data group and predicted values $f(x_i)$ by the linear model is the crucial problem of the OLSR algorithm. The objective function of OLSR can be formed as below:

$$\min_{\beta} \sum_{i=1}^{N} (f(x_i) - y_i)^2$$

Where y_i represents the actual behavioural score. The minimization problem of this objective function was solved using the Moore-Penrose pseudo-inverse method and singular value decomposition. If X is full column rank, the analytical solution of the estimator of β value is represented as follows:

$$\hat{\beta} = \mathrm{X}^{+}\mathrm{y} = (X^T X)^{-1} X^T y$$

Where $X^{+} = (X^T X)^{-1} X^T$ indicates Moore-Penrose pseudo-inverse, and X is a $N * p$ matrix in which each row is a feature vector of one subject.

The limitations of OLSR make it impossible to be directly used for linear regression fitting in many cases. Especially in the following two issues: 1) the X is not a full-rank matrix or positive definite matrix, that is, the number of features is larger than that of observations, increasing the difficulty of solving the inversion of the $\mathrm{X^TX}$ matrix and 2) a strong linear correlation between the features are prone to overfitting. In contrast, LSVR, LASSO regression, ridge regression, and elastic net regression adopted multiple regularization rules to help minimize the overfitting problem in machine learning models. OLSR estimator may provide a good fitting to the training dataset. However, it will not fit well with the test dataset. The OLSR has no parameters, which is an advantage, but it cannot control the complexity of the model.

3.2.2 Ridge regression

If multicollinearity exits in the observed data, OLSR is very sensitive to the noisy input variables, and its solution will be extremely unstable. If the growth of the parameter can be restricted, then the sensitivity of the model to noisy the inputs will be reduced. To limit the size of the model parameters, a penalty term (regularization term)

is included in the objective function of the model, which is called regularization. For example, the regression model uses "squared magnitude" of coefficient as penalty term (L2 regularization) added to the loss function termed ridge regression. The complete optimization function is calculated as follows:

$$\min_{\beta} \sum_{i=1}^{N} (f(x_i) - y_i)^2 + \lambda \sum_{j=1}^{p} \| \beta_j \|^2$$

In the ridge algorithm, λ can regulate the trade-off between the prediction accuracy within the training data and L2 regularization. Additionally, L2 regularization drives down the overall size of the weight values during optimization and reduces the overfitting problem. Compared with OLSR, ridge regression is a more restrained model, making it less possible to overfit. In general, a simpler model performs worse on the training set but performs better in generalization. The ridge model makes a trade-off between the simplicity of the model (coefficients are all close to 0) and the performance of the training set. The importance of both simplicity and training set performance to the model can be specified by the user by setting the alpha parameter. The optimal setting of alpha depends on the specific data set used. Increasing alpha will make the coefficients more towards 0, thereby reducing training set performance, but may improve generalization performance.

3.2.3 LASSO regression

Unlike ridge regression, L1-norm regularization applied to the OLSR loss function is termed as LASSO regression, making the coefficients of determination shrunk to zero. Therefore, the loss function has the form as below:

$$\min_{\beta} \sum_{i=1}^{N} (f(x_i) - y_i)^2 + \lambda \sum_{j=1}^{p} | \beta_j |$$

Lasso regression penalizes less important features, which cause high variance and model over-fitting issues of training data and makes their respective coefficients zero, thereby eliminating them, which benefits feature selection and reduces the model complexity. Meanwhile, the trade-off between the prediction accuracy with the training data group and L1 regularization, i.e. the trade of penalties between bias and variance, is controlled by parameter λ. If an easy to explain model is required, LASSO can give a model that is easier to understand because it only selects a part of the input features. LASSO performed poorly on the training set and the test set. This indicates that there

is underfitting. To reduce underfitting, we try to reduce alpha. While doing this, we also need to increase the maximum number of iterations to run.

3.2.4 Elastic net regression

Elastic net regression is another regularized linear regression model involving L1-norm regularization used by LASSO and L2-norm regularization used by ridge regression in the loss function during training. The loss function is set to the formula as follows:

$$\min_{\beta} \sum_{i=1}^{N} (f(x_i) - y_i)^2 + \lambda \sum_{j=1}^{p} (\alpha \mid \beta_j \mid + \frac{1}{2}(1-\alpha) \parallel \beta_j \parallel^2)$$

Elastic net regression, which includes both L1-norm and L2-norm penalties, produces better performances than other models with only L1 or L2 regularization.

Hyperparameter λ is provided to control the sum weight of both penalties in the loss function, controlling the trade-off between the prediction accuracy in the training samples and regularizations, i.e., the trade of penalties between bias and variance. The fully-weighted penalty is used by default with a value of 1; a value of 0 is used to exclude the penalty. Another hyperparameter α is utilized to distribute the relative weight given to L1 and L2 regularization. The value α is from 0 to 1.

3.2.5 Linear support vector regression

Compared with the squared loss function described in the previous models, LSVR implements Vapnik's ε-sensitive loss function to fit the linear model. The aim of the objective function is to identify a function $f(x_i)$, which produces a predicted value with less than ε deviation from the actual value y_i for all training samples. Besides, the flatness of this function needs to be maximized at the same time. Precisely, maximizing the flatness is calculated by an L2-norm regularization to minimize the squared sum of the coefficients. The loss function is written as below to learn the model parameters:

$$\min_{\beta} \frac{1}{2} \sum_{j=1}^{p} \parallel \beta_j \parallel^2 + C \sum_{i=1}^{l} (\xi_i + \xi_i^*)$$

$$\text{Subject to } \begin{cases} y_i - f(x_i) \le \varepsilon + \xi_i \\ f(x_i) - y_i \le \varepsilon + \xi_i^* \\ \xi_i, \xi_i^* \ge 0 \end{cases}$$

Where ξ_i and ξ_i^* are the positive and negative errors at the i-th observed data, respectively. This loss function can be solved by the linear programming approach. The algorithm is used to generate weights (i.e. α_s) for the support vectors, then the weighted sum of these feature vectors was used to calculate the regression coefficients of all features, shown as follows,

$$f(x_i) = \sum_{j=1}^{p} \beta_j x_{i,j} + \beta_0 = \sum_{j=1}^{p} (\sum_{s=1}^{l} \alpha_s x_{s,j}) x_{s,j} + \beta_0 = \sum_{s=1}^{l} \alpha_s (x_i^* x_s) + \beta_0$$

Where $x_s^* x_i$ is referred to as the linear kernel. The penalty coefficient of the loss function is controlled by parameter C, which is equivalent to the regularization coefficient in linear regression. The default value of the penalty coefficient is 1. The larger the C is, the greater the penalty for incorrect samples, resulting in increased training sample accuracy but less generalization ability. That is, the test data classification accuracy is lowered. However, if C is lowered, some incorrect misclassification examples can be included in the training data group, and the generalization ability is higher. The larger the C value, the weaker the corresponding regularization. In other words, if the parameter C value is large, then LSVR will fit the training set as best as possible (the model will be more complicated). If the C value is small, the model emphasizes making the coefficient vector (w) close to 0. A small C value (corresponding to strong regularization) allows the algorithm to adapt to "most" data points as much as possible. In contrast, a larger C value (corresponding to weak regularization) emphasizes the correct classification of each data point. For training samples with noise, the latter is generally used, and the samples with the wrong classification in the training sample set are regarded as noise.

This section gives description of the five commonly used machine learning regression models including the definition, formula and parameters. In Chapter 4, a novel prediction approach of sensation-seeking based on elastic net regression was developed. This provides a novel way to investigate the relationship between behavioural measures and brain functional connectivity with a prediction model instead of ordinary correlation analysis. A schematic overview of this approach is shown in Fig. 4.1. In Chapter 5, for the first time, the prediction efficiency of the effective connectivity and the Granger causality was compared by developing a nested-5-fold cross validation prediction models with five regression models as described above.

Details of the structure of this nested-5-fold prediction model is shown in Fig 5.1, and in section 5.2.

Chapter 4

Prediction of Sensation-seeking from Functional Connectivities of the Medial Orbitofrontal Cortex with the Anterior Cingulate Cortex

4.1 Introduction

Sensation seeking is a multifaceted personality trait with components that include experience-seeking, thrill and adventure seeking, disinhibition, and susceptibility to boredom (Zuckerman, 1994). High sensation seekers, compared to low sensation seekers, are more vulnerable to reckless driving (Jonah, 1997), physical risk sports (Ruedl et al., 2012), unprotected sexual activities (Hoyle et al., 2000), problem gambling (Harris et al., 2015), and substance use (Bardo et al., 1996). One critical issue is the mechanisms predisposing those high in sensation seeking to such risky behaviors. Addressing this issue is of great importance in prevention programs aimed at reducing the occurrence of sensation-seeking behaviours where these may be dangerous (Sargent et al., 2010) and in the development of risk-taking models (Schonberg et al., 2011).

Individuals with high sensation-seeking have a stronger orienting response and greater cortical arousal in response to intense visual or auditory stimuli. They also show a preference for and have stronger skin conductance responses to sexually explicit and violent stimuli (Smith et al., 1990). Taken together, this evidence suggests that high sensation seekers show hypersensitivity to intense and novel stimuli.

Previous research on brain processing related to sensation-seeking has typically involved activation studies with relatively low numbers of participants. In one study, activation in the ventral striatum in a delayed incentive task was related to individual differences in sensation-seeking and novelty seeking (Abler et al., 2006). In another study, Joseph et al. (2009) found that high sensation seekers had larger responses in the posteromedial orbitofrontal cortex and insula to arousing pictures. In a gambling task, it was found that those with high scores for thrill and adventure-seeking had larger activations in the ventral striatum, insula, precuneus and superior frontal gyrus (Kruschwitz et al., 2012). In another gambling task, high sensation seekers had greater responses to Wins in the prefrontal cortex and insula (Cservenka et al., 2013).

Activation of the ventrolateral prefrontal cortex to reward expectancy has also been related to impulsive sensation seeking (Chase et al., 2017).

In the present study, we used a different approach with no task being performed by analysing resting-state functional connectivity and relating this to sensation seeking. A highlight of the investigation described here is the large number of participants involved (414). Another feature of the present study is the use and further development of methods. In addition to measuring correlations of sensation-seeking with functional connectivities, we also made predictions about sensation-seeking from the functional connectivities. The prediction approach provides another way to identify functional connectivity links related to sensation-seeking. The prediction method used was to identify relevant links by finding the connections with which the optimal prediction could be made (Liu et al., 2018a). The predictions were made with an elastic net linear regression model because an elastic net operates reasonably when the features are correlated (Cui and Gong, 2018). We know of no other large-scale study of the relation between sensation-seeking and functional connectivity. Because sensation-seeking may be related to some types of impulsivity, we also measured the correlations in this dataset between sensation-seeking and different types of impulsivity. Further, we investigated whether the functional connectivities related to sensation-seeking were also associated with impulsivity.

The hypotheses we investigated were: (1) Are some resting-state functional connectivities significantly related to sensation-seeking? (2) Can sensation-seeking be predicted from functional connectivities? (3) Are some of the functional connectivities related to sensation-seeking also related to impulsive behaviour? (4) Are functional connectivities in brain areas related to emotion, such as the orbitofrontal cortex, amygdala, and anterior cingulate cortex (Rolls, 2014b, 2019b) related to sensation-seeking? Although (4) was a hypothesis, we did not exclude any brain area from consideration and performed a whole-brain analysis.

4.2 Method

4.2.1 Participants, resting-state fMRI

The data used in this study is provided by the enhanced Nathan Kline Institute-Rockland Sample dataset (Nooner et al., 2012). NKI-RS is an ongoing, institutionally centered endeavor aimed at creating a large-scale (N > 1000) community sample of

participants across the lifespan, which was approved by an Ethics committee (Nathan Kline Institute and Montclair State University). Measures include a wide array of physiological and psychological assessments, genetic information, and advanced neuroimaging. In addition, anonymized data is made available (fcon_1000.projects.nitrc.org/index/enhanced). Four hundred fourteen participants were involved in this prediction analysis, ageing from 18 to 85. All of these participants have available resting-state fMRI data and the behaviour scores of sensation seeking.

The resting-state fMRI data were acquired on a 3T Siemens Trio Scanner with a BOLD-weighted multiband echo-planar imaging sequence (TR=645 ms, voxel size=3 mm, duration=10 min), with the participants awake and looking at a fixation cross on the screen (Nooner et al., 2012).

4.2.2 Data Preprocessing

Resting-state fMRI data were preprocessed using FSL (Jenkinson et al., 2012) and AFNI toolbox (Cox, 1996). For each individual, the preprocessing steps included: slice timing correction (FSL slicetimer), motion correction (FSL mcflirt), spatial smoothing by a 3D Gaussian kernel, despiking motion artifacts using the brain-wavelet toolbox (Patel et al., 2014), registering to a 3×3×3 mm3 standard space by first aligning the functional image to individual T1 structural images using boundary-based registration (Greve and Fischl, 2009) and then to standard space using FSL's linear and non-linear registration tool (FSL flirt and fnirt), regressing out nuisance covariates including Friston's 24 head motion parameters (Friston et al., 1996), white matter signal, and the cerebrospinal fluid signal. No temporal filtering was used to ensure compatibility for possible analysis for effective connectivity. All the images were manually checked to ensure successful preprocessing. The resulting time courses were used for the construction and analysis of the brain network. Global signals were not regressed out, for reasons described elsewhere (Cheng et al., 2016).

After preprocessing, the whole brain was parcellated to reduce the high dimensionality of the voxel-level data. In this study, 94 regions for the brain (excluding the cerebellum) were defined by the Automated-Anatomical-Labelling Atlas 2 because it has been tailored to include clear subdivisions of the orbitofrontal cortex (Rolls et al., 2015). The names of the brain areas are shown in Appendix-1. Then the time series were extracted for each region by averaging the signals of all voxels within that region.

4.2.3 Construction of the whole-brain functional network

Functional connectivity is defined as the correlation of the BOLD signal averaged across time between pairs of brain regions or voxels (Biswal et al., 1995). For each pair of brain regions, the Pearson correlation was calculated from the BOLD signal across the time series for that pair of brain regions to measure functional connectivity between the 94×94 brain regions for each participant. Fisher's r-to-z transformation was then implemented to improve the normality of the correlation coefficients, resulting in a 94 by 94 symmetric matrix that represented the links between every pair of brain regions (Fig. 4.1A).

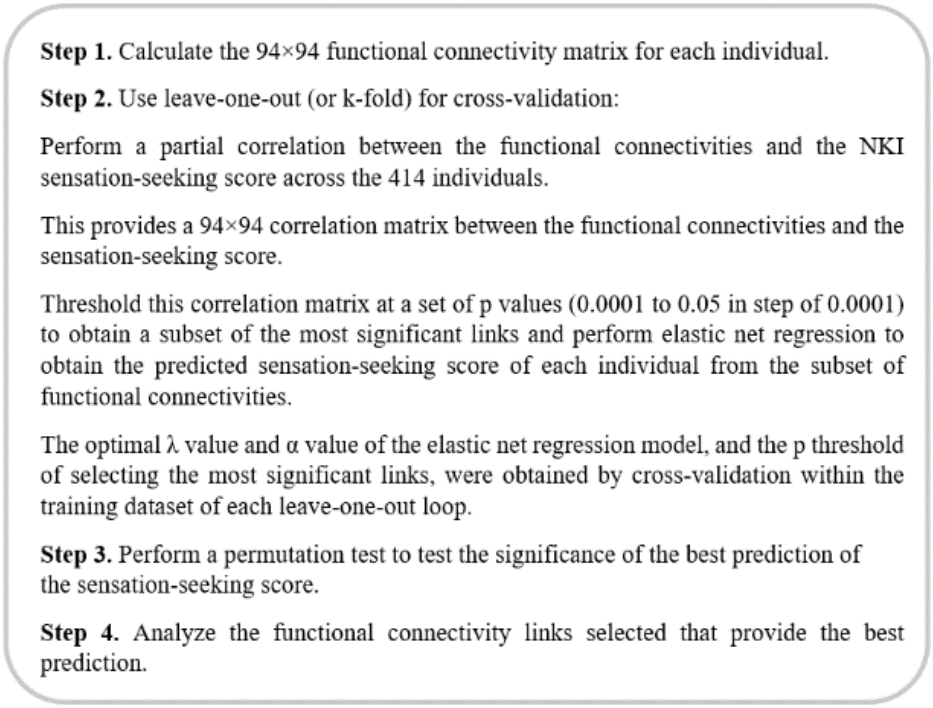

Figure 4.1. A) Schematic overview of the method.

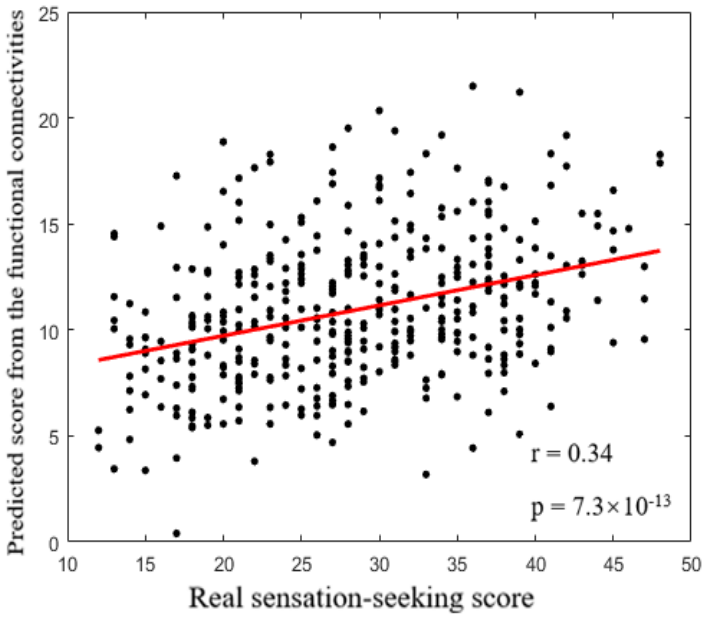

B) The correlation was 0.34 between the predicted sensation-seeking score from the functional connectivities and the actual score of each of the 414 individuals obtained with the optimal p-threshold value for selecting which functional connectivity links to use, which was 0.001. Each data point is from a different individual.

4.2.4 Correlation of the functional connectivities with sensation-seeking

Interest in sensation-seeking as a measure was developed by Zuckerman (1994) and came to be included in the UPPS as a result of factor analysis (Whiteside and Lynam, 2001). The UPPS-P is a 59-item self-report inventory in its revised version (originally UPPS) that quantifies five different aspects of impulsive behaviour (Lynam et al., 2006): (i) negative urgency, which refers to the tendency to experience strong impulses under conditions of negative affect; (ii) lack of perseverance that reflects the experience of having problems with remaining focused on a task that might be boring or too difficult; (iii) lack of premeditation that describes the tendency to engage in an act without reflecting the consequences of that act beforehand; (iv) sensation seeking that further comprises two aspects: (a) the propensity to enjoy and chase exciting activities; (b) an openness to engage in new experiences that might be dangerous; and (v) positive urgency that involves the tendency towards rash actions in response to very positive mood. Each item can be scored on a four-point Likert scale, ranging from 1 (strongly agree) to 4 (strongly disagree). Reversed items are recoded afterwards so that higher scores indicate a more pronounced level of self-reported trait impulsivity. Reliability analyses revealed an adequate level of internal consistency (Cronbach's

alpha) for each of the five subscales (Golchert et al., 2017). The questions used to produce the sensation-seeking score are available (Whiteside and Lynam, 2001) and are shown in the next section, and included: “I generally seek new and exciting experiences and sensations”, “I welcome new and exciting experiences and sensations, even if they are a little frightening and unconventional”, and “I quite enjoy taking risks”.

After the functional connectivity matrices of all participants had been calculated, correlations between the functional connectivities and the sensation-seeking scores across all participants were calculated to investigate which brain regions have connectivities related to sensation-seeking. In more detail, a partial correlation was performed between the functional connectivities and the sensation-seeking scores with age, sex, ethnicity, race and head motion regressed out. In this study, false discovery rate (FDR) correction ($p<0.05$) for multiple comparisons (Benjamini and Hochberg, 1995) for the functional connectivity between any pair of AAL2 brain regions was used.

4.2.5 Full sensation-seeking question list

The sensation-seeking question list is part of the full list of UPPS questionnaires (Whiteside and Lynam, 2001). For each statement, please indicate how much you agree or disagree with the statement. If you ‘Agree Strongly’ circle 1, if you ‘Agree Somewhat’ circle 2, if you ‘Disagree somewhat’ circle 3, and if you ‘Disagree Strongly’ circle 4. Be sure to indicate your agreement or disagreement for every statement below. All items in sensation-seeking are reversed, which means that the item needs to be reverse scored such as 1=4, 2=3, 3=2, 4=1.

1. I generally seek new and exciting experiences and sensations.
2. I'll try anything once.
3. I like sports and games in which you have to choose your next move very quickly.
4. I would enjoy water skiing.
5. I quite enjoy taking risks.
6. I would enjoy parachute jumping.
7. I welcome new and exciting experiences and sensations, even if they are a little frightening and unconventional.
8. I would like to learn to fly an airplane.
9. I sometimes like doing things that are a bit frightening.
10. I would enjoy the sensation of skiing very fast down a high mountain slope.

11. I would like to go scuba diving.

12. I would enjoy fast driving.

4.2.6 Prediction of the sensation-seeking scores from the functional connectivities

A schematic overview of the method used in this study is shown in Fig. 4.1A. The method used was developed from methods described by Liu et al. (2018a) and Cui and Gong (2018) in which the links optimal in making the prediction, and an elastic net linear regression model was used to make the predictions because it is a powerful approach when there is some correlation between the features. The functional connectivity matrix includes functional connectivity links which have some correlations with each other. We made a comparison and found that the elastic net regression had a considerably better prediction performance than an LSVR in the current study.

Elastic net regression combines L1-norm and L2-norm regularizations in the standard linear regression loss function to make predictions (Zou and Hastie, 2005). The regression model used is as follows:

$$\hat{Y} = \sum_{j=1}^{p} \widehat{\beta_j} X_j + \widehat{\beta_0}$$

where $\hat{Y}$ is the best estimate of the predicted value of the sensation-seeking scores, X_j is the value of the j^{th} feature used in the prediction model, β_j is the regression coefficient of the j^{th} feature and p is the number of features. The aim of the regression model is to find a function $F(X) = \sum_{j=1}^{p} \beta_j X_j + \beta_0$ that can best predict the actual behavioural score by examining the regression coefficients. The objective function takes the form:

$$\min_{\beta} \sum_{i=1}^{N} (f(x_i) - y_i)^2 + \lambda \sum_{j=1}^{p} (\alpha|\beta_j| + \frac{1}{2}(1-\alpha)\|\beta_j\|^2)$$

where $f(x_i)$ is the value of the predicted behavioural score for the i^{th}subject, y_i is the observed behavioural score, and N is the number of subjects. A mixing parameter α is used to control the relative weighting of the L1-norm and L2-norm contributions. In addition, a regularization parameter λ is used to control the trade-off of penalties between bias and variance.

The LASSO function in MATLAB was used to implement elastic net regression. The optimal λ value and a-value were obtained by cross-validation within the training dataset of each leave-one-out loop.

4.2.7 Individual prediction framework

Leave one out cross-validation was performed in the prediction stage to test the accuracy (Fig.4.1A). In each leave-one-out iteration, the most significantly correlated group of FC links were selected by performing a partial correlation between the functional connectivity and the sensation-seeking score across all samples in the training set except for the single test sample. The effects of age, sex, ethnicity, race and head motion were regressed out. The individual prediction was performed with groups of functional connectivities more significant than a certain p threshold (i.e. the p value of the partial correlation between the functional connectivity and the sensation-seeking score had to be under the p threshold) (Liu et al., 2018a). The p threshold was obtained by cross-validation within the training dataset of each leave-one-out loop. The elastic net regression model was trained with the training set with the group of the most significant functional connectivities defined in this way and tested by predicting the test sample with leave one out cross-validation. Example code of feature selection and optimizing the model parameters is attached in Appendix-6. The Pearson correlation coefficients between the actual scores and the predicted scores were computed to quantify the accuracy of the prediction (Erus et al., 2015; Siegel et al., 2016). To yield the final accuracy, the predicted score of each participant in each iteration was saved in one vector, and the correlation between the predicted scores and actual scores was calculated across all 414 participants.

4.2.8 Statistical test: permutation analysis

To determine whether the predicted scores obtained from the prediction model were significantly better than random, a nonparametric permutation procedure was adopted. The symptom scores across all participants were randomly shifted in each permutation. Then the elastic net prediction analysis was conducted. The null distribution for the highest correlation between the actual scores and predicted scores was formed by running the permutation procedure 10000 times, resulting in a significance level of $p < 0.0001$ (Fig. 4.4).

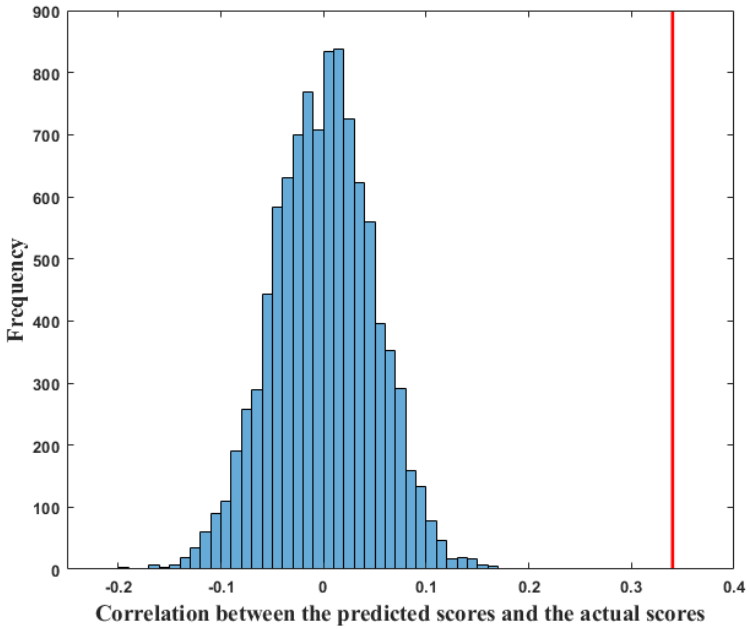

Figure 4.4. Permutation test results for the sensation-seeking score predicted from the functional connectivities when the participants' scores were shuffled with respect to their functional connectivities. The blue lines stand for the null distribution formed by 10000 iterations. The red line stands for the correlation r value between the actual score and the predicted score obtained by the unshuffled prediction model.

4.2.9 Association of sensation-seeking with risk-taking, and substance use

The correlation between the sensation-seeking score and the risk-taking score was also measured to examine whether the sensation-seeking score is associated with risk-taking behaviours. The risk-taking score was provided by the domain-specific risk-taking scale (DOSPERT) (Blais and Weber, 2006), which assesses risk-taking in five content domains: financial decisions (separately for investing versus gambling), health/safety, recreational, ethical, and social decisions. The associations between sensation-seeking and the overall risk-taking score and its five subscales were examined.

In addition, the correlation between the sensation-seeking score and the substance use scores available in the NKI dataset was also measured to examine whether the sensation-seeking score is associated with substance use behaviours. The measure of substance use was obtained with the adult self-report questionnaire (ASR) (Achenbach and Rescorla, 2003) results available in the NKI dataset. The associations between sensation-seeking and alcohol, tobacco, and drug use were examined.

4.3 Results

4.3.1 Functional connectivities that predict and are correlated with sensation-seeking

After the functional connectivity matrices of all participants had been calculated, the partial correlation between each functional connectivity and the sensation-seeking score across all participants was calculated with age, sex, ethnicity, race and head motion regressed out. Five functional connectivities were significantly correlated with the sensation-seeking score at $p < 0.05$ FDR corrected, corresponding to a p threshold of 3.83e-05 in the partial correlations (Table 4.1).

Region 1	Region 2	r value	p value
Amygdala_L	Rolandic_Oper_L	0.175	3.81E-04
OFCmed_L	Cingulate_Ant_R	0.220	7.28E-06 *
OFCmed_L	Cingulate_Ant_L	0.206	2.75E-05 *
OFCmed_R	Cingulate_Ant_R	0.192	9.00E-05
OFCpost_L	Cingulate_Ant_L	0.191	1.03E-04
Olfactory_L	Cingulate_Ant_R	0.207	2.43E-05 *
Olfactory_L	Cingulate_Ant_L	0.203	3.61E-05 *
Olfactory_L	Frontal_Inf_Orb_2_L	0.188	1.35E-04
Rectus_R	Cingulate_Ant_R	0.236	1.34E-06 *
Rectus_R	Cingulate_Ant_L	0.202	3.83E-05
Rectus_R	Frontal_Sup_2_R	0.189	1.23E-04

Table 4.1. The eleven functional connectivities were optimal for use in predicting sensation-seeking using an elastic net regression model. The r values show the correlation between the functional connectivity and the sensation-seeking score, and the p values show the significance level. Five functional connectivities that were significantly correlated with the sensation-seeking score at $p < 0.05$ FDR corrected are indicated by *.

For the predictions, the functional connectivity matrix was thresholded with many different p values for the correlation between the sensation-seeking score and the connectivities to find the links optimal for making the prediction. An elastic net regression model was used to predict the sensation-seeking score with leave-one-out cross-validation. The overall accuracy of this prediction model given by the correlation

r value between the predicted score and the actual score across all 414 participants was 0.34 ($p = 7.3x10^{-13}$) (shown in Fig. 4.1B). (The result was shown to remain highly significant with 10-fold cross-validation, as described in the next section.) Random permutation analysis was used to test the significance level of the prediction. The sensation-seeking scores were shuffled concerning the values predicted from the functional connectivities across all participants randomly in each iteration. In ten thousand iterations of the random permutation test, the results were significant at the maximum level obtainable of $p < 0.0001$ (Fig. 4.4).

Eleven functional connectivities were found to be optimal in making the prediction of sensation-seeking (Table 4.1). 10 of these 11 links involved medial orbitofrontal cortex areas and eight of the medial orbitofrontal cortex links were with the anterior cingulate cortex (Fig. 4.2).

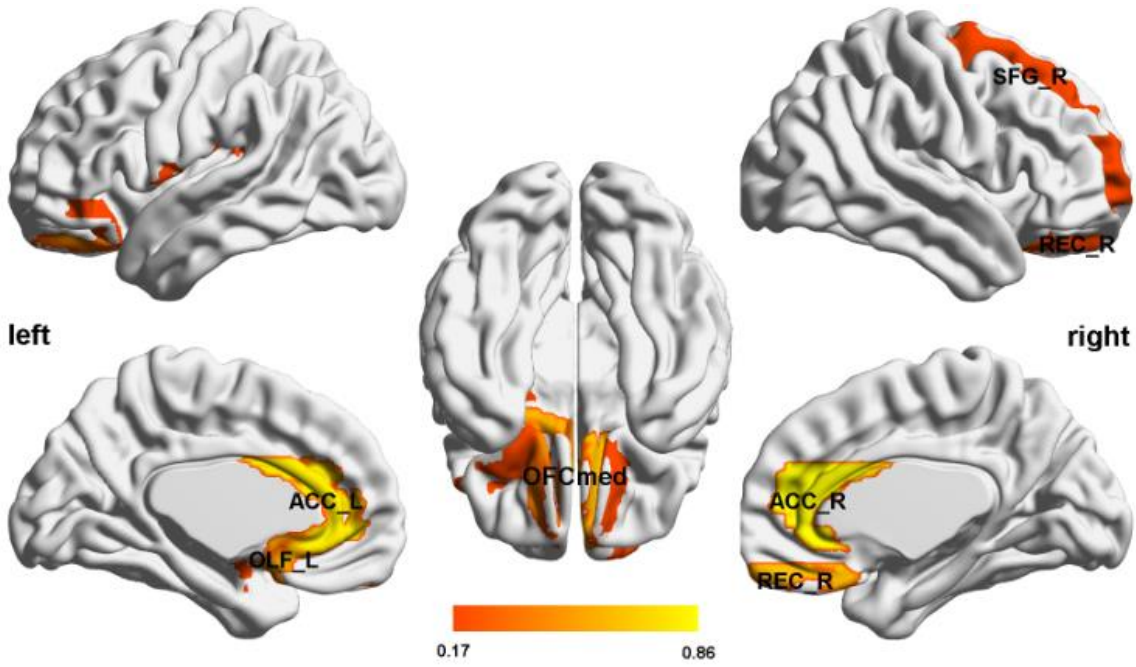

Figure 4.2. The brain regions related to the 11 functional connectivities were optimal in predicting sensation-seeking. The AAL2 regions shown in this figure with labels are medial OFC (OFCmed), olfactory (OLF), rectus, ACC, and superior frontal gyrus (SFG).

One link involved the lateral orbitofrontal cortex, and one the amygdala. Five of the links, all involving the medial orbitofrontal cortex and anterior cingulate cortex, were individually significantly correlated ($p<0.05$ after FDR correction) with sensation-seeking with all the participants involved (Fig. 4.3). The AAL2 areas (Rolls et al., 2015) included here as medial orbitofrontal cortex were medial OFC, posterior OFC, anterior

OFC, the rectus, and the olfactory tubercle (Rolls et al., 2018). (The olfactory tubercle is included in these medial areas because, in the AAL2 atlas, it is at least continuous with the posterior orbitofrontal cortex; and has high correlations of its resting-state functional connectivity with the other AAL2 medial orbitofrontal cortex areas listed (Rolls et al., 2018)).

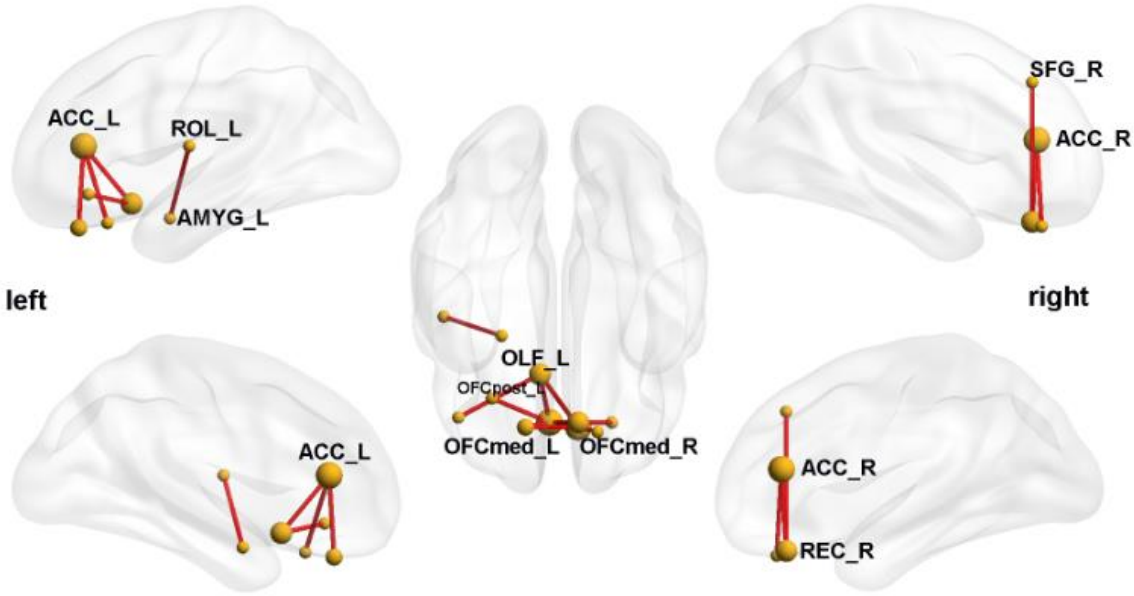

Figure 4.3. The eleven functional connectivities that were used in the optimal prediction of sensation-seeking. Lateral, medial and dorsal views are shown. The AAL2 regions shown in this figure with labels are medial OFC (OFCmed), posterior OFC (OFCpost), olfactory (OLF), rectus, ACC, amygdala (AMYG), superior frontal gyrus (SFG), and rolandic operculum.

In more detail, these 11 links were those that were common to all runs of the leave-one-out cross-validation, which typically used 18 links with a threshold for the correlation matrix that gave the optimal prediction. We checked that these 11 links were able, if used alone, to obtain a good prediction, and that was found to be the case, in that the predicted sensation-seeking scores were correlated with $r=0.335$ ($p=2.4\times10^{-12}$) with just the 11 links (Table 4.1). We can, therefore, have confidence that good predictions can be made from just the 11 functional connectivity links shown in Table 4.1.

In addition, to provide another way of assessing how well the functional connectivities could make predictions, they were used in an analysis to predict who was high on sensation-seeking and who was low. The participants were split at the median into two groups, high and low on sensation-seeking. In a leave-one-out cross-validation

using support vector classification, the prediction was 63% correct ($p<0.001$) using a permutation test. The procedure used was as described above, selecting the optimal number of functional connectivity links from those with the most significant differences between the two groups. Eleven links were used and included nine from the medial orbitofrontal cortex, of which six were with the anterior cingulate cortex. These links are similar to those that successfully predict the sensation-seeking score in the elastic net regression model.

In addition, we showed that with only links between the medial orbitofrontal cortex areas and the anterior cingulate cortex (i.e. part of the common links in the elastic net regression model) used for the prediction of high vs low sensation-seeking individuals, then the prediction was 62% correct (where chance is 50%). Thus, a reasonable prediction of the high sensation-seeking individuals could be made from just the eight functional connectivity links between the medial orbitofrontal cortex and the anterior cingulate cortex (Table 4.1) which were used to make the optimal prediction of the sensation-seeking score in Fig. 4.1B.

4.3.2 Further statistical tests

An elastic net regression model was used to predict from the functional connectivities the sensation-seeking score with leave-one-out cross-validation. To test whether the cross-validation method will affect the statistical significance of the prediction model, this result was checked with 10-fold cross-validation, which resulted in a highly significant correlation with $p=5.6\times10^{-5}$, $r=0.20$. The ten-fold cross-validation was performed by using each fold to predict the sensation-seeking score of the approximately 41 individuals (of the 414 participants) used as the test set in that fold, and then after all folds had been run, calculating the correlation between the 414 predicted and actual scores. The procedures for cross-validation to obtain parameter values for lambda and alpha were analogous to those used for the leave-one-out analysis.

4.3.3 Other UPPS-P subscales

In the present study, only the sensation-seeking subscale of the UPPS-P had significant correlations with functional connectivities after FDR correction, and in addition, the scores could be predicted from the functional connectivities for the sensation-seeking scores. The other four subscales were investigated, but none had a

significant correlation with any functional connectivity after FDR correction, and the prediction from the functional connectivities for these four subscales were low.

As these five subscales stand for different dimensions of impulsivity, there could be similarities and differences between these subscales. Hence, correlation analyses between the five subscales were performed to check their similarity. The sensation-seeking subscale showed a relatively low correlation with the other four subscales, explaining the different results for sensation-seeking compared to the other four subscales of impulsive behaviour in the UPPS (Table 4.2).

	Negative Urgency	**Lack of Premeditation**	**Lack of Perseverance**	**Sensation Seeking**	**Positive Urgency**	**Total score**
Negative Urgency	1.000	0.353	0.402	0.240	0.691	0.795
Lack of Premeditation	0.353	1.000	0.473	0.154	0.312	0.589
Lack of Perseverance	0.402	0.473	1.000	0.045	0.293	0.553
Sensation Seeking	0.240	0.154	0.045	1.000	0.317	0.616
Positive Urgency	0.691	0.312	0.293	0.317	1.000	0.802
Total score	0.795	0.589	0.553	0.616	0.802	1.000

Table 4.2. The correlation matrix between the five subscales and the total score of the UPPS-P. The number of participants was 414.

4.3.4 Relation between sensation-seeking, risk-taking behaviours and NEO five factor personality inventory

A correlation between the sensation-seeking score and the risk-taking score was also performed to examine whether the sensation-seeking score is associated with risk-taking behaviours. The risk-taking score was provided by DOSPERT (Blais and Weber, 2006), which assesses risk-taking in five content domains: financial decisions (separately for investing versus gambling), health/safety, recreational, ethical, and social decisions. The associations between sensation-seeking and the overall risk-taking score and its five subscales were examined. The sensation-seeking score was significantly correlated with the overall-risk taking score with $r=0.49$ ($p=3.92\times10^{-26}$) across 412 participants (the intersection of the number of participants having fMRI data and UPPS-P and DOSPERT scores available). The correlations between the sensation-

seeking and risk-taking subscales are shown in Table 4.3. The highest correlation of sensation-seeking was with the 'recreational' risk-taking subscale.

Risk-Taking	r value	p value
Ethical	0.26	7.16e-08
Financial	0.25	4.56e-07
Health	0.35	1.21e-13
Recreational	0.58	4.11e-39
Social decision	0.19	8.36e-05

Table 4.3. Correlations between the different risk-taking subscales of the DOSPERT and sensation-seeking across 412 participants.

In addition, of the five functional connectivities significantly correlated with sensation-seeking after FDR correction, three all involving the medial orbitofrontal cortex and the anterior cingulate cortex were significantly associated ($p<0.05$) with the overall risk-taking score as shown in Table 4.4.

Region1	Region2	Risk-Taking		Drug Use		Drinking		Smoking	
		r val	p val	r val	p val	r val	p val	r val	p val
Rectus_R	Cingulate_Ant_R	0.108	0.030	-0.012	0.832	-0.009	0.873	-0.147	0.012
OFCmed_L	Cingulate_Ant_R	0.082	0.101	0.031	0.596	0.021	0.718	-0.064	0.273
Olfactory_L	Cingulate_Ant_R	0.107	0.031	0.041	0.489	0.026	0.655	-0.084	0.153
OFCmed_L	Cingulate_Ant_L	0.088	0.078	0.028	0.628	0.022	0.714	-0.026	0.653
Olfactory_L	Cingulate_Ant_L	0.144	0.004	0.055	0.351	0.038	0.513	-0.036	0.542

Table 4.4. Correlations and associated p values for the relation between the five links related to sensation-seeking after FDR correction and other behaviours, including risk-taking.

Similarly, association analysis between the sensation-seeking with a five-factor personality inventory was performed. The NEO-FFI-3 is a 60-item psychological personality inventory that assesses based on the five-factor model: Openness to Experience, Conscientiousness, Extraversion, Agreeableness, and Neuroticism. The sensation-seeking score was significantly correlated with the Extraversion score ($r=0.23$, $p=1.37\text{x}10^{-11}$), with the Openness to Experience score ($r=0.24$, $p=6.01\text{x}10^{-13}$),

with the Agreeableness score (r=-0.24, $p=1.61x10^{-12}$), with the Conscientiousness score (r=-0.03, p=0.36), and with the Neuroticism score (r=-0.01, p=0.70).

4.3.5 Relation between sensation-seeking and substance use (drinking, smoking and other drugs)

A correlation between the sensation-seeking score and the substance use scores available in the NKI dataset was also performed to examine whether the sensation-seeking score is associated with substance use behaviours. The measure of substance use was obtained with ASR (Achenbach and Rescorla, 2003). The sensation-seeking score was correlated with the drug usage (including cannabis and cocaine) per day r=0.29 ($p=3.13x10^{-7}$), correlated with alcohol usage per day r=0.21 ($p=1.89x10^{-4}$), and correlated with tobacco usage per day r=-0.024 (p=0.67) across 298 participants (intersection number of participants having fMRI data, UPPS-P score and DOSPERT score available).

The five functional connectivities that were significantly correlated with sensation-seeking after FDR correction did not, in general, have significant correlations with these measures of drug abuse, as shown in Table 4.4.

4.4 Discussion

In this investigation, it was found that it was possible to predict the sensation-seeking score of 414 individuals from resting-state functional connectivities, which mainly involved the medial orbitofrontal cortex and anterior cingulate gyrus. The method used involved the selection of an optimal threshold for the functional connectivity correlation matrix to predict the sensation-seeking score, which was r=0.34, $p=7.3x10^{-13}$. The prediction method used an elastic net regression model, which was found to be more effective than support vector regression. 10 of the 11 common links used in each leave-one-out iteration to predict sensation-seeking involved medial orbitofrontal cortex areas and eight of the medial orbitofrontal cortex links were with the anterior cingulate cortex. This was supported by the finding that 5 of these links were significantly correlated with the sensation-seeking score after FDR correction.

The behavioural assessment used was UPPS, which measures impulsive behaviour. The sub-score of the UPPS, which produced the most significant correlations with the functional connectivities, was the sensation-seeking score, and for that reason is the focus of this project. Sensation-seeking may be one factor that can lead to impulsive

behaviour. Impulsive behaviour has many components or subtypes (Dalley and Robbins, 2017), and one component may be related to decreased sensitivity to non-reward, which might imply lower functional connectivity of the lateral orbitofrontal cortex (Deng et al., 2019). The lateral orbitofrontal cortex, especially on the right, continues round the inferior convexity to the inferior frontal gyrus, but this does not happen on the left as much because the inferior frontal gyrus on the left includes Broca's area. However, in the research of Cheng et al. (2019b), it was found that increased functional connectivity involving medial orbitofrontal areas in drinkers of alcohol was also associated with increased impulsivity, so they argued that increased sensitivity to reward might also lead to high impulsivity. That could be another component or type of impulsivity. The association of sensation-seeking with impulsivity was supported in the present investigation by the finding that risk-taking (an aspect of impulsivity) was somewhat correlated with the sensation-seeking score with r=0.49 and that three of the five medial orbitofrontal cortex links with the anterior cingulate cortex that were implicated in sensation-seeking had significant correlations with risk-taking as measured by the DOSPERT (Blais and Weber, 2006). A concept then related to the present investigation is that some types of impulsive behaviour can be related in part to increased functional connectivity of the medial orbitofrontal cortex reward system with the anterior cingulate cortex action-outcome system; and that this functionality contributes to sensation-seeking. Consistent with this concept, we found that the sensation-seeking score was correlated with positive affect ($r=0.14$, $p<0.003$), which relates the sensation-seeking score to some types of positive behaviour.

The method of making optimal predictions of behaviour from functional connectivity by searching for the best threshold for the functional connectivity correlation matrix has been used in only a few studies before (Liu et al., 2018a; Liu et al., 2018b) to the best of our knowledge. Its use in combination with an elastic net regression for making the prediction was found to be more powerful than using support vector regression.

A previous task-related fMRI study showed that high sensation seekers have a high activation to arousing images in the posterior medial orbitofrontal cortex (Abler et al., 2006; Joseph et al., 2009). Activations in the nucleus accumbens (which receives from the orbitofrontal cortex) are high in sensation-seekers in a monetary incentive delay task (Abler et al., 2006). There is also extensive evidence that the human medial OFC areas, including Brodmann area (BA) No.13, are activated by rewarding stimuli

that are subjectively pleasant (including pleasant odours, pleasant touch, pleasant flavor, and monetary reward) (O'Doherty et al., 2001; Grabenhorst and Rolls, 2011; Rolls, 2014a; Rolls, 2017b). It was very interesting that in our study, without any task, differences in the functional connectivity of the medial orbitofrontal cortex were related to sensation-seeking.

The anterior cingulate cortex is relevant to emotion for it receives input from the orbitofrontal cortex about the value of emotional stimuli and implements instrumental goal-directed actions using action-outcome learning. In this study, five functional connectivities which were significantly correlated with sensation-seeking scores after FDR correction was between the ACC areas and the medial OFC areas. This provides evidence to elucidate further the hypothesis that the orbitofrontal cortex sends reward and non-reward information to the ACC where the reward/non-reward signals can be interfaced to cingulate systems that learn actions to obtain reward and avoid non-reward and punishers (Rushworth et al., 2011; Rushworth et al., 2012; Rolls, 2014a; Rolls, 2017b). The effects of high functional connectivity described here between the medial orbitofrontal cortex and the anterior cingulate cortex may be related to a strong effect of reward on promoting actions, which is expressed as sensation-seeking.

In conclusion, this research reveals a clear association between functional connectivity involving the medial orbitofrontal cortex and sensation-seeking, with connectivity involving medial orbitofrontal cortex areas and the anterior cingulate cortex especially prominent. It was quite remarkable was that it was possible to predict the sensation-seeking score only from 8 links involving different medial orbitofrontal cortex areas and the anterior cingulate cortex with a correlation of $r=0.300$ ($p<4.8\times10^{-10}$). (The corresponding value with the best 11 links shown in Table 4.1 was $r=0.335$ ($p<2.4\times10^{-12}$).) This provides clear evidence that the relation between these two brain areas, the medial orbitofrontal cortex and the anterior cingulate cortex, is strongly involved in sensation-seeking. Moreover, the concept was advanced that one type of impulsivity, which is related to sensation-seeking, is related to increased functional connectivity of a reward-related cortical region, the medial orbitofrontal cortex.

Chapter 5

Comparison of Granger Causality and Effective Connectivity Features with Machine Learning Prediction Models

5.1 Motivation

The applications of functional connectivity measured from resting-state fMRI data have helped to understand the mechanism of brain connections, as reported in many studies and many of my projects. However, the functional connectivity can only give an undirected temporal correlation of BOLD signal change between pairs of brain areas, with no explanation of which direction these brain areas interact with each other. Therefore, it is worth exploring more methods to measure the projection relations of these interactions. In this project, the Granger causality modelling (Hamilton et al., 2011) and effective connectivity modelling (Gilson et al., 2018) were performed to measure the directional connectivity of the brain. Furthermore, the effects of these two directional connectivity methods on measuring the brain were examined by performing predictions on the behavioural measure (verbal intelligence) with five different machine learning regression algorithms.

5.2 Method

5.2.1 Granger causality and effective connectivity

The concept of cross prediction was the base of the Granger causality. To be specific, if including the previous values of time series X enhances the future forecast of time series Y, X is defined to have a causal effect on Y (Granger, 1969). The efficacy of cross-prediction could be deduced from the residual error after the prediction (Roebroeck et al., 2005) or the magnitude of the predictor coefficients (Blinowska et al., 2004) in any two time-series X and Y. Both of these two approaches are identical, and the detailed analyses on the relationship of these two methods are given by Granger (1969). The model order was typically determined by the Akaike information criterion (AIC). (Akaike, 1974). The calculation of Granger causality values between pairs of brain regions was performed by the toolbox developed by Luo et al. (2013). Detailed method description of Granger causality is as shown in the method chapter (Chapter 3).

Effective connectivity is defined as an estimation of the strengths of dynamical interactions between neural populations in the cortex hypothesized to shape functional connectivity. Effective connectivity in this project was calculated by the effective connectivity method developed by Gilson et al. (2016). To assess effective connectivity, this method used a cortical model that incorporates data from Diffusion-weighted MRI and fMRI. This method can be applied to the whole brain, while the traditional effective connectivity 'dynamical causal modelling' (Marreiros et al., 2008) can only be used to very few brain regions due to its high computational complexity. Detailed method description of effective connectivity is as shown in the method chapter (Chapter 3).

5.2.2 Participants, dataset, and behavioural measure

The data used in this investigation is from the enhanced Nathan Kline Institute-Rockland Sample dataset (Nooner et al., 2012). Details of this dataset are described in Chapter 4 (section 4.2.1) and preprocessing of the fMRI data is in Chapter 4 (section 4.2.2). In this project, 477 participants with available fMRI data and verbal intelligence measures were investigated, aged 18 to 85.

The verbal intelligence measure came as a subscale of the Wechsler Abbreviated Scale of Intelligence (WASI-II) (McCrimmon and Smith, 2013). The WASI-II is a general intelligence trail of overall cognitive performance, which includes four subtests: block design (13-item), vocabulary (31-item), matrix reasoning (30-item), and similarities (24-item). The verbal intelligence score was obtained as a combination of the vocabulary and similarities subsets. More descriptions of WASI-II can be found on the NKI website (http://fcon_1000.projects.nitrc.org/indi/enhanced/assessments/wasi-ii.html). The verbal intelligence score ranges from 65 to 143 of these 477 participants (mean=103.8, SD=12.3).

5.2.3 Prediction models with Granger causality and effective connectivity

To compare how Granger causality and effective connectivity model the brain efficiently, prediction models with Granger causality and effective connectivity as predictors independently were built to examine which connectivity feature of the brain will produce higher prediction accuracy on the same behaviour measure. To be more comprehensive and analyse the efficiency of different prediction models, five commonly used prediction models in machine learning were compared in this investigation, including ordinary least squares regression (OLSR), linear support vector

machine regression (LSVR), LASSO regression, ridge regression, and elastic net regression. Detailed method descriptions of these five regression algorithms can be found in Chapter 3 (section 3.2). The scikit-learn library of Python was utilized to perform OLSR, LSVR, ridge regression, LASSO regression, and elastic net regression (http://scikit-learn.org/) in this project.

5.2.4 Individualized prediction framework

Five prediction models were performed on the Granger causality and effective connectivity features separately. A schematic overview of the prediction framework is shown in Fig. 5.1. In this project, all features, i.e., whole brain connectivity links were included in the prediction model without prior feature selection, as the aim of this investigation was comparing the efficiency of Granger causality and effective connectivity on modelling the whole brain connectivity instead of getting high prediction accuracy. 5-fold cross-validation was applied to examine the prediction accuracy of these models. For the LSVR, LASSO regression, ridge regression, and elastic net regression, a nested 5-fold cross-validation was used to optimize parameters in these models. Details are as follows.

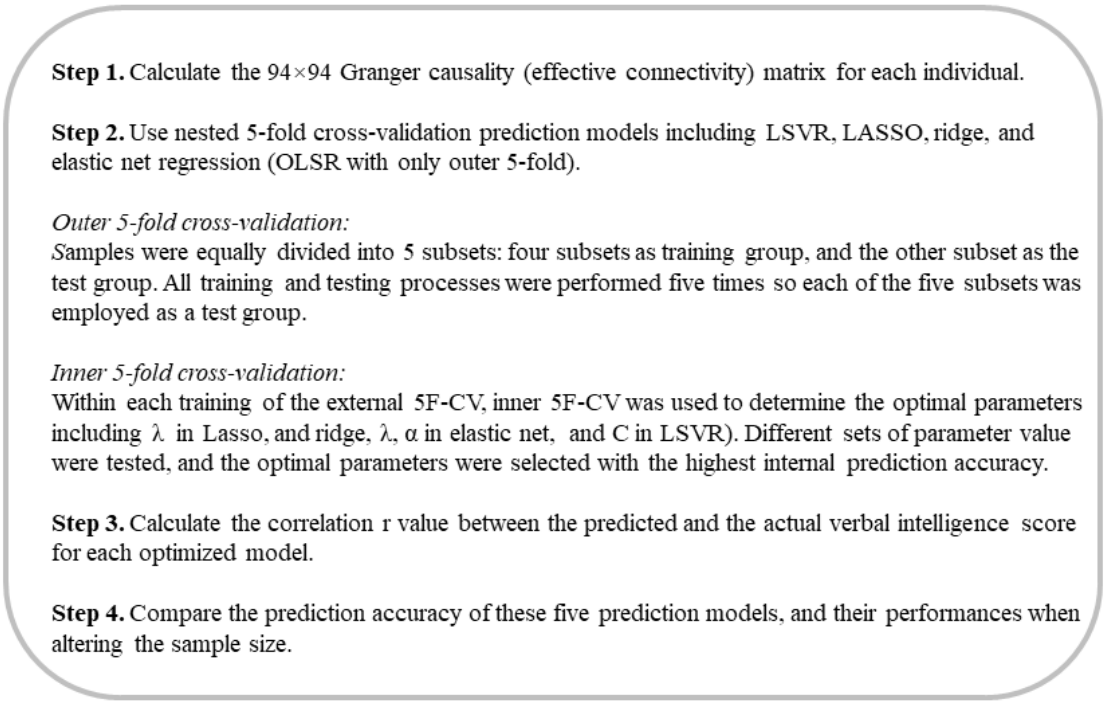

Figure 5.1. Schematic overview of the method.

Outer 5-fold cross-validation

For outer 5-fold cross-validation, all samples were approximately equally divided into 5 sample subsets. All samples were sorted from small to large according to the size of the verbal intelligence value of the data set and then regard the samples sorted as (1, 6, 11, ...) as the first sample subgroup. By analogy, (2, 7, 12, ...) was the second sample subgroup, (3, 8, 13, ...) was the third sample subgroup, (4, 9, 14, ...) was the fourth sample subgroup, (5, 10, 15, ...) was the last sample subgroup, which was the fifth sample subset. This method of splitting the data set avoided the random deviation between the subsets and the large calculation cost caused by repeating the random splitting procedure many times. Among the five sample subsets, four subsets were used as the training group, and the other subgroup was employed as the test group. Here, all the training sample data was used to construct the prediction models, and then the prediction results of the test samples were computed. To quantify the prediction accuracy of the regression models, the Pearson correlation coefficient and the mean absolute error (MAE) between the predicted score and the actual score were computed. All training and testing processes were performed five times to ensure that each of the five subsets was employed as a test group. The final model accuracy was achieved by averaging the correlation and MAE of the five iterations.

Inner 5-fold cross-validation and parameter tuning

In addition to the OLSR model, the remaining four models all needed to find the optimal parameters that suited them during the training process. Therefore, in each training of the external 5F-CV, the inner 5F-CV was used to determine the optimal parameters of the correlation regression algorithm (Lasso, ridge λ, elastic net λ, α and LSVR C). Since the values of C and λ were opposite to each other, the value range of C is $[2^{-5},2^{-4},...,2^{9},2^{10}]$, so the value range of λ is $[2^{-10},2^{-9},..., 2^{4}, 2^{5}]$. For the value range of α in the elastic net regression was [0,0.1,...,0.9,1]. Based on the given C and λ, a grid search was performed on the elastic net regression, and 176 (16 * 11) sets of the (λ, α) parameters was obtained.

For LSVR with parameter C, ridge and LASSO with parameter λ, and elastic net regression with parameters λ and α, the training and the test groups were divided according to the external 5F-CV described above. Four sample training subsets were used to determine the parameter C (LSVR) or λ (LASSO and ridge regression) or a given parameter set (λ, α) (elastic net regression) to train the optimal prediction model

and the remaining subset was used to test. The above process was repeated five times so that each subset was the test set once, and the results of 5 internal CVs were obtained. For each internal 5F-CV iteration, a correlation coefficient value and MAE were generated for each parameter. Then the average value of the five inner loops of MAE and correlation coefficient was obtained. The mean correlation r values and the reciprocal of the mean MAE were denoted as the internal prediction accuracy. Finally, the optimal parameters were determined by holding the highest internal prediction performance.

5.2.5 Sampling and model fitting method

To study the impact of the training set size on the prediction effect of the regression models, different numbers of training subsets were extracted from the entire sample set. In theory, with the gradual increase of the training sample size, the prediction performance of the machine learning model will no longer be sensitive to the size of the sample size. At the same time, to reduce the amount of calculation, we increased from 30 to 450 samples with 30 as the increment, thereby generating 15 training sample sizes. Fifty random samplings were used for every sample size to achieve a stable result. Then the average value of these fifty prediction accuracy (i.e., correlation r) were calculated. Next, how the average accuracy of the prediction results was affected by the number of samples was the focus of this investigation.

5.3 Result

5.3.1 Prediction effect of Granger causality and effective connectivity

Firstly, prediction models with the EC and GC feature with five machine learning regression algorithms with all samples available in the NKI dataset were built to predict the verbal intelligence measure and provided an overall prediction effect comparison. Four hundred seventy-seven subjects with available fMRI and behavioural data were included in this investigation. The plots between the predicted score and the actual verbal intelligence score by different regression algorithms are illustrated in Fig. 5.2. Regardless of the algorithm, the EC features-based prediction performed slightly less efficiently than the GC feature-based prediction on the same behaviour with a mean correlation r value across these five EC models at r=0.17 and of GC at r=0.2. In the EC feature-based prediction models, the ridge regression model provided the highest

prediction accuracy at r=0.22. In contrast, in the GC based prediction models, the elastic net model achieved the highest prediction accuracy at r=0.23. Except for the ridge regression model, the correlation r values of five regression models using GC feature were higher than those of regression models using EC feature. In all the regression algorithms, the dispersion degrees of the actual and predicted scores points were different based on EC and GC features. In the prediction results of Lasso regression, the overlapping area was the smallest among the five algorithms (Fig. 5.2).

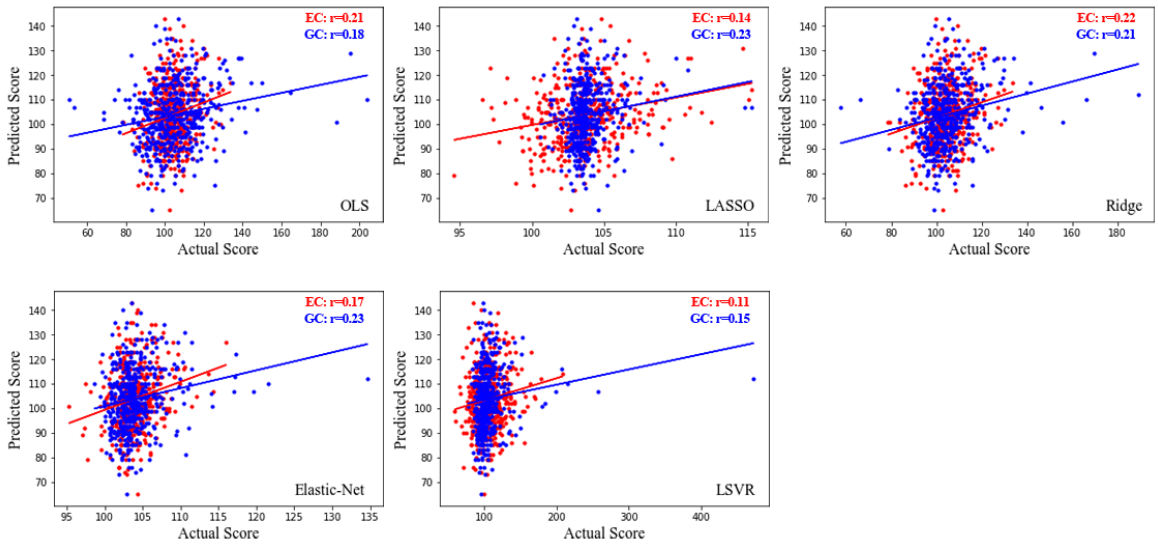

Figure 5.2. Scatter plots and model fitting curves between the actual and predicted scores with five regression algorithms including OLSR, LASSO, ridge, elastic net and LSVR with all 477 participants included.

5.3.2 Sample size effect of the algorithms

To further investigate the relationship between the prediction effect of each algorithm and sample size, similar prediction procedures with each algorithm with 15 different sample sizes were performed. The prediction effect was indicated by the mean value of the correlation r value between the predicted score and actual score over 50 random selection of sample groups of each sample size (Fig. 5.3). When modelling with the whole-brain EC features to predict verbal intelligence, LSVR regression yielded highest prediction accuracies for sample sizes smaller than 90 among these five models (Fig. 5.3A). The performance of the LSVR model began to be lower than the other four models when sample sizes were bigger than 90. In contrast, the OLSR, LASSO, ridge, and elastic net, provided better prediction accuracy results when the sample size

increased. The elastic net model provided the highest prediction accuracy among all these five prediction models when the sample size was larger than 150. Additionally, the improvement of the prediction accuracy of the OLSR model with the sample size increasing was not obvious comparing with the other three algorithms, i.e., LASSO, ridge and elastic net models. In the prediction models using the whole-brain GC features, the prediction accuracy of all the algorithms except for the LSVR, increased when the sample size increased. Similar to the EC feature-based model, the elastic net provided the highest accuracy when the sample size was bigger than 150. Regardless of the algorithm, when the sample size was smaller than 240, EC feature-based prediction models provided better prediction results than the GC feature-based prediction models. When the sample size achieved and beyond 240, the GC models provided better prediction accuracy than EC models. Besides, no matter EC or GC features were used, the performance of elastic net regression was better than the other four regression models when sample sizes were larger than 150.

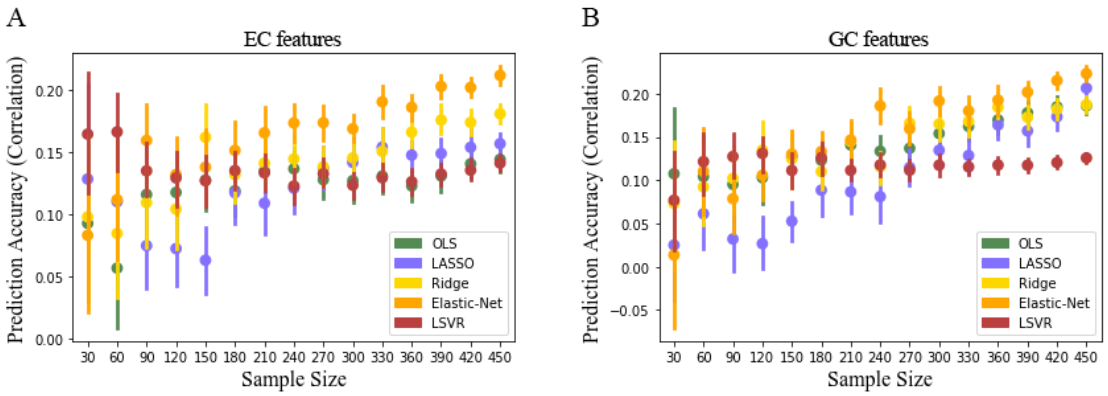

Figure 5.3. Prediction accuracy of EC and GC based prediction models with five regression algorithms. Different prediction algorithms were marked with different colours, and 15 sample sizes were selected from 30 to 450. With a certain sample size, 50 subsets were selected randomly within the whole dataset, and the mean prediction accuracy was shown in this figure to show a robust result. A) The plot of EC feature-based prediction accuracy (mean correlation) trend with 15 different sample sizes with 50 sample subsets of each sample size; B) The plot of GC feature-based prediction accuracy (mean correlation) trend with 15 different sample sizes with 50 sample subsets of each sample size.

5.3.3 Algorithm-to-algorithm similarity

To further investigate the similarity of the prediction results between these five algorithms, the correlation of the prediction scores with all participants between each pair of algorithms were calculated to form a similarity matrix between these algorithms

(Fig. 5.4). The algorithm-to-algorithm similarity results of five regression algorithms were calculated based on the predicted scores across all participants using both EC features (Fig. 5.4A) and GC features (Fig. 5.4B). The results of EC features-based algorithm-to-algorithm similarity was quite different from that of GC features-based. Regardless of the features used, LASSO regression showed very low similarity with all other algorithms except elastic net using EC features. This was consistent with its lower prediction accuracy compared to other algorithms. For the EC feature-based prediction models, taking the elastic net model as reference (which provided the highest prediction accuracy), the correlation between the elastic net model and the other four models, from high to low, was LASSO, LSVR, ridge regression, and OLSR. When using GC features, the similarity of OLSR and ridge regression was close to 1 (Fig. 5.4B), which indicated that the parameter λ in the ridge regression model was close to 0, which was equivalent to OLSR regression. Because of the larger number of GC features and relatively lower number of EC features, the problem of multicollinearity greatly influenced the predicted scores of ridge regression with GC features. Compared with the algorithm-to-algorithm similarity results using EC features, the similarity results of the elastic net and OLSR, elastic net and ridge, and ridge and OLSR raised in the GC feature models.

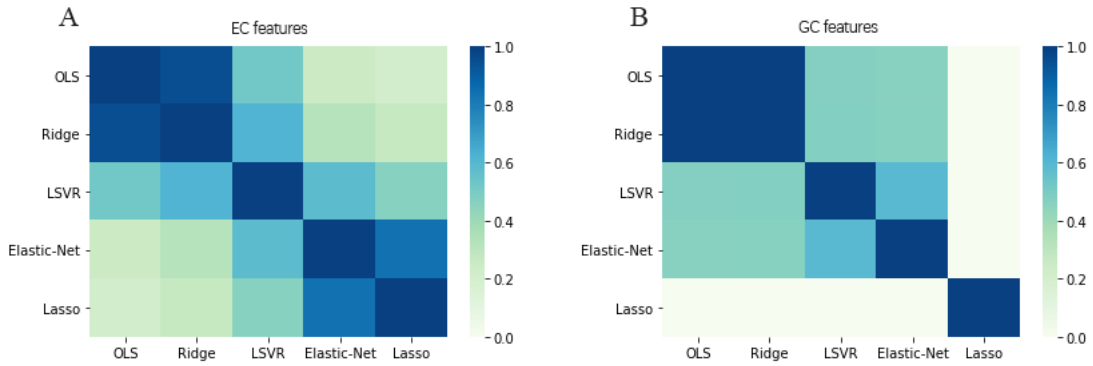

Figure 5.4. A) A 5 by 5 matrix representing the algorithm-to-algorithm similarity of EC features-based predicted scores. B) A 5 by 5 matrix representing the algorithm-to-algorithm similarity of GC features-based predicted scores. The darker the colour, the higher the correlation.

5.4 Discussion

Regardless of the algorithms, the GC feature-based models predicted better than the EC feature-based model in the prediction models with EC feature and GC feature with all participants included, with a mean correlation r value across these five EC models at r=0.17 and of GC at r=0.2. The best prediction model with the EC feature was with the ridge regression algorithm resulting in r=0.22. The best prediction model with GC feature was with the elastic net regression with r=0.23. The correlation r value between the predicted and the actual score is not very high, but acceptable according to existing connectome-based prediction literature (Cai et al., 2020; Itahashi et al., 2021; Ren et al., 2021). As we focus on comparing the efficiency of the Granger causality and effective connectivity on the whole brain, no feature selection was performed as in Chapter 4. Hence, this can be a reason of low accuracy. The five prediction models performed differently with EC and GC feature in the further analysis with sample size changes. However, the elastic net regression provided better prediction accuracy than the other four algorithms in both EC and GC based models.

For the OLSR prediction models, there were significant differences in the prediction performance based on EC and GC features. According to the previous introduction, no regularization terms were involved in the OLSR algorithm. Ridge regression and LSVR, on the other hand, used L2 norm regularization, LASSO used L1 norm regularization, while elastic net regression used both L1 and L2 norm regularization. In all linear regression algorithms, the lack of regularization in the OLSR model resulted in a high probability of inconsistent prediction results. According to the existing research, the regularization problem in the linear regression models with high dimensional features may depend on the related matrix. By using regularization, the negative impact of data noise on the model can be effectively overcome. In summary, the impact of regularization on the predictive performance of regression algorithms will depend on the ill-conditioned degree and noise level of a given problem. Therefore, when the feature dimension is high, and the sample size is small, the prediction performance of the model will be very unstable, so the OLSR should be used with extreme caution.

As shown in Fig. 5.3, the prediction models of the LASSO regression, ridge regression, and elastic net regression with both the EC and GC features had stable prediction accuracy than the OLSR. Additionally, the prediction accuracy of these three

algorithms raised with the increase of sample size generally. LASSO regression, ridge regression, and elastic net regression are all improved versions for the problems of OLSR. In simple terms, OLSR fits the parameters to minimize the squared loss function. Besides, LASSO regression is based on the square loss function plus the L1-norm penalty term to fit the parameters, and ridge regression optimizes based on OLSR based on the application of the L2-norm penalty term. Elastic net regression adopted both L1 norm and L2 norm for regularization. The LASSO objective function is convex and easy to calculate, and the coefficient of the unrelated variable is 0, and the robustness is good. Ridge regression only has a display solution, and the calculation is simple; Elastic net and Lasso regression can compress small coefficients to 0 and selectively compress one of the collinear variables. Notably, because of the larger number of GC features and relatively lower number of EC features, the problem of multicollinearity greatly influenced the predicted scores of ridge regression with GC features, which resulted in a relatively lower accuracy with EC features than the GC feature and low stability especially with small sample sizes ($n<210$, Fig. 5.3A). To further investigate the similarity of the prediction results between these five algorithms, the correlation of the prediction scores with all participants between each pair of algorithms were calculated to form a five-by-five similarity matrix (Fig. 5.4). Regardless of the features used, LASSO regression showed very low similarity with all other algorithms except elastic net using EC features. This was consistent with its lower prediction accuracy compared to other algorithms.

In conclusion, five commonly used prediction algorithms, including OLSR, ridge, LASSO, elastic net and LSVR, were performed to explore the efficiency of the EC and GC feature of the brain. Generally, the GC feature provided slightly better prediction accuracy than the EC feature, indicating that the GC feature model the directional connectivity of the brain better than the EC based on this study. From the prediction accuracy point of view, regardless of the algorithms used, the prediction accuracy with both EC and GC features were not high ($r=0.23$ in this study vs $r=0.34$ in our previous study on sensation-seeking with FCs). This can be due to the high dimensional features but the small sample size available. Additionally, by comparing the efficiency of these five commonly used prediction models, the elastic net regression provided better prediction accuracy than the other four algorithms in both EC and GC based models. We propose that the elastic net fits better with high dimensional feature data and handle multicollinearity better than other algorithms. The OLSR, which does not involve any

regularization terms in this method, should not be used in high dimensional data with a small sample size, which will provide a very unstable result. In addition, the multicollinearity problem greatly influences the predicted result of ridge regression worse than the other algorithms. The elastic net, which combines both L1 norm and L2 norm for regularization, provided better prediction results in this study and fits better for neuroimage data based on this study and our previous study on sensation-seeking with FC features in Chapter 4.

Further investigations with other independent datasets and predictions on different behaviours can be performed to validate the finding on examining the efficiency of Granger causality and effective connectivity on modelling the whole brain directional connectivity network. In addition, in terms of the prediction accuracy, further investigations can be developed on a larger dataset or try feature selections in advance to narrow the feature dimension down to achieve higher prediction accuracy. As in this project, the aim was to compare the whole brain EC and GC differences, no feature selection was applied in advance.

Chapter 6

Risk-taking in humans and the medial orbitofrontal cortex

6.1 Introduction

Risk-taking is a fundamental difference between different people. Here we analysed the basis of this difference and show that it relates to how strongly the medial orbitofrontal cortex relates to other brain systems. Given that the medial orbitofrontal cortex is involved in reward, an implication is that it is differences in the reward value of potential goals that is a key factor in whether individuals show risky behaviours (rather than for example sensitivity to punishment). The findings provide new insights into human behaviour that have potential applications in many walks of life.

Risk-taking is used to describe the tendency of taking certain risks when people were making decisions or aiming for higher targets, which is highly associated with sensation-seeking and impulsivity (Green and Myerson, 2013). Besides, risk-taking was reported to be associated with drug use, alcohol use, and gambling problems. Significant associations between the frequencies of drug use, a large number of drinking problems, and sexual risky behaviours were found in different studies (Bjork and Pardini, 2015; Braams et al., 2016). In a review of current neural and biochemical findings of impulsivity by Dalley and Robbins (2017), a fractionation of impulsive behaviour was proposed, which suggested that impulsivity may have many subtypes, and these subtypes depend on distinct neuron systems. Three subtypes were described in this paper, including: 'waiting impulsivity', 'stopping impulsivity', and 'risky impulsivity'. Risky impulsivity is about risky decision making and is associated with sensation-seeking (Green and Myerson, 2013). The neural mechanisms underlying risky impulsivity include the lateral prefrontal cortex involving a preference for ambiguity with unknown probabilities of outcomes and the posterior parietal cortex involving the tendency for risk with known probabilities (Huettel et al., 2006). Individual differences in risk-taking behaviours have been linked to several brain areas, as reported in different studies. For example, the ventral striatum was positively correlated with a higher tendency in pursuing rewards and a higher likelihood of seeking fun (Braams et al., 2016). In the study of Blankenstein et al. (2017), greater risk preferences were found related to higher activation of the ventral medial prefrontal areas.

Furthermore, the tendency to risky impulsivity is often associated with sensation-seeking (MacPherson et al., 2010; Ruedl et al., 2012). Sensation-seeking was found positively correlated with the medial OFC areas in our previous study with the NKI dataset (N=414) (Wan et al., 2020). This study suggested that sensation-seeking, which is an aspect of impulsivity, may be driven by reward involving the medial OFC areas. Besides, a modest association between risk-taking and sensation-seeking found in the sensation-seeking study indicates that the risk-taking may be led by the reward associated with sensation-seeking. Association between risk-taking and substance use, especially alcohol and drug use, has been reported in many studies, although different genetics and neuro systems were reported relevant in different studies. In one of our previous studies, increased FCs involving the medial OFC regions in alcohol drinkers were found correlated with increased impulsiveness (Cheng et al., 2019b). This supports the hypothesis that one type of impulsivity is led by reward, which is associated with substance use. A more detailed literature review on the current risk-taking studies is in Chapter 2.

The aim of the present study is to investigate how brain functional connectivity is related to risk-taking using a very large neuroimaging sample of 18,740 participants from the UK Biobank. Functional connectivity is measured by the correlation between the fMRI BOLD signal between each pair of brain areas, with a high functional connectivity providing an indication of strong interactions between areas. A feature of the investigation is that risk-taking was measured by self-report from the human participants, whereas performance in tasks thought to be related to risky behaviour need to be used in animal studies. The measure of risky behaviour used here was shown to be valid, in those other measures such as whether the individual is a worrier were (negatively) correlated with it, and alcohol and drug use were positively correlated with the report measure of risky behaviour. The hypotheses investigated were whether some neural systems had their functional connectivity significantly related to self-reported human risk-taking; whether the reward-related medial orbitofrontal cortex had high functional connectivity in risk-takers; whether the punishment/non-reward lateral orbitofrontal cortex has low functional connectivity in risk-takers; and whether the report measure of risk-taking was related to substance use and other behavioural measures such as worrier status.

6.2 Method

6.2.1 Dataset and resting-state fMRI data

The UK Biobank is a large-scale biomedical database and research resource dedicated to improving the prevention, diagnosis, and treatment of various diseases. It follows the health status, medical history, and well-being of 500,000 volunteers aged between 37 and 73 years and recruits health information to approved researchers from academia and industry. These participants underwent cognitive performance, mental health and physical assessments, provided detailed information of their backgrounds, living environment, and general behavioural pattern, and agreed to have their health followed longitudinally. 19,528 participants with available resting-state fMRI data after quality control are mainly investigated in this study, with 10323 females and 9205 males (ageing from 45 to 79, mean 61.80).

6.2.2 Behaviour measures

The risk-taking measure used (UK Biobank data field ID 2040) was the response to the question: "Would you describe yourself as someone who takes risks?". An answer of 'Yes' was scored 1, and of 'No' 0. Participants who reported 'Do not know' or 'Prefer not to answer' were excluded, leaving 29,956 participants with risk-taking data from release 1 of the UK Biobank.

A worrier/anxious feelings measure (UK Biobank data field ID 1980) also used was the response to the question: "Are you a worrier?". Scoring was as for the risk-taking measure, and provided 30,237 participants, 15,134 of whom provided a response of 'Yes'.

6.2.3 A t-test on functional connectivity

Functional connectivity is computed by performing a Pearson correlation of the BOLD signal averaged across time between each pair of voxels or brain areas (Biswal et al., 1995). In this study, the brain regions were used and defined by AAL2 (Rolls et al., 2015). This AAL2 atlas includes 94 brain regions spanning the whole cerebrum, excluding the cerebellum. The time series of each pair of brain areas were extracted first. Then, the Pearson correlation between these two time courses was calculated to measure functional connectivity for each participant. To improve the normality of the correlation coefficients, the Fisher's r-to-z transformation was performed, which results

in a 94 by 94 symmetric matrix that each value represents one link between every pair of brain regions.

Two-sample two-tailed t-tests were used to test whether risk-taking is associated with functional connectivity in this investigation. The confounding effects of age, sex, education, head motion (mean framewise displacements), and site information were removed in this analysis. 18,740 participants who have both available resting-state fMRI and risk-taking data were included in the t-test, including 4891 risk-taking people and 13849 non-risk-taking people. Example MATLAB code for the t-test analysis is attached in Appendix-5.

6.2.4 Longitudinal analysis

In the UK Biobank dataset, the behaviour measures, including risk-taking and worrier/anxious feeling, were tested more than once for each participant. To be specific, the measures were tested at baseline time when the participants were first circulated in this UK Biobank project, and then another test was taken when the participants returned to have an imaging scanning. This follow-up study enables a longitudinal analysis for behaviour measures to investigate the changes of certain behaviour and longitudinal associations of this behaviour with other behaviours. In this analysis, the longitudinal association of risk-taking with other measures, including worrier/anxious and other addiction measures, were explored by performing a two-wave cross-lagged panel model (CLPM). Covariances including age, sex, and education were regressed out before this analysis. The CLPM were implemented with the Lavaan package in R. Parameters in this model were estimated by maximum likelihood estimation, and the standardized beta coefficients and standard errors were reported in this analysis.

6.3 Results

6.3.1 Functional connectivity changes for the risk-taking vs non-risk-taking groups

778 functional connectivities were found significantly different between the risk-taking and non-risk-taking groups ($p<0.001$, FDR corrected). The brain regions, including the VMPFC, the rectus, the medial OFC, the postcentral, the parahippocampal, the middle temporal pole and the superior temporal pole, were significantly different in the risk-taking group (Fig. 6.1). The full matrix of the t values

of functional connectivities is shown in Fig. 6.2A. The lower triangle of the matrix shows the t value of all FCs of the risk-taking group vs the non-risk-taking group; the upper triangle of the matrix shows which FCs were significantly different between these two groups (p<0.001 uncorrected). Most of these significant different links were higher in the risk-taking group compared to the non-risk-taking group, while only 42 links were lower in the risk-taking group. Links involving the medial orbitofrontal cortex areas (the rectus, the medial OFC, and the posterior OFC) and the VMPFC were higher in the risk-taking the non-risk-taking group. Besides, links involving the paraHippocampal and the temporal lobe (the temporal pole: superior and middle temporal gyrus) were higher in the risk-taking group than in the non-risk-taking group. A square of higher functional connectivity links within the temporal lobe is shown in Fig. 6.2A.

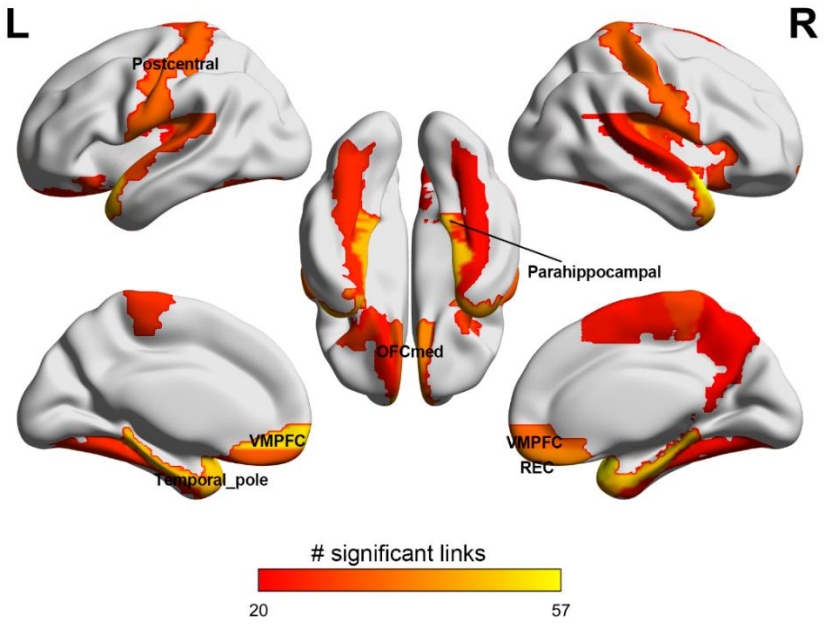

Figure 6.1. Functional connectivity links were significantly higher in the risk-taking group (p<0.001, FDR corrected). The number of links higher involving different brain regions is shown in this figure, and only the brain regions which have more than 20 links were significant are shown.

6.3.2 Worrier/anxious feelings, drug use and alcohol use with risk-taking behaviour

The worrier/anxious feeling was associated with risk-taking with r=-0.122 (p=7.62e-98) at the behavioural level. Besides, 712 functional connectivities were

significantly different between the worrier/anxious feelings and the non-worrier/anxious feeling groups ($p<0.01$, FDR corrected) (shown in Fig. 6.2B). Links involving the VMPFC, the rectus, the posterior OFC, the cingulate cortex, the hippocampus, and the temporal lobe (the temporal pole: superior and middle temporal gyrus) were significantly lower in the worrier/anxious feelings group. In summary, the functional connectivity links involving the VMPFC, the rectus, the medial OFC areas, the hippocampus/parahippocampal, and the temporal lobe (the temporal pole: superior and middle temporal gyrus) were significantly negatively associated with the worrier/anxious feelings group and significantly positively associated with the risk-taking group. In addition, for the 778 links significantly associated with risk-taking (shown in Fig. 6.2), 767 of these links were positively associated with risk-taking and 762 of which were negatively associated worrier/anxious feelings; 11 of these links were negatively associated with risk-taking and all of that were positively associated worrier/anxious feelings.

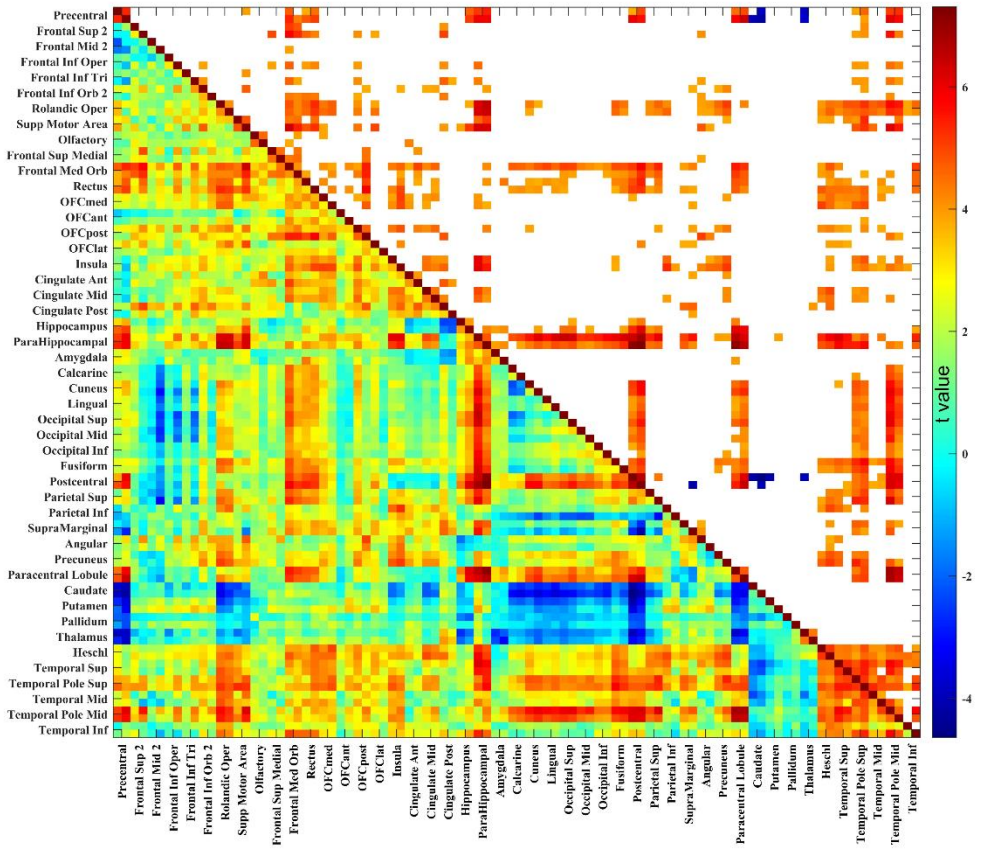

Figure 6.2. A) The difference in functional connectivity in the risk-taking group. The matrix of t values for the risk-taking group. The lower triangle matrix shows the functional

connectivity across all links of the risk-taking group relative to the non-risk-taking group. The upper triangle matrix shows significant links with p<0.001 FDR corrected.

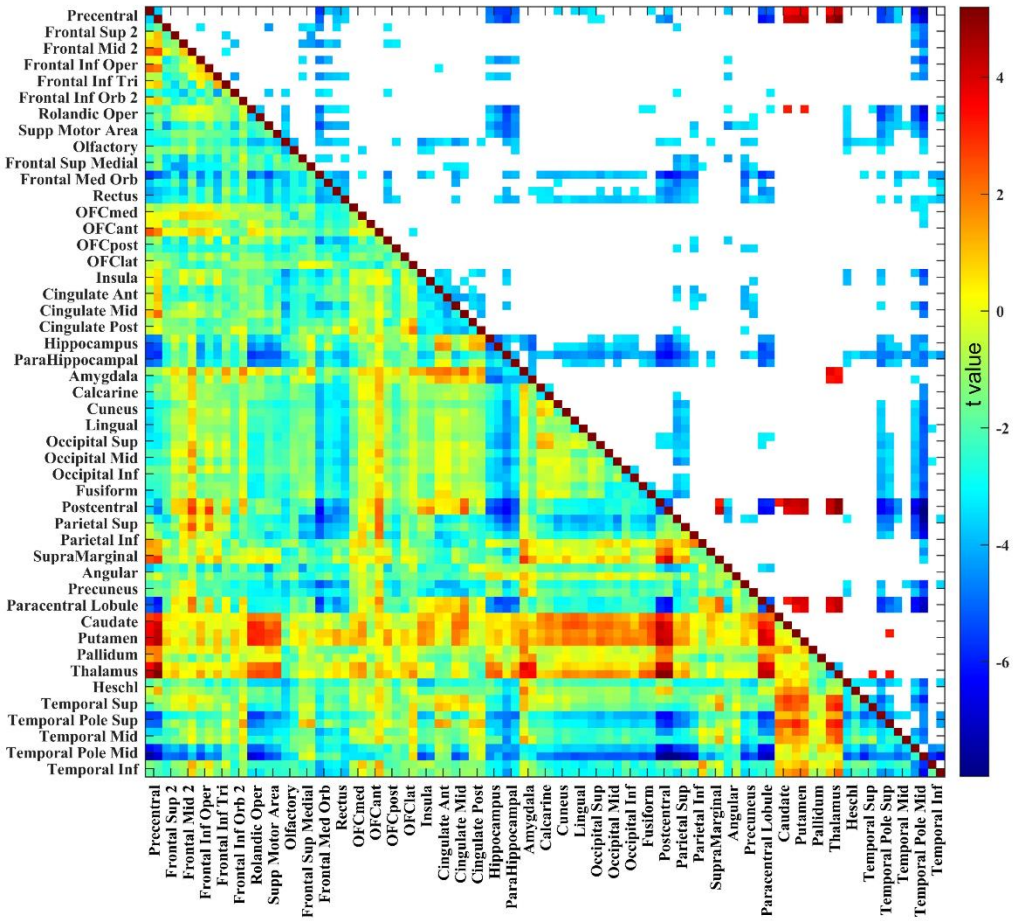

B) The difference in functional connectivity in the worrier/anxious feelings group. The matrix of t values for the worrier/anxious feelings group. The lower triangle matrix shows the functional connectivity across all links of the worrier/anxious feelings group relative to the non-worrier/anxious feelings group. The upper triangle matrix shows significant links with p<0.01 FDR corrected.

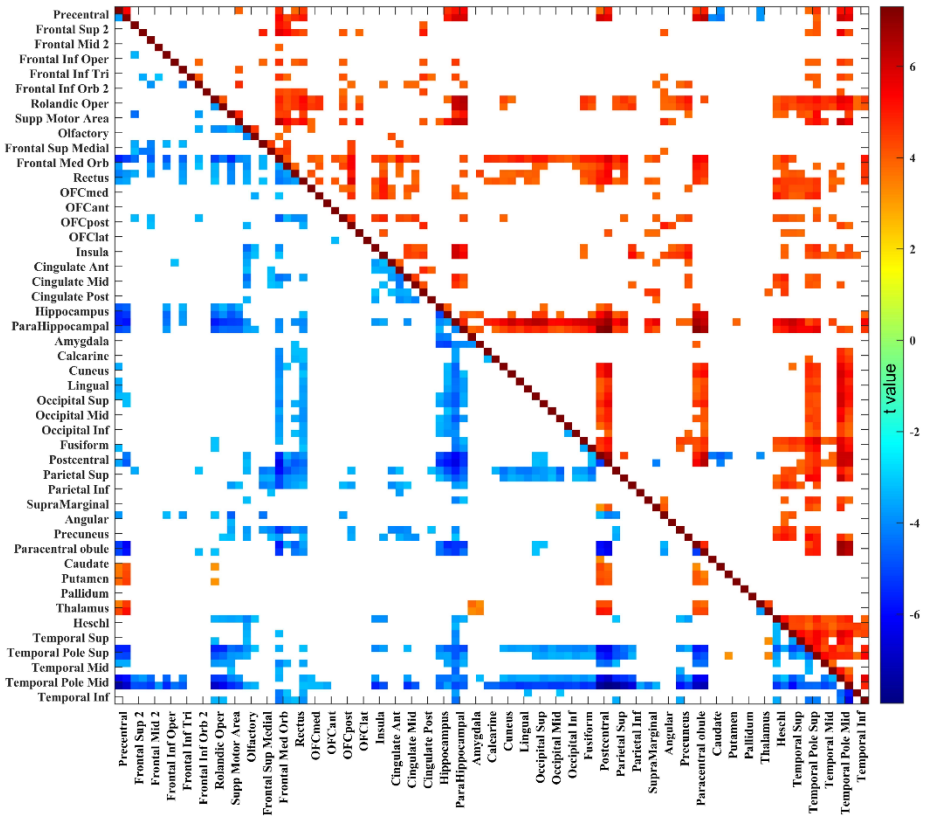

C) Only the significantly different functional connectivity links in the risk-taking group (as in A)) (upper triangle) and in the worrier/anxious feelings group (as in B))(lower triangle) are shown together as a comparison.

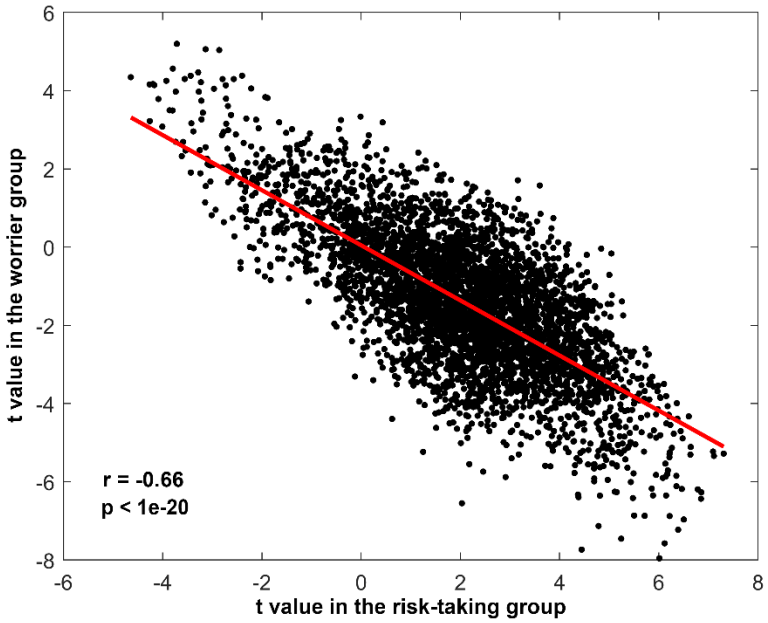

D) Scatter plots and fitting curves between the t values (differences of functional connectivity) in the risk-taking group and the worrier/anxious feelings group.

In the longitudinal analysis performed by the Lavaan package, the associations of risk-taking with worrier/anxious feelings at baseline and imaging visit time were investigated (result as shown in Fig. 6.3). Risk-taking at the baseline time was associated with the imaging visit worrier/anxious scores in the longitudinal analysis (β=-0.046, p<0.001). The baseline worrier/anxious score was associated with the imaging visit risk-taking score with β=-0.035 (p<0.001). In addition to the association between the risk-taking and worrier/anxious measures at the same measuring time, the former measures of risk-taking and the successive worrier/anxious measure were associated significantly, and vice versa.

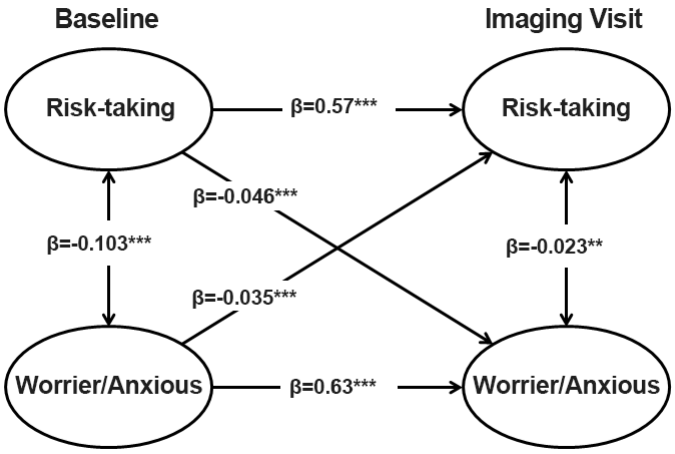

Figure 6.3. Longitudinal association of risk-taking with worrier/anxious. Covariances including age, sex, and education were regressed out. The standardized beta coefficients are shown in the figure (* p<0.01, ** p<0.005, ***p<0.001).

Besides, the risk-taking was associated with cannabis use (r=0.116, p=8.763e-65), with the frequency of consuming large amount alcohol (r=0.096, p=1.175e-41), and with the amount of alcohol drunk (r=0.078, p=5.140e-28) (Table 6.1).

	Drinking Amount		Heavy Drink Frequency		Cannabis Use	
Risk-taking	r value	p value	r value	p value	r value	p value
	0.078	5.14E-28	0.098	1.18E-41	0.117	5.99E-66
Worrier	r value	p value	r value	p value	r value	p value
	-0.039	5.15E-08	-0.053	4.96E-14	-0.026	1.53E-04

Table 6.1. Behaviour level association between risk-taking, worrier/anxious feelings, drug use, and alcohol use.

6.3.3 Sensation-seeking, impulsiveness, and validation with independent data groups

Validations with the risk-taking and impulsiveness in other datasets were performed to test whether the findings are consistent. With the same brain atlas, the correlation between the risk-taking and the functional connectivities with all participants from the NKI dataset was performed. Then, the correlation between the correlation matrix of risk-taking with FCs in the UK Biobank dataset and the correlation matrix of risk-taking with FCs in the NKI dataset was 0.12 ($p=3.3e-15$), as shown in Fig. 6.4A. Impulsiveness measures are available in the HCP dataset, a set of delay discounting trials with different amounts of money and length, including 12 different trail scores and two summary scores. The same analysis with the risk-taking in the NKI dataset was performed. The correlation between the correlation matrix of risk-taking with FCs in the UK Biobank dataset and the correlation matrix of the delay discounting score with FCs in the HCP dataset was -0.38 ($p<1e-20$), as shown in Fig 6.4B.

Besides, validation was also performed in the same dataset with the same risk-taking measure. The functional connectivity changes for the risk-taking and non-risk-taking groups were conducted with newly released data in the UK biobank (with 5699 participants with available risk-taking scores and fMRI data). The correlation between the correlation matrix of risk-taking with FCs in the UK Biobank dataset and the correlation matrix of risk-taking with FCs in the newly released data in the UK biobank was 0.67 ($p<1e-20$) shown in Fig 6.4C, providing cross-validation in the form of support from independent participants. (It was confirmed that the correlation measures utilized were not significant with measures from the UK Biobank that are unlikely to be related to risk-taking. These included total food weight consumed on the previous day (field ID 100001) for which $r=-0.00043$ $p=0.98$; and body mass index (field ID 21001) for which $r=-0.024$ $p=0.11$.)

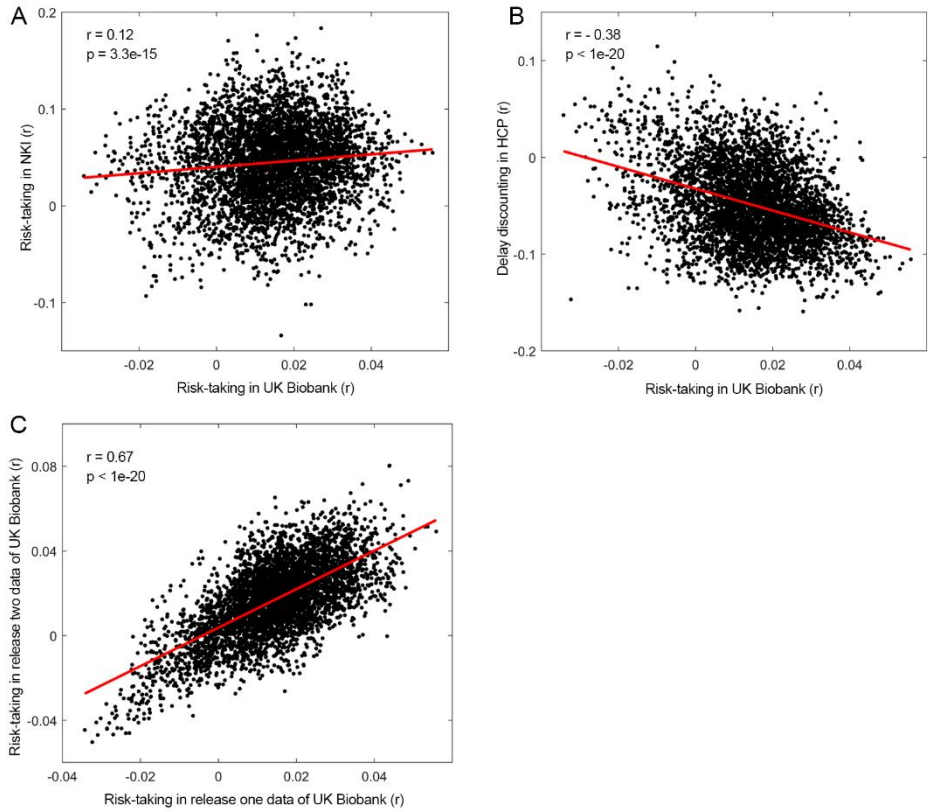

Figure 6.4. Validations. A) The correlation between the correlation matrix of risk-taking with FCs in the UK Biobank dataset and the correlation matrix of risk-taking with FCs in the NKI dataset was 0.12 (p=3.3e-15). B) The correlation between the correlation matrix of risk-taking with FCs in the UK Biobank dataset and the correlation matrix of the delay discounting score with FCs in the HCP dataset was -0.38 (p<1e-20). C) The correlation between the correlation matrix of risk-taking with FCs in the UK Biobank dataset and the correlation matrix of the risk-taking with FCs in the newly released data in the UK biobank was 0.67 (p<1e-20).

6.4 Discussion

In the t-test of functional connectivities between the risk-taking and non-risk-taking groups, links involving the medial OFC areas, the rectus, and the VMPFC were higher in the risk-taking group than in the non-risk-taking group. Risk-taking is an aspect of impulsive behaviour. The medial OFC and the VMPFC are in function of reward. Therefore, the positive correlation between risk-taking and the links with the medial OFC and the VMPFC indicates the risk-taking behaviour can be a reward-driven impulsive behaviour. Enhanced functional connectivity involving the medial orbitofrontal regions was also associated with increased impulsivity in alcoholics, according to Cheng et al. (2019a), implying that increased reward sensitivity could potentially lead to high impulsivity. In a previous study on sensation-seeking (Chapter

4), we found positive correlations between sensation-seeking and the FCs between the medial OFC and the ACC. Besides, a high association between sensation-seeking and risk-taking was found in the sensation-seeking study in the NKI dataset with r=0.49 (p=3.92e-26). This supports the argument that enhanced reward sensitivity may lead to high impulsivity. A theory that is related to the present analysis, also consistent with previous studies, is that some kinds of impulsiveness might be associated with increased functional connectivity with the reward system, including the medial orbitofrontal cortex and the VMPFC. In contrast, conventional impulsiveness was believed to be involving the reduced sensitivity to the non-reward system, which includes the lateral orbitofrontal cortex.

Links involving the paraHippocampal gyrus were higher in the risk-taking group than in the non-risk-taking group. The hippocampus and paraHippocampal areas are involved in episodic memory, which might indicate that the risk-taking behaviour can be associated with the previous memories and experiences (Rolls, 2016; Rolls, 2018a). As shown in a study on hypertension with the UK Biobank dataset, FC links involving the hippocampus and paraHippocampal areas were correlated with blood pressure (Feng et al., 2020). Hence, the same t-test of FCs between the risk-taking and non-risk-taking groups was also performed with additional co-variances, the diastolic and systolic blood pressures to evaluate whether the paraHippocampal showed in this study is associated with blood pressure. The resulting links and regions were similar to those without blood pressures regressed out but less significant. The FC links with the paraHippocampal were still significantly higher in the risk-taking group. This provides evidence that the FCs involving the paraHippocampal areas were not related to blood pressures. Hence, the blood pressure was not regressed out in this analysis. Links involving the temporal lobe (the temporal pole: superior and middle temporal gyrus) were higher in the risk-taking group than in the non-risk-taking group. The temporal lobe provides input signals to the frontal lobe as the association cortex, and this can cause higher FCs involving the paraHippocampal.

The worrier/anxious feelings measure is correlated with risk-taking with r=-0.122 (p<1e-20) in the behaviour level. In relation to the brain, the FC links involving the medial OFC areas were positively correlated with risk-taking and negatively correlated with worrier/anxious feelings (Fig. 6.2C). An interesting implication of these findings is that the type of risk-taking considered here was related to increased FCs of reward-related medial OFC areas. Furthermore, these FCs were also associated with reduced

feelings of anxiety. Thus, we suggest that the same functional connectivities involving the medial OFC areas that may promote risk-taking because of increased reward are also involved in the reduced anxiety associated with such risk-taking behaviours. Besides, drug use and alcohol use were positively correlated with risk-taking, as consistent with our previous study on impulsiveness in the NKI dataset. Besides, the FC links involving the medial orbitofrontal cortex, which were significantly correlated with the impulsiveness measure, were found modestly associated with drug and alcohol use. This may indicate the association between risk-taking and drug/alcohol use is related to the medial orbitofrontal cortex of the brain.

In conclusion, the medial orbitofrontal cortex, which is in the function of the reward system, was found related to risk-taking, which is associated with impulsivity. This proves to support the hypothesis that one type of reward-driven impulsivity is related to the medial orbitofrontal cortex of the brain. Besides, the medial orbitofrontal cortex was found negatively correlated with anxious feelings, which is the opposite direction with risk-taking. In the behaviour level, drug/alcohol use was positively correlated with risk-taking, which is consistent with our previous found with another dataset. This suggests the association between risk-taking and drug/alcohol use is related to the medial orbitofrontal cortex of the brain.

Chapter 7

Brain Functional Connectivities that Mediate the Association between Traumatic Events in Childhood and Mental Health in Later Life

7.1 Introduction

Childhood traumatic events are an established risk factor for psychopathology. Children who experience sexual, physical or emotional abuse, or physical and emotional neglect may feel overwhelmed, and this can be associated with lasting mental and physical differences. Despite the century-old debate on the origins of this association, the association and possible causality of an individual's childhood traumatic events and psychopathology, and how brain differences related to that, is still an important topic and needs more findings with large sample sizes (Susser and Widom, 2012; Teicher and Samson, 2016; Baldwin et al., 2019).

Meta-analyses indicated that childhood traumatic events were correlated with a twenty to thirty percentage increase in the risk of psychosis (van Dam et al., 2012; Varese et al., 2012; Trotta et al., 2015). Also, such childhood traumatic events were found associated with the development of mental disorders including depression (McLaughlin et al., 2017; Copeland et al., 2018), and physical ill-health including non-communicable diseases (Basu et al., 2017; Suglia et al., 2018). Particularly on individuals who had experiences of exposing to stressful events and early-life traumas, depression was commonly reported (Kessler, 1997; Green et al., 2010; McLaughlin et al., 2010; Nanni et al., 2012; Rolls, 2018b). In addition, reported trauma was robustly associated with a range of adverse life differences including depression (Kessler et al., 1997; Collishaw et al., 2007; Baldwin et al., 2019). The relationship between depression and reported trauma is unclear and complicated. The reported trauma was associated with both subsequent depression and prior depression (Kendler et al., 1999). However, most of the people who had exposure to traumatic events do not report depression (Kessler et al., 1997; Collishaw et al., 2007; Baldwin et al., 2019). In addition, there is evidence that childhood traumatic events are associated with poorer cognitive performance in adults (Petkus et al., 2018; Velikonja et al., 2021).

In addition to behaviour-level association analyses, there is converging evidence from substantial studies linking childhood traumatic events to brain structure and

function (Teicher and Samson, 2016). A large amount of research supported the enduring associations between childhood maltreatment and adversity and stress-susceptible brain circuitry (Shonkoff et al., 2012; Marusak et al., 2016). In a study with a large dataset, participants with childhood emotional abuse experiences ('felt hated by family member as a child') were found to have smaller ventral striatum volumes compared to those who did not have traumatic events in their childhood (Gheorghe et al., 2021). Reviews on the neuroimaging literature suggested that a history of childhood traumatic events was associated with volumes and/or function alterations of (midline) prefrontal cortex and with limbic regions and related functional connectivities (Whittle et al., 2009; Morey et al., 2016; Bolsinger et al., 2018). Furthermore, this idea was supported by a longitudinal behavioural study which revealed that smaller prefrontal cortex volume associated with childhood traumatic events was linked to later poor cognitive function (Hanson et al., 2012) and poorer illness courses (Frodl et al., 2010). In the studies of McLaughlin et al. (2014); Sheridan and McLaughlin (2014), traumatic events were found to have strong associations with neural systems which were related to emotion regulation, salience processing, and threat detection and learning. These neural systems included the fronto-amygdala system (Tottenham, 2015), which is also referred as the limbic (Yeo et al., 2011), comprising the medial prefrontal cortex, the amygdala, and the hippocampus.

Nonetheless, the exact pathways involved in the association between childhood traumatic events and brain development and behaviour have yet to be firmly delineated. Furthermore, significant variations in effect sizes were observed in different studies (Gibson et al., 2016). These variations might be explained by methodological difficulties, including small sample size, cross-site data, differences in how childhood traumatic events and mental health symptoms were measured, and the level of confounding adjustment. Therefore, it is unclear if the relationship between childhood traumatic events and psychotic experiences is causal and reliable and how the underlying biological pathways are related.

To understand the underlying neural pathways more comprehensively, large population samples are likely to be important. Most of the previous studies have focused on the underlying brain structure associated with childhood trauma, not on brain functioning. In addition, the studies described investigated the relationship between childhood trauma and the mental health problems of only adolescent or young

adults, not the long-lasting associations between childhood trauma and people in more mature adulthood to assess the persistence of the associations.

The study described here has three main objectives. First, we aimed to assess the association between traumatic events in childhood and a wide range of mental health problems and cognitive performance in later life using large scale data from 19,535 participants from the UK Biobank dataset. Second, we aimed to examine the association between childhood traumatic events and brain functional connectivity and to test whether functional connectivity mediates the association between childhood traumatic events and mental health problems in later adulthood. Third, we aimed to validate the results using an independent dataset with 17,747 participants.

7.2 Method

7.2.1 Participants and data preprocessing

The UK Biobank is a health resource aiming to improve the prevention, diagnosis and treatment of a wide range of illnesses (Miller et al., 2016; Alfaro-Almagro et al., 2018). It follows the health and well-being of 500,000 volunteer participants and provides health information to approved researchers from academia and industry. The participants have assessments of cognitive function, mental health problems and physical health, provide detailed information about their backgrounds and lifestyles, and agree to have their health followed longitudinally. The UK Biobank received ethical approval from the research ethics committee (REC reference 11/NW/0382). The current investigation was performed under UK Biobank application number 1954. The demographic characteristics of individuals who were included in this investigation are summarized in Table 7.1.

A standard Siemens Skyra 3T running VD13A SP4 with a standard Siemens 32-channel RF receive head coil was used to acquire the multi-modal imaging. 22,331 participants with available resting-state functional MRI data were collected and processed in the UK Biobank dataset. The details of the image acquisition can be found in the form of a protocol on the UK Biobank website (http://biobank.ctsu.ox.ac.uk/crystal/refer.cgi?id=2367).

Characteristics	**No. (%)**
Age, mean (SD), y	62.77 (7.73)
Female	86,523 (56.31%)
BMI	26.77(4.55)
Townsend deprivation index, mean (SD), points	-1.71 (2.83)
Alcohol Drinker Status	
Prefer not to answer	53 (0.03%)
Never	4,335 (2.82%)
Previous	4,124 (2.69%)
Current	145,058 (94.46%)
Smoking Status	
Never	88,605 (57.70%)
Previous	53,905 (35.10%)
Current	11,061 (7.20%)
Education Qualifications	
College or University degree	69,753 (45.69%)
A levels/AS levels or equivalent	20,648 (13.52%)
O levels/GCSEs or equivalent	30,268(19.82%)
CSEs or equivalent	5,640 (3.69%)
NVQ or HND or HNC or equivalent	7,715 (5.05%)
Other professional qualifications, e.g., nursing, teaching	7,735 (5.07%)
None of the above	10,921 (7.15%)

Table 7.1. Demographic Characteristics of the 153,642 UK Biobank Participants.

The UK Biobank performed all the quality control and pre-processing procedures using the FSL (FMRIB Software Library), and the details of the pre-processing can be referred to on the UK Biobank website (http://biobank.ctsu.ox.ac.uk/crystal/refer.cgi?id=1977) and also as described in Miller et al. (2016). Correction for spatial and gradient distortions, as well as head motion, intensity normalization and bias field removal, registration to the T1 weighted structural image, transformation to 2 mm Montreal Neurological Institute (MNI) space, and the FIX artefact removal procedure were all part of the data pre-processing (Smith et al., 2013; Navarro Schroder et al., 2015). Finally, by using ICA+FIX processing

(Independent Component Analysis followed by FMRIB's ICA-based X-noiseifier), the head motion parameters were regressed out, and structural artefacts were removed (Griffanti et al., 2014; Salimi-Khorshidi et al., 2014)). The FMRIB (Oxford University Centre for Functional MRI of the Brain) data preprocessing pipeline used here has been frequently used in resting-state fMRI investigations (Navarro Schroder et al., 2015; Smith et al., 2015; Colclough et al., 2017; Vidaurre et al., 2018). 19,535 participants were retained for the investigation on neuroimaging with available behavioural data, after the imaging quality control procedure.

7.2.2 Construction of the whole-brain functional network

After pre-processing, the whole brain was parcellated into 228 regions of interest using the Shen atlas (Shen et al., 2013). The Shen atlas was applied in this study for two main reasons. First, the Shen atlas was developed based on functional connectivity, which can help the explanations with functional connectivity results. This has been validated in different resting-state fMRI investigations (Finn et al., 2015; Rosenberg et al., 2016). Second, the Shen atlas was more helpful in this study because it parcels the brain into more areas than the AAL2 atlas (Rolls et al., 2015).

We presented the mapping of Shen atlas areas to AAL2 atlas areas in Appendix-3 and adopted the AAL2 area names when referring to particular brain regions and the related functional connectivities because the Shen atlas areas do not have region names (Rolls et al., 2015). To quantify functional connectivity between pairs of brain regions, for each individual, the Pearson correlation was calculated from the time series for that pair of brain regions. Then the Fisher's z transformation was performed to increase the normality of these correlations, yielding a 228 by 228 symmetric matrix which indicates the connections between each pair of brain areas.

7.2.3 Childhood traumatic event score

The childhood traumatic event score was calculated based on five questions related to childhood traumatic events available in the UK Biobank dataset. These five questions are as follows: (field ID question)

20487 Felt hated by family member as a child

20488 Physically abused by family as a child

20489 Felt loved as a child

20490 Sexually molested as a child

20491 Someone to take to doctor when needed as a child

The answers to these five questions are encoded the same way: score from 0 to 4 representing the answer from ‘never true’ to ‘very often true’ (data-coding 532 in the UK Biobank data field) in the UK Biobank dataset, hence no normalization was needed. The childhood traumatic events score describes the severity of the traumatic events of each participant as a child. Specifically, a correlation between each pair of these five measures was performed to check whether these questions measure traumatic events in the same direction (i.e., whether a higher score in the questions was related to a higher traumatic score). The scores of questions 20489 and question 20491 were reversed, and then the childhood traumatic event score was calculated as a sum of the scores of these questions. The sum score based on 5 point responses (0:4) across all childhood traumatic questions was used in this investigation instead of the number of adverse childhood events, which provides a wide range of distribution of the childhood trauma score from 0 to 20 for further analyses (Gheorghe et al., 2021).

7.2.4 Association of childhood traumatic events with mental health problems and cognitive performance

First, the correlations between the childhood traumatic events scores and the mental health problems later in life . To be specific, a partial correlation was performed between mental health problems scores and the childhood traumatic events scores with age, gender, body mass index, education, Townsend index, alcohol use, and tobacco use regressed out. The Townsend deprivation index is named after Prof Peter Townsend, which is a simple census-based index of material deprivation calculated by the combination of four census variables including households without a car, overcrowded households, households not owner-occupied, and persons unemployed (Wilkinson, 1997). A greater Townsend index score implies a greater degree of deprivation. Areas may be “ranked” according to their Townsend score as a means of expressing relative deprivation.

The mental health problems scores included nine aspects: addiction, anxiety, cannabis use, depression, mania, mental distress, unusual and psychotic experiences, self-harm, and wellbeing, which are categories specified under the mental health tab of the online questionnaires in the UK Biobank dataset (https://biobank.ctsu.ox.ac.uk/crystal/label.cgi?id=136). For each category, a mean

score of all the questions was calculated as an overall score of that category of mental health problems.

The correlation was also measured between the childhood traumatic event score and cognitive performance including fluid intelligence, numeric memory and prospective memory. The score of each category of cognitive performance was the score of single questions recommended by the UK Biobank dataset instead of the calculated sum scores of all measures under each category.

To validate the result, in the main analysis, all participants with available behavioural data except for the participants who were included in the second release of the dataset were included (around 480,000 participants, with the exact number varying for different behaviours). For the data in the second release of the UK Biobank dataset, we performed validation with these 17,747 independent participants.

In addition to the behaviour level associations, the functional connectivity related to the mental health problems, cognitive performance, and the childhood traumatic events scores were investigated. Hadamard products were performed on the mean correlation r values of significant brain regions with childhood traumatic events and mental health problems/cognitive performance to calculate the commonalities of the brain regions related to the different measures. The functional connectivities significant with childhood traumatic events were FDR corrected at $p<0.01$, and the functional connectivity significant with other measures (mental health problems and cognitive performances) was FDR corrected at $p<0.05$.

7.2.5 Association between the functional connectivities with childhood traumatic events

A Spearman correlation was performed to assess the association between whole-brain functional connectivity and the childhood traumatic event scores across all participants. Specifically, partial correlations were performed between functional connectivities and the childhood traumatic scores with 9 confounding variables regressed out including age, gender, body mass index, education, Townsend index, alcohol use, tobacco use, site information and head motion (mean framewise displacement). To take into account multiple comparisons, FDR correction was applied to identify the functional connectivities significantly correlated with the childhood traumatic event score. To validate the results, the same analyses were performed with 17,747 independent participants in the second release of the UK Biobank dataset.

7.2.6 Mediation analysis and structural equation modelling

Mediation analyses were conducted to interrogate the relationship between the childhood traumatic events, related brain imaging variables, mental health problems, and cognitive performance: path a represents a relationship between childhood traumatic events and functional connectivity links; path b represents the relationship between functional connectivity links and mental health problems/cognitive measures; path c represents the relationship between childhood traumatic events and mental health problems/cognitive measures; path a*b represents an indirect path which is the relationship between childhood traumatic events and mental health problems/cognitive measures that is mediated by the mean strength of the functional connectivity links which were significantly correlated with the childhood traumatic events. The mediation analysis was conducted by the Mediation Toolbox of Tor Wager (https://github.com/canlab/MediationToolbox), with a 1,000 bias-corrected bootstrap sample for significance testing. Age, gender, body mass index, education, Townsend index, alcohol use, tobacco use, site information and head motion (only for functional connectivities) were regressed out as covariances in the mediation analyses.

Structural equation modelling (SEM) was used to further test the role of the functional connectivities in the relationship between the childhood traumatic events scores, mental health problems, and cognitive performance scores in groups modelled by latent variables. Four latent variables were estimated in this model including childhood traumatic events, mental health problems, cognitive performance, and functional connectivity strength. Using latent variables helps control measurement error, artificially reducing the relationship between measured variables in standard univariate analyses (McDonald, 1990). Calculations of SEM were performed with the Lavaan toolbox in Matlab (Rosseel, 2012). For preprocessing, age, gender, body mass index, education, Townsend index, alcohol use, tobacco use, site information and head motion were regressed out as covariances for each latent variable (site information and head motion were only for functional connectivities). A latent variable representing the childhood traumatic events was estimated based on the score of five childhood traumatic event questions. Latent variables for the mental health problem and cognitive performance were estimated in the same model. Finally, a latent variable representing the functional connectivity strength of brain regions was based on the mean functional connectivity value of the links which were significantly correlated with childhood

traumatic events for the top 25 most involved brain regions. Multiple regression was adopted to measure the multivariate relationship between functional connectivity strength, childhood traumatic events, mental health problems and cognitive performance. Standardized beta coefficients were used to indicate the effect sizes of the relationship between pairs of latent variables. The comparative fit index (CFI) and root mean square error of approximation (RMSEA) were used to indicate the fitting degree of the structural equation model (Bentler, 1990; Browne and Cudeck, 1992). The brain regions included in this model were selected as those with a significant correlation with the childhood traumatic event score. The hypotheses about the directions to test in the structural equation model were set up a priori, based on arguments that the early childhood trauma might influence the brain functional connectivities; and that the childhood traumatic events and related brain changes might influence the cognitive performance and mental health problems (Bolsinger et al., 2018; Copeland et al., 2018).

7.3 Results

7.3.1 Association between childhood traumatic events, and mental health and cognitive performance

Association analysis was performed between childhood traumatic events and mental health problems (N=151,009). All the mental health problems were positively correlated with the childhood traumatic events, while well-being was negatively correlated (all $p<1.0\times10^{-200}$, Fig. 7.1). Of special interest, childhood traumatic events were associated with anxiety at r = 0.19 ($p<1.0\times10^{-323}$), with depression at r = 0.21 ($p<1.0\times10^{-323}$), with self-harm at r = 0.24 ($p<1.0\times10^{-323}$), and with well-being at r = -0.22 ($p<1.0\times10^{-323}$). Cognitive performance, including fluid intelligence, numeric memory and prospective memory, were negatively correlated with childhood traumatic events (all $p<1.0\times10^{-3}$, Fig. 7.1). Fluid intelligence was the most significantly correlated cognitive performance with childhood traumatic events with r=-0.05 ($p=2.8\times10^{-10}$).

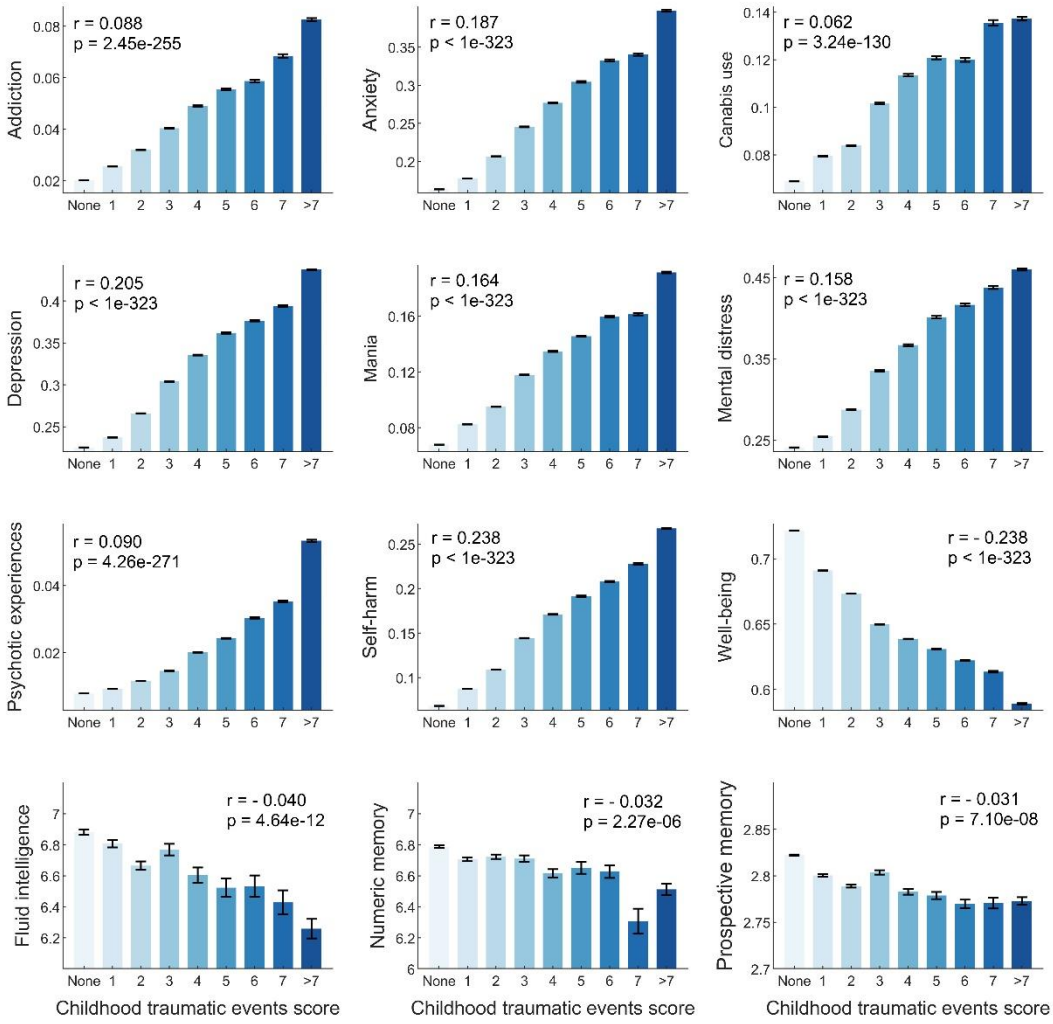

Figure 7.1. Mental health problems and cognitive performance are all related to childhood traumatic events. They include addiction, anxiety, cannabis use, depression, mania, mental distress, psychotic experiences, self-harm, well-being, fluid intelligence, numeric memory and prospective memory. The correlation coefficient r values of each mental health problem with childhood traumatic events are shown in each subplot.

7.3.2 Functional connectivity correlated with childhood traumatic events

Next, the association between childhood traumatic events and brain functional connectivity was investigated with the first release of neuroimaging data of the UK Biobank dataset (N=19,535). One hundred ninety-four FC links were significantly negatively correlated with the childhood traumatic event score ($p<0.01$, FDR corrected, Fig. 7.2). The brain areas related to these significant links included the middle temporal gyrus, the inferior temporal gyrus, the precentral cortex, the inferior frontal gyrus (the triangular part), the middle frontal gyrus, the superior medial prefrontal cortex, and the precuneus (Fig 7.2). The top 100 significantly correlated functional connectivity links

with the childhood traumatic events score are shown in Table 7.2, and a full list of these 194 significant links are shown in Appendix 4.

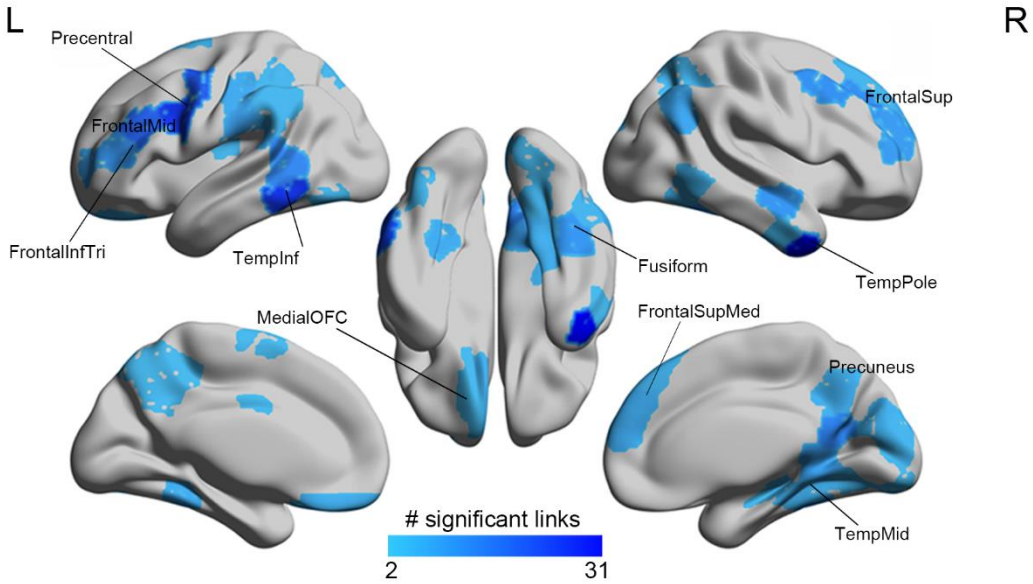

Figure 7.2. Correlation of the functional connectivity links with childhood traumatic events ($p<0.01$, FDR corrected). The numbers of links for each brain region in the Shen atlas showing a significant negative correlation with the childhood traumatic events score are shown.

Region 1	Region 2	r val	p val	Region 1	Region 2	r val	p val
Temporal_Inf_R	Temporal_Inf_L	-0.046	4.95E-08	Precuneus_R	Cingulate_Mid_L	-0.037	1.03E-05
Angular_R	Precentral_L	-0.045	1.03E-07	Precentral_R	SupraMarginal_L	-0.037	1.04E-05
Angular_R	Temporal_Inf_L	-0.045	1.25E-07	Occipital_Mid_R	Precentral_L	-0.037	1.08E-05
Temporal_Inf_R	Temporal_Mid_L	-0.044	2.40E-07	Frontal_Mid_2_R	Precentral_L	-0.037	1.10E-05
Lingual_R	Temporal_Inf_L	-0.043	2.82E-07	Fusiform_R	Precentral_L	-0.037	1.10E-05
Temporal_Inf_R	Postcentral_L	-0.043	3.36E-07	Precuneus_R	Frontal_Inf_Tri_L	-0.037	1.12E-05
Precuneus_R	Temporal_Inf_L	-0.042	5.09E-07	Temporal_Inf_L	Rectus_L	-0.037	1.16E-05
Frontal_Sup_2_R	Precentral_L	-0.042	8.92E-07	Precuneus_R	Precentral_L	-0.037	1.17E-05
Precuneus_R	Precentral_L	-0.041	9.50E-07	Angular_R	Frontal_Inf_Tri_L	-0.037	1.22E-05
Precuneus_R	Precentral_L	-0.041	1.07E-06	Temporal_Inf_R	Temporal_Inf_R	-0.037	1.23E-05
Temporal_Inf_R	Parietal_Inf_L	-0.041	1.10E-06	Parietal_Sup_R	Temporal_Inf_R	-0.037	1.25E-05
Precuneus_R	Precentral_L	-0.041	1.11E-06	Frontal_Sup_2_R	Precentral_L	-0.037	1.26E-05
SupraMarginal_R	Temporal_Inf_R	-0.041	1.21E-06	Frontal_Sup_Medial_R	Frontal_Inf_Tri_L	-0.037	1.26E-05
Temporal_Inf_R	Parietal_Inf_L	-0.041	1.25E-06	Temporal_Mid_R	Temporal_Mid_L	-0.037	1.27E-05
Temporal_Mid_R	Temporal_Inf_L	-0.041	1.31E-06	Temporal_Inf_R	Frontal_Sup_2_L	-0.037	1.28E-05
Temporal_Inf_R	Frontal_Inf_Tri_L	-0.041	1.42E-06	Lingual_R	Precentral_L	-0.037	1.44E-05
Angular_L	Temporal_Inf_L	-0.040	1.92E-06	Temporal_Inf_R	Rolandic_Oper_R	-0.037	1.44E-05
Temporal_Inf_R	Parietal_Sup_L	-0.040	2.44E-06	Cuneus_L	Temporal_Inf_L	-0.037	1.45E-05
Temporal_Inf_R	Frontal_Inf_Tri_L	-0.040	2.61E-06	Temporal_Inf_R	Precentral_L	-0.037	1.49E-05
Temporal_Inf_R	SupraMarginal_L	-0.040	2.82E-06	Frontal_Sup_2_R	Parietal_Inf_L	-0.037	1.54E-05
Temporal_Inf_R	Precentral_L	-0.039	3.47E-06	Frontal_Sup_2_R	Fusiform_L	-0.037	1.59E-05
Temporal_Mid_R	Frontal_Inf_Tri_L	-0.039	3.69E-06	Cuneus_R	Temporal_Inf_L	-0.036	1.63E-05
Precuneus_R	Temporal_Inf_L	-0.039	3.90E-06	Frontal_Mid_2_R	Frontal_Inf_Tri_R	-0.036	1.67E-05
Lingual_R	Frontal_Inf_Tri_L	-0.039	4.16E-06	Supp_Motor_Area_L	Rolandic_Oper_L	-0.036	1.67E-05
Temporal_Pole_Sup_L	Temporal_Inf_L	-0.039	4.22E-06	Fusiform_R	Precentral_L	-0.036	1.76E-05
Frontal_Sup_Medial_R	Temporal_Mid_L	-0.039	4.26E-06	Postcentral_R	Temporal_Inf_R	-0.036	1.80E-05
Frontal_Sup_2_R	Postcentral_L	-0.039	4.29E-06	Temporal_Mid_L	Temporal_Mid_L	-0.036	1.80E-05
Frontal_Sup_2_R	Parietal_Inf_L	-0.039	4.30E-06	Angular_R	Precentral_L	-0.036	1.84E-05
Temporal_Mid_R	Precentral_L	-0.039	4.61E-06	Fusiform_R	Frontal_Inf_Tri_L	-0.036	1.90E-05
Rolandic_Oper_R	Temporal_Inf_R	-0.039	4.97E-06	Postcentral_L	Temporal_Mid_L	-0.036	1.91E-05
Temporal_Inf_R	Postcentral_L	-0.039	5.09E-06	Frontal_Sup_2_R	Frontal_Inf_Tri_L	-0.036	1.95E-05
Temporal_Mid_L	Temporal_Inf_L	-0.039	5.13E-06	Temporal_Pole_Sup_R	Temporal_Inf_L	-0.036	1.97E-05
Temporal_Inf_R	Parietal_Inf_L	-0.039	5.27E-06	Temporal_Inf_R	Fusiform_L	-0.036	2.01E-05
Precuneus_L	Rectus_L	-0.039	5.30E-06	Occipital_Sup_R	Precentral_L	-0.036	2.04E-05
Temporal_Inf_R	Temporal_Mid_R	-0.038	5.36E-06	Fusiform_R	Precentral_L	-0.036	2.10E-05
Temporal_Inf_R	Temporal_Sup_R	-0.038	5.37E-06	Frontal_Sup_2_R	SupraMarginal_R	-0.036	2.15E-05
ParaHippocampal_R	Precentral_L	-0.038	5.38E-06	Frontal_Sup_2_R	Frontal_Inf_Tri_L	-0.036	2.21E-05
Cuneus_R	Frontal_Inf_Tri_L	-0.038	5.65E-06	Precentral_L	Fusiform_L	-0.036	2.34E-05
Temporal_Inf_L	ParaHippocampal_L	-0.038	5.73E-06	Fusiform_R	Frontal_Sup_2_L	-0.036	2.40E-05
Precentral_L	Precuneus_L	-0.038	5.75E-06	Lingual_R	Cingulate_Mid_L	-0.036	2.40E-05
Frontal_Mid_2_R	Precentral_L	-0.038	6.58E-06	Temporal_Sup_R	Temporal_Inf_R	-0.036	2.41E-05
Temporal_Inf_R	Temporal_Mid_L	-0.038	6.84E-06	Frontal_Mid_2_R	Precuneus_L	-0.036	2.41E-05
ParaHippocampal_R	Temporal_Mid_L	-0.038	6.99E-06	Lingual_R	Temporal_Mid_L	-0.036	2.53E-05
Frontal_Inf_Tri_L	Rectus_L	-0.038	7.66E-06	OFCmed_L	OFCant_R	-0.036	2.54E-05
Precentral_L	Fusiform_L	-0.038	7.69E-06	Temporal_Inf_L	Precuneus_L	-0.036	2.55E-05
Angular_R	Temporal_Mid_R	-0.038	8.29E-06	Hippocampus_R	Temporal_Mid_L	-0.036	2.58E-05

Temporal_Inf_R	Rolandic_Oper_L	-0.037	9.44E-06	Frontal_Sup_Medial_R	Precentral_L	-0.036	2.68E-05
Frontal_Sup_2_R	Fusiform_R	-0.037	9.80E-06	Temporal_Inf_R	Fusiform_R	-0.036	2.71E-05
Temporal_Inf_R	Temporal_Sup_L	-0.037	9.85E-06	Frontal_Sup_2_L	Fusiform_L	-0.035	2.72E-05
Frontal_Mid_2_R	Precuneus_R	-0.037	9.97E-06	Frontal_Sup_2_R	Precentral_R	-0.035	2.73E-05

Table 7.2. Top 100 significantly correlated functional connectivity links with the childhood traumatic events score. All the links shown in this table are significant at $p<0.01$, FDR corrected.

7.3.3 Common brain regions correlated with both childhood traumatic events and mental health problems and cognitive performance

In addition to the association between childhood traumatic events and behavioural measures, we also found correlations between the functional connectivity significantly correlated with childhood traumatic events and the functional connectivity associated with mental health problems and cognitive performance, especially for anxiety ($r=0.35$, $p=8.3\times10^{-8}$), depression ($r=0.23$, $p=5.1\times10^{-4}$), well-being ($r=-0.30$, $p=3.8\times10^{-6}$) and numeric memory($r=-0.23$, $p=5.6\times10^{-4}$) (Fig. 7.3).

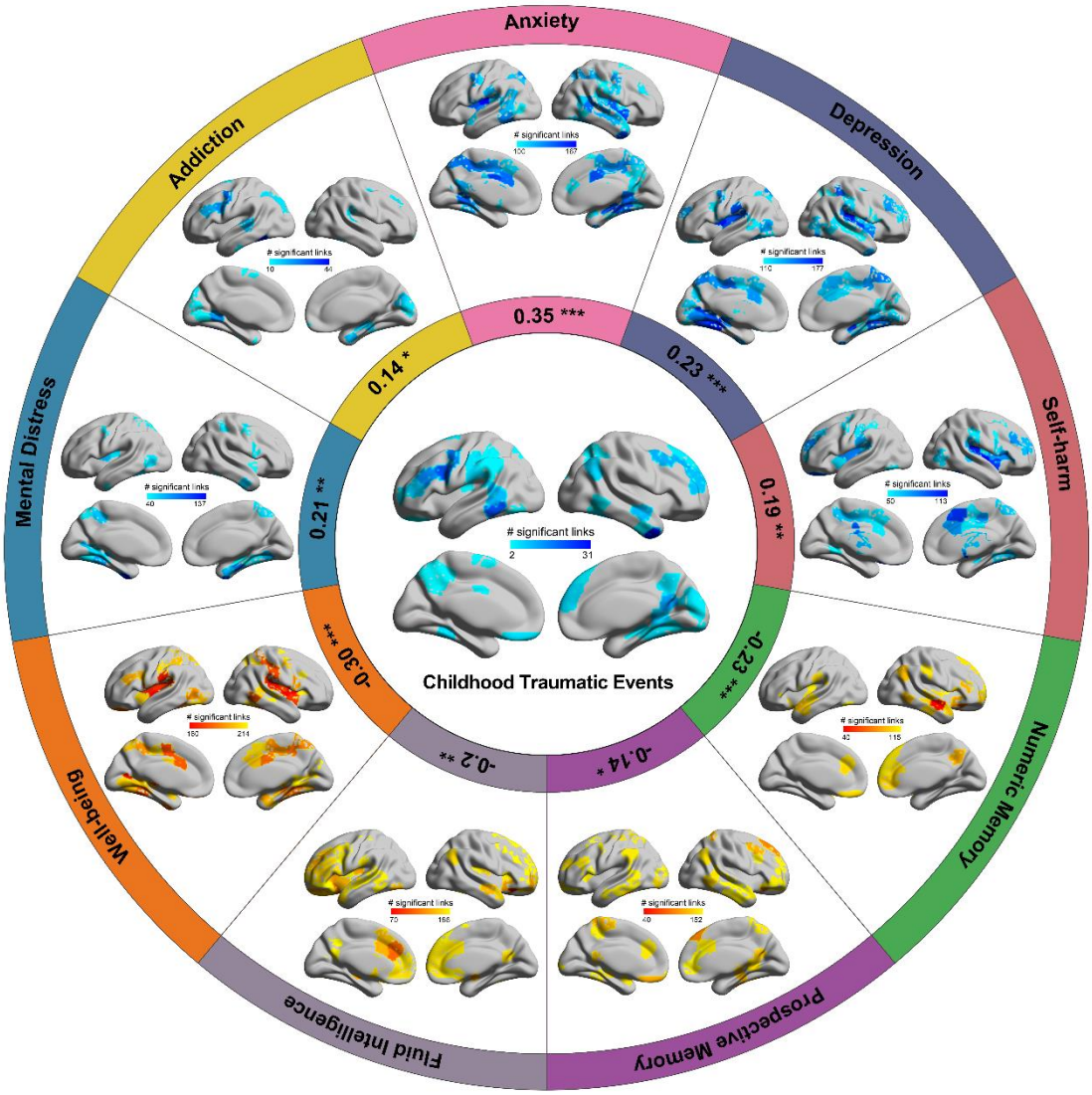

Figure 7.3. Correlation of the functional connectivity links with mental health problems and cognitive performance ($p<0.05$, FDR corrected). The number of links that are different in different brain regions for different mental health problems and cognitive performance is shown. In the centre, brain regions with reduced functional connectivity correlated with the childhood traumatic event score are shown (from Figure 7.2) to provide a reference for the other measures. The coefficients shown in the inner circle are the correlation r value of the mean correlation coefficient of significant links in all brain regions between the childhood traumatic event score and mental health problems and cognitive performance (* $p<0.05$, ** $p<0.01$, ***$p<0.001$).

To be specific, the precentral cortex and anterior areas to it were correlated with childhood traumatic events and with addiction, depression, mental distress, well-being, prospective memory, fluid intelligence. The middle temporal gyrus showed as a common area for anxiety, depression, well-being, numeric memory, prospective memory, fluid intelligence, and childhood traumatic events. The superior medial prefrontal area was common between only numeric memory and childhood traumatic

events. (The utility of this is that it suggests that impairments in numeric memory in those with childhood traumatic events may be related to reduced functional connectivity in the superior medial prefrontal cortex.) The hippocampus / paraHippocampal gyrus was common between addiction, anxiety, mental distress, well-being, numeric memory and childhood traumatic events. Hadamard products were also calculated to explore the common brain regions correlated with childhood traumatic events and mental health problems/cognitive performances (Table 7.3). The inferior temporal gyrus and the middle temporal gyrus was found common between the childhood traumatic events and anxiety in the top 10 highest Hadamard products of all brain regions. The precuneus was found common between the childhood traumatic events, numeric memory and prospective memory in the top 10 highest Hadamard products of all brain regions.

Addiction		**Anxiety**		**Depression**		**Mental Distress**	
Regions	**HP**	**Regions**	**HP**	**Regions**	**HP**	**Regions**	**HP**
Precentral_L	0.653	Temporal_Inf_R	5.100	Temporal_Inf_R	4.253	Precentral_L	0.893
Precentral_L	0.582	Temporal_Inf_L	3.083	Precentral_L	2.710	Fusiform_R	0.484
Frontal_Inf_Tri_L	0.331	Precentral_L	2.307	Precentral_L	2.628	Fusiform_L	0.480
Frontal_Sup_2_R	0.162	Fusiform_R	1.349	Fusiform_R	1.541	Lingual_R	0.278
Fusiform_R	0.143	Precuneus_R	1.346	Precuneus_R	1.394	Fusiform_R	0.238
Fusiform_L	0.102	Temporal_Mid_R	1.259	Frontal_Sup_2_R	1.331	ParaHippocampal_R	0.203
Cuneus_R	0.099	Lingual_R	1.189	Fusiform_L	1.145	Precuneus_L	0.195
ParaHippocampal_R	0.093	Temporal_Mid_L	1.144	Temporal_Mid_R	1.094	Temporal_Inf_R	0.179
Calcarine_R	0.056	ParaHippocampal_R	0.842	Temporal_Mid_L	1.073	Rolandic_Oper_L	0.156
Hippocampus_R	0.053	Fusiform_R	0.734	Lingual_R	1.034	Fusiform_L	0.141
Well-being		**Numeric Memory**		**Prospective Memory**		**Fluid Intelligence**	
Regions	**HP**	**Regions**	**HP**	**Regions**	**HP**	**Regions**	**HP**
Precentral_L	-4.094	Temporal_Mid_R	-1.687	Temporal_Inf_L	-0.889	Temporal_Inf_L	-1.798
Frontal_Inf_Tri_L	-2.830	Angular_R	-0.630	Precuneus_R	-0.803	Precentral_L	-1.345
Fusiform_R	-2.180	Precuneus_R	-0.461	Frontal_Mid_2_R	-0.741	Precentral_L	-1.336
SupraMarginal_L	-1.665	SupraMarginal_L	-0.413	Precentral_L	-0.659	Temporal_Mid_R	-1.076
Lingual_R	-1.531	Frontal_Sup_Medial_R	-0.358	Frontal_Inf_Tri_L	-0.657	Precuneus_R	-0.962
Fusiform_L	-1.371	Rectus_L	-0.348	Fusiform_R	-0.554	Frontal_Inf_Tri_L	-0.926
Fusiform_R	-1.210	Temporal_Mid_R	-0.336	Lingual_R	-0.431	Temporal_Mid_L	-0.700
ParaHippocampal_R	-1.079	Frontal_Sup_2_R	-0.253	Temporal_Mid_L	-0.414	Frontal_Sup_2_R	-0.677
Postcentral_L	-1.037	ParaHippocampal_R	-0.243	Frontal_Sup_2_R	-0.367	Fusiform_R	-0.672
Temporal_Mid_R	-0.946	Rolandic_Oper_L	-0.158	Angular_R	-0.363	Frontal_Inf_Tri_L	-0.640

Table 7.3. List of top 10 brain regions that were significant in the childhood traumatic events and mental health problems/cognitive performances. HP is initial for Hadamard product.

7.3.4 Mediation analysis and structural equation modelling

The functional connectivities that were significantly correlated with childhood traumatic events (Fig. 7.2) significantly mediated the relationship between the childhood traumatic events and mental health problems including addiction (1.9% of the variance explained), anxiety (1.3% explained), depression (1.0% explained) and well-being (1.4% explained) (all p<10-3) (Fig. 7.4). The interpretation is that the functional connectivities correlated with childhood traumatic events significantly mediate the association between childhood traumatic events and addiction, anxiety, depression and well-being. Similar results were also found for the cognitive performance measures including fluid intelligence (3.0% explained), and prospective memory (3.3% explained) (p<0.05) (Fig. 7.4). The interpretation is that the functional connectivities correlated with childhood traumatic events significantly mediate the association between childhood traumatic events and fluid intelligence and prospective memory. A full list of the mediation results for all measures of mental health problems and cognitive performance can be found in Table 7.4.

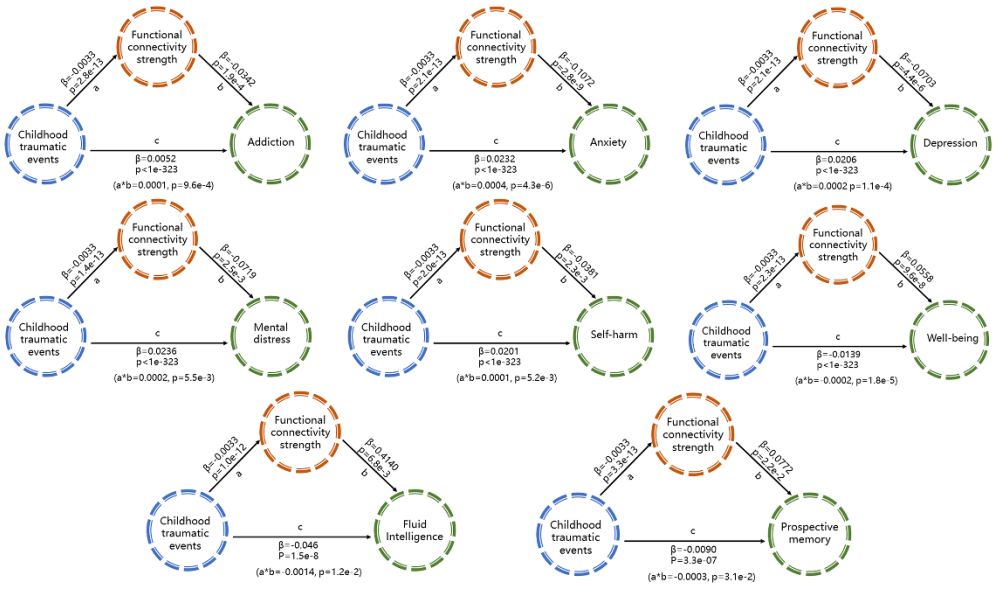

Figure 7.4. Mediation analysis between the childhood traumatic events, the mental health problems and cognitive measures with a mean strength of functional connectivity links which were significantly correlated with the childhood traumatic events as a mediator. Path a: relationship between childhood traumatic events and functional connectivity links; Path b: the relationship between functional connectivity links and mental health problems/cognitive measures; Path c: the relationship between childhood traumatic events and mental health problems/cognitive measures; Path a*b represents an indirect path which is the relationship between childhood traumatic events and mental health problems/cognitive measures that is mediated by the mean strength of the functional connectivity links which were significantly

correlated with the childhood traumatic events. Path a*b indicates the extent to which taking the functional connectivity strength into account can explain the effect of the childhood traumatic events on mental health and cognitive measures including: addiction (1.9% of the variance explained), anxiety (1.3% of the variance explained), depression (1.0% of the variance explained), mental distress (0.8% of the variance explained), self-harm (0.5% of the variance explained), well-being (1.4% of the variance explained), fluid intelligence (3.0% of the variance explained), and prospective memory (3.3% of the variance explained).

	Path a		**Path b**		**Path c**		**Path a*b**	
	beta	**p**	**beta**	**p**	**beta**	**p**	**beta**	**p**
Addiction	**-0.0033**	**2.8E-13**	**-0.0342**	**1.9E-04**	**0.0052**	**0**	**0.0001**	**9.6E-04**
Anxiety	**-0.0033**	**2.1E-13**	**-0.1072**	**2.8E-09**	**0.0232**	**0**	**0.0003**	**4.3E-06**
Cannabis use	-0.0033	2.3E-13	-0.0144	2.4E-01	0.0034	1.23E-07	0.0000	2.5E-01
Depression	**-0.0033**	**2.1E-13**	**-0.0703**	**4.4E-06**	**0.0206**	**0**	**0.0002**	**1.1E-04**
Mania	-0.0033	1.4E-13	-0.0172	1.6E-01	0.0125	0	0.0001	1.7E-01
Mental distress	**-0.0033**	**1.4E-13**	**-0.0719**	**2.5E-03**	**0.0236**	**0**	**0.0002**	**5.5E-03**
Unusual and psychotic experiences	-0.0033	2.1E-13	-0.0012	7.9E-01	0.0034	0	0.0000	7.9E-01
Self-harm	**-0.0033**	**2.0E-13**	**-0.0381**	**2.3E-03**	**0.0201**	**0**	**0.0001**	**5.2E-03**
Wellbeing	**-0.0033**	**2.3E-13**	**0.0558**	**9.6E-08**	**-0.0139**	**0**	**-0.0002**	**1.8E-05**
Fluid intelligence	**-0.0033**	**1.0E-12**	**0.4140**	**6.8E-03**	**-0.046**	**1.5E-08**	**-0.0014**	**1.2E-02**
Numeric memory	-0.0035	3.7E-07	0.2469	1.4E-01	-0.0204	2.1E-02	-0.0009	1.6E-01
Prospective memory	**-0.0033**	**3.3E-13**	**0.0772**	**2.2E-02**	**-0.0090**	**3.3E-07**	**-0.0003**	**3.1E-02**

Table 7.4. Mediation analysis between childhood traumatic events, mental health problems, and cognitive performances with a mean strength of functional connectivity links shown in Table 7.2 as mediator.

Structural equation modelling was performed to measure the multivariate relationship between childhood traumatic events, mental health problems, cognitive performance, and the functional connectivity in the frontal lobe, the temporal lobe, the precuneus, etc. (comparative fit index (CFI) = 0.99, root mean square error of approximation (RMSEA) = 0.032), and as shown in Fig. 7.5, all the paths in the model were significant at $p<0.001$. The functional connectivities that were significantly correlated with childhood traumatic events had a significant association with mental health problems ($\beta=-0.04$, $p<0.001$) and with cognitive performance ($\beta=0.05$, $p<0.001$), suggesting that childhood traumatic events and the associated brain changes related to those events may contribute to the mental health problems and cognitive performance differences.

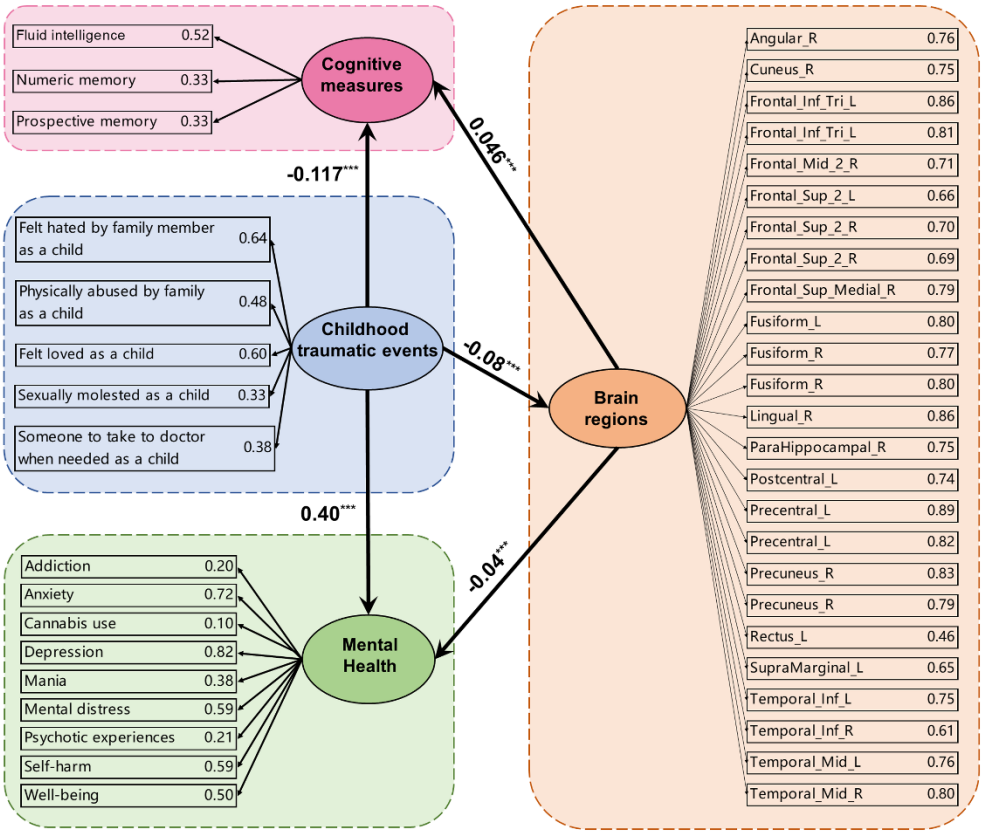

Figure 7.5. Structural equation model: for the brain regions indicated with functional connectivity of some links associated with the childhood trauma score, the correlation of its significant links with the childhood trauma score was entered into structural equation model with the behavioural measures indicated and grouped to form latent variables. The numbers in bold font show the standardised beta coefficients involving the latent variables. All paths between the latent variables were significant at $p < 0.001$ (indicated by 3 stars). After the Brain Regions, the functional connectivity between the significant links for that brain area with the childhood trauma score is shown. The structural equation model used here enables the different measures for cognition to be grouped, and similarly for the childhood trauma and mental health measures, so that relationship between the grouped variables can be measured. The direction of the effects to be tested was as shown by the arrows, and was based on a priori hypotheses.

7.3.5 Validation with an independent data group

Validation was performed with the second release of neuroimaging data from the UK Biobank (N=17,747). Firstly, the behavioural associations between childhood traumatic events, mental health problems and cognitive performance were well-validated, with anxiety ($r=0.19$, $p=3.8\times10^{-93}$), depression ($r=0.19$, $p=3.2\times10^{-95}$), self-harm ($r=0.25$, $p=2.5\times10^{-155}$), well-being ($r=-0.22$, $p=1.9\times10^{-126}$), fluid intelligence ($r=-0.03$, $p=1.4\times10^{-3}$), and numeric memory ($r=-0.03$, $p=5.3\times10^{-3}$) (Table 7.5).

	Main analysis		Validation	
	r value	p value	r value	p value
Addition	0.09	4.5E-235	0.09	2.9E-22
Anxiety	0.19	<E-323	0.19	3.8E-93
Cannabis use	0.06	1.2E-117	0.07	1.3E-14
Depression	0.21	<E-323	0.19	3.2E-95
Mania	0.16	<E-323	0.17	3.4E-72
Mental distress	0.16	<E-323	0.16	1.2E-68
Psychotic experiences	0.09	2.1E-253	0.08	2.0E-19
Self-harm	0.24	<E-323	0.25	2.5E-155
Well-being	-0.22	<E-323	-0.22	1.9E-126
fluid Intelligence	-0.05	2.8E-10	-0.03	1.4E-03
numeric memory	-0.04	1.1E-04	-0.03	5.3E-03
prospective memory	-0.04	6.8E-08	-0.02	4.5E-02

Table 7.5. Association between childhood traumatic events, mental health problems and cognitive performances with the first and second released data group.

Secondly, the correlation between childhood traumatic events and functional connectivity was well-validated (Fig. 7.6). For example, areas with many links correlated with childhood trauma in the second release include prefrontal cortical areas (superior, middle and inferior frontal and medial superior frontal), the middle and inferior temporal cortex and temporal pole, and the orbitofrontal cortex including the posterior and lateral orbitofrontal cortex (Fig. 7.6A). It was found that the correlation of the association pattern of functional connectivity with childhood traumatic events between the first and second released data group was $r=0.40$, $p < 10^{-323}$ (Fig. 7.6B). (It was confirmed that the correlation measures utilized were not significant with measures from the UK Biobank that are unlikely to be related to risk-taking. These included total food weight consumed on the previous day (field ID 100001) for which r=-0.00043 p=0.98; and body mass index (field ID 21001) for which r=-0.024 p=0.11.) This cross-validation analysis thus provides evidence that the associations between childhood traumatic events, mental health problems and functional connectivity described above can be confirmed with an independent dataset.

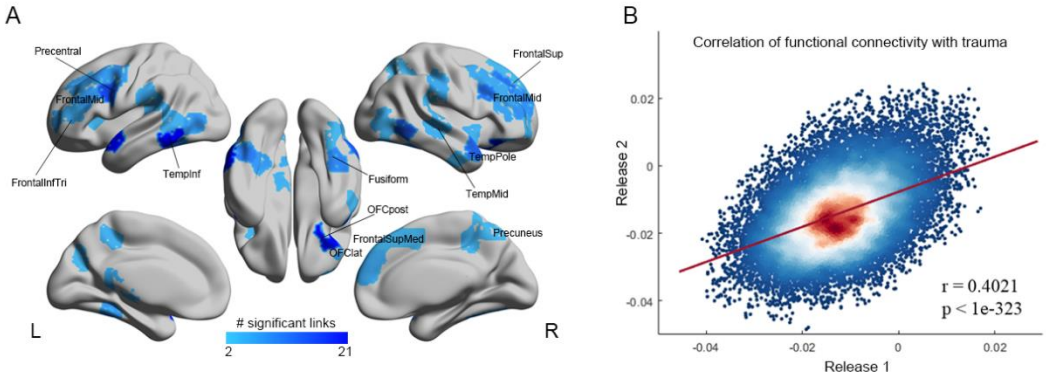

Figure 7.6. Comparison of the findings from the second release of the UK Biobank with 17,747 participants. A) For the second release, correlation of the functional connectivity links with childhood traumatic events ($p<0.01$, FDR corrected). The numbers of links for each brain region in the Shen atlas showing a significant negative correlation with the childhood traumatic events score are shown. B) Scattergram of the functional connectivity r values between the first and second releases. There is one data point for each region in the Shen atlas.

7.4 Discussion

This is the first study, to our knowledge, to examine the association between childhood traumatic events, brain function, mental health problems, and cognitive performance, with a large sample size in the UK Biobank dataset. A strong correlation was shown between the mental health problems, cognitive performance, and low functional connectivity in brain regions with childhood traumatic events. The main brain regions with functional connectivity negatively correlated with the childhood traumatic events scores included the precentral areas extending into the prefrontal cortex (superior, middle, inferior and medial parts), the temporal cortex (lateral and medial), the precuneus, the fusiform gyrus, and the medial orbitofrontal cortex. The results were well validated with an independent data group with the correlation between the two correlation matrices with childhood traumatic events $r=0.4$, $p<10^{-323}$. The low functional connectivities of these brain regions were shown to significantly mediate the association between childhood traumatic events, and mental health problems including addiction, anxiety, depression, and well-being (all $p<10^{-3}$).

A range of mental health problems including addiction, anxiety, cannabis use, depression, mania, mental distress, psychotic experiences, self-harm, and well-being in later life was found to be positively significantly associated with childhood traumatic events ($p<1\times10^{-117}$) (Fig. 7.1). Brain regions for which functional connectivity was

associated with childhood traumatic events and mental health problems included the middle temporal gyrus, the medial orbitofrontal cortex and in the second release lateral orbitofrontal cortex, the prefrontal and precentral cortex, and the precuneus (Fig. 7.3).

The middle temporal gyrus, which was common between anxiety and childhood traumatic events, is implicated in facial emotional expression and face movements, and theory of mind (Hasselmo et al., 1989; Critchley et al., 2000; Hein and Knight, 2008; Cheng et al., 2015; Cheng et al., 2017; Rolls, 2021). The association between the middle temporal gyrus and childhood traumatic events suggests that childhood traumatic events are associated with differences in the neural mechanisms for detecting face emotional expression and in the theory of mind (Cheng et al., 2015), which may relate to emotional problems such as anxiety, depression, and mental distress in later adulthood.

The medial orbitofrontal cortex is involved in reward value and hence in emotion and decreases in functional connectivity here are associated with depression (Rolls, 2019a, b; Rolls et al., 2020a). The lateral orbitofrontal cortex is involved in changing behaviour to non-reward and punishment and reduced functional connectivity here may be associated with rule-breaking and impulsive types of behaviour (Rolls, 2019a, b; Rolls et al., 2020a).

The functional connectivity of the fusiform gyrus was found to be significantly associated with childhood traumatic events and mental health measures including addiction, anxiety, depression, mental distress, and well-being. The fusiform gyrus is implicated in face processing (Schirmer and Adolphs, 2017; Grill-Spector et al., 2018).

The precentral cortex and areas extending anteriorly into the lateral prefrontal cortex, which were significantly associated with childhood traumatic events and mental health problems including addiction, depression, mental distress, and well-being, contains mirror neurons that are implicated in observational learning as proposed by Rizzolatti and Craighero (2004). Mirror neurons in area F5 of the premotor areas in both humans and monkeys fire when actions are being performed, or are observed in another individual (human or monkey) performing the same action (Rizzolatti, 2014). Impairment in this type of learning may be related to the cognitive and mental problems associated with childhood traumatic events. Executive function, implemented in the prefrontal cortex (Shallice and Cipolotti, 2018; Cristofori et al., 2019), may also be involved.

The precuneus is a part of the medial parietal cortex involved in self-awareness, autobiographical memory, and spatial function (Cavanna and Trimble, 2006; Freton et al., 2014). The low functional connectivity of the precuneus suggests that childhood traumatic events are associated with a reduced or low sense of self. In addition, a low functional connectivity of the precuneus with some cortical areas is associated with depression (Peng et al., 2015; Cheng et al., 2018; Schreiner et al., 2019). The lower connectivity of the precuneus reported here in the participants with childhood traumatic events may be related to depression and contribute particularly to the low self-esteem in depression.

Cognitive performance measures including fluid intelligence, numeric memory and prospective memory were also found to be negatively correlated with childhood traumatic events ($p<0.001$) (Fig. 7.1). Although not as significant as the mental health problems, negative associations between childhood traumatic events and cognitive functions were observed. Brain regions associated with childhood traumatic events and lower cognitive performance included the superior medial prefrontal cortex, and the middle frontal gyrus (Fig. 7.3).

The superior medial prefrontal area was related to both childhood traumatic events and numeric memory. The superior medial prefrontal area is involved in planning / executive function (Mizuhara and Yamaguchi, 2007). Numerical information is represented and processed by regions of the prefrontal and posterior parietal lobes, according to studies in humans and nonhuman primates utilizing a variety of approaches (Nieder and Dehaene, 2009). In a more recent study on the representation of numerical and sequential patterns, activations in the medial prefrontal areas were found when participants were processing number change tasks (Wang et al., 2015). Childhood traumatic events may relate to numeric memory and the superior medial prefrontal cortex because of the role of this region in low executive function.

Further, the superior and middle frontal gyri are part of the frontoparietal network, which is involved in cognitive control and working memory (Sheridan and McLaughlin, 2014). The negative association between childhood traumatic events and cognitive performance may also relate to the reduced functional connectivity of this system.

The mediation analyses provided evidence that the reduced functional connectivities related to childhood traumatic events mediated the relationship between the childhood traumatic events and the mental health problems including addiction (1.9% variance explained), anxiety (1.3% variance explained), depression (1.0% variance

explained) and well-being (1.4% variance explained) (all $p<10^{-3}$) (Fig. 7.4), and the cognitive measures including fluid intelligence (3.0% variance explained), and prospective memory (3.3% variance explained) ($p<0.05$).

The SEM analysis was performed to measure the associations between the grouped variables for Cognitive Effects, Mental health problems, and brain regions for the measures associated with childhood trauma in one regression model. In this modelling, the mean functional connectivity strengths of the brain regions which were significantly correlated with the childhood traumatic events score were also significantly associated with mental health problems ($\beta=-0.04$, $p<0.001$) and cognitive performance ($\beta=0.05$, $p<0.001$), suggesting that childhood traumatic events and consequent brain changes related to that may contribute to the mental health problems and cognitive performance measured in later life (Fig. 7.5).

Because this is an association study, causality cannot be directly addressed. One possibility is that childhood trauma produces brain differences, behavioural problems, and cognitive differences. Another possibility is that the general socio-economic environment during childhood made a contribution. However, we did regress out as a covariate on no interest the Townsend index, which measures a set of socio-economic variables. We also tested whether the Townsend index was correlated with the childhood trauma score. The Townsend index was significantly associated with childhood traumatic events score ($r=0.08$, $p=5.3\times10^{-200}$). In addition, the association between childhood traumatic events and other factors which might contribute to brain differences, behavioural problems, and cognitive differences were tested, including BMI ($r=0.06$, $p=2.8\times10^{-103}$), smoking ($r=0.09$, $p=3.8\times10^{-284}$), and drinking ($r=-0.03$, $p=7.7\times10^{-30}$). (These variables were regressed out of all the analyses described here.) Another factor might have been that some children, for genetic or possibly other reasons, were more likely to have traumatic events. Besides, another limitation in this study is the brain functional differences were focused while the brain volume loss is not checked, as the functional connectivity alteration could be reduced by either fewer axons (due to cell/volume loss) or reduced synaptic weight. The present findings do though make it clear that there are significant and long-lasting associations between childhood traumatic events, brain functional differences, and behavioural and cognitive problems.

It is interesting and remarkable that a rather similar constellation of mental health and cognitive problems involving similar brain regions to those described here are associated in children with prolonged nausea and vomiting of the mother in pregnancy

(Wang et al., 2020), with conflict in the family environment (Gong et al., 2021), and with a young age of the mother (Du et al., 2021). Whether these similar associations reflect the vulnerability of some brain regions during development or other factors, is not yet known, but the similarities are of considerable interest for neurology.

Strengths of the present investigation are the large sample size (over 20,000 participants), which leads to robust findings; a focus on brain functional differences related to childhood traumatic events instead of structure as in many other studies; validation with a large independent sample group in the same dataset (around 20,000 participants); comprehensive analysis of the long-lasting relation into mature adulthood between childhood traumatic events and a range of mental health problems and lower cognitive performance; and the mediation analysis, which links the findings to recent advances in understanding brain mechanisms associated with childhood traumatic events and mental health problems.

In summary, this investigation provides evidence in a very large population that childhood traumatic events are associated with many kinds of mental health problems in later life including anxiety, depression, and well-being; that lower functional connectivity involving the precentral areas extending into the prefrontal cortex (superior, middle, inferior and medial parts), the temporal cortex (lateral and medial), the precuneus, and the medial orbitofrontal cortex, which are involved in executive function, face processing, emotion, and memory were associated with childhood traumatic events; and that the low functional connectivities mediated the correlation between the childhood traumatic events and mental health problems including addiction, anxiety, depression and self-harm, and cognitive measures including fluid intelligence and prospective memory. These advances have implications for the care and treatment of people who very many years previously have had childhood traumatic events, for these results indicate which functions may benefit from treatment given the insight from knowing the brain regions that are involved.

Chapter 8
Conclusion and Open Problems

8.1 Discussion

This thesis, by exploring novel computational methods and modelling approaches on large scale neuroimaging data for analyses of the brain function and various behaviour measures, contributes to the understanding the brain mechanism of impulsivity (including sensation-seeking and risk-taking) and its association with alcohol/drug use in two dependent datasets. In addition, long-lasting relationships were revealed between childhood traumatic events, brain functional connectivity, and various psychological disorders, including depression, anxiety, and addiction. To our knowledge, this is the first time such relationships have been shown in a large sample from the UK Biobank dataset. Detailed discussion section of each topic is included at the end of the main chapters: here, brief conclusions drawn from the findings of different projects are provided.

In Chapter 4, a novel prediction model was developed, based on the elastic net regression of the sensation-seeking personality from brain functional connectivity of the medial OFC areas and the ACC areas. A sensation-seeking score was found to be optimally predicted with a correlation of $r=0.34$ ($p=7.3\times10^{-13}$) between the predicted and the actual sensation-seeking score across all participants. This provides a novel way to investigate the relationship between behavioural measures and brain functional connectivity, replacing the usual correlation analysis with a prediction model. Furthermore, the prediction model examines groups of functional connectivity links, instead of an individual link, which is usual in correlation analysis; this indicates the relationship between behaviour measures and a group of links as community. Biologically, this provides clear evidence that functional connectivities between the medial OFC and the ACC were strongly involved in sensation-seeking. Moreover, our study advanced the concept that one type of impulsivity, related to sensation-seeking, is associated with increased functional connectivity of a reward-related cortical region, the medial orbitofrontal cortex.

Following the same research interest in exploring the underlying mechanism of impulsivity, Chapter 6 found a significant association between risk-taking and the functional connectivity of the medial OFC areas with 18,740 participants from the UK

Biobank dataset ($p<0.001$, FDR corrected). This supports the hypothesis proposed in Chapter 4 that one type of reward-driven impulsivity is related to the medial orbitofrontal cortex of the brain, which is highly associated with risk-taking and sensation-seeking. In addition, the relationship between risk-taking and worry/anxiety was investigated through an advanced approach in this project. Instead of performing the traditional correlation between behaviour scores, the association pattern of behaviour measures with functional connectivity was analysed. This enabled the analysis of behavioural differences in association with differences in functional connectivity in the brain. Interestingly, the significantly associated functional connectivity links between risk-taking and anxiety involved similar regions of the brain, including the medial orbitofrontal cortex, VMPFC, and the parahippocampal gyrus, but in the opposite direction ($p<0.001$, FDR corrected). This investigation revealed, to my knowledge for the first time, that risk-taking individuals were not normally worriers, and the medial orbitofrontal cortex, which is a key area of the reward system, was associated positively with risk-taking, and negatively with anxiety.

Apart from functional connectivity, an exploration of directional connectivity measures was conducted in Chapter 5, including the effective connectivity (EC) measure and Granger causality (GC) of the brain. Five commonly used prediction algorithms, i.e., OLSR, ridge, LASSO, elastic net and LSVR, were performed to explore the efficiency of the EC and GC feature of the brain. Generally, the GC feature provided slightly better prediction accuracy of verbal intelligence than the EC feature, indicating that the GC feature modelled the directional connectivity of the brain in this study better than the EC. This study explored the currently developed measures of directional connectivity of the whole brain and compared their efficiency using different prediction models. This provides a way to examine the efficiency of different brain connectivity measures in terms of their prediction accuracy on behaviour measures. Our comparison of the efficiency of these five commonly used prediction models found that elastic net regression provided better prediction accuracy than the other four algorithms in both EC and GC based models. Further investigations can be tried with other large-scale datasets and predictions on different behaviour measures to validate these findings, and the functional connectivity analysis can be included for comparison.

Chapter 7 investigated childhood traumatic events in relation to cognitive performance, various psychological disorders, including anxiety, depression and

addiction in adulthood. Childhood traumatic events are established risk factors for psychopathology and can be associated with lasting mental differences. The UK Biobank dataset, which includes various health status reports, cognitive performance data and mental health measures from 500,000 volunteers, provides a great opportunity to explore the relationship between childhood traumatic events and various psychological disorders. Childhood traumatic events were found to be significantly associated with adult mental health problems, including anxiety ($r=0.19$, $p<1.0\times10^{-323}$), depression ($r=0.21$, $p<1.0\times10^{-323}$), addiction ($r=0.09$, $p<1.0\times10^{-230}$), and self-harm ($r=0.24$, $p<1.0\times10^{-323}$), as well as with adult cognitive performance, including fluid intelligence ($r=-0.05$, $p=2.8\times10^{-10}$) and prospective memory ($r=-0.04$, $p=6.8\times10^{-8}$). Functional connectivities of the precentral areas, the frontal lobe (middle and superior part), the temporal cortex (inferior and middle part), and the precuneus were negatively correlated with childhood traumatic events (FDR corrected, $p<0.01$). Notably, this investigation focused on the long-lasting relationship of childhood trauma with other behaviours over 30 years later, while most childhood trauma studies are limited to childhood or early adolescence. Moreover, with the massive datasets of various behaviour measures available, the relationships were investigated with nine mental health measures and three cognitive measures in adults, and the associated patterns of functional connectivity. These findings highlight the long-lasting relationship between childhood traumatic events and a wide range of mental health problems and cognition in later life. They also provide insights into the neural mechanisms of the long-lasting relationship, including brain areas involved in executive function, emotion, face processing, and memory.

8.2 Open Problems

The development of model imaging techniques and more available public datasets provides great opportunities for researchers to explore more about human behaviours and their underlying neuro pathways. However, with massive sample sizes and high-dimensional neuroimaging data, it is also a great challenge in terms of methodology. Further investigations can be developed, applying more complex and novel machine learning methods to model neuroimaging data more effectively with massive data. Furthermore, efficient dimensional reduction methods for neuroimaging data should be explored and developed to solve the very high-dimensional brain features (over

thousands of features) at the level of the whole brain. In addition, multi-modal analysis methods are also of great importance for the exploration of neuroimaging data, behavioural data, and genetic data together.

Although the literature may include thousands of reported results on the same question, limited convergence and conflicting findings may be disappointing and confusing in the search for a consistent understanding. This may be caused by different datasets, different pre-processing procedures, or inefficient methods which produce biased results. Developing a systematic approach that can summarize and extract the important and consistent findings from a large number of studies will benefit future researchers.

With specific reference to this thesis, there are some open problems to work on following the current research. First, further exploration is needed into the parcellation of impulsivity and how different brain regions are related to different subtypes of impulsivity. As proposed in the projects presented in Chapters 4 and 6, one type of impulsivity, which is related to sensation-seeking, is related to increased functional connectivity of a reward-related cortical region, the medial orbitofrontal cortex. Other subtypes of impulsivity and related brain regions may be of interest to investigate with a large-scale dataset and proper validation, aiming to deepen the understanding of impulsivity.

Second, machine learning methods are of great value in dealing with neuroimaging data with a high number of dimensions and large population, as described in Chapters 4 and 5. In particular, prediction models help to predict behaviour measures from brain connectivities. For example, a reliable prediction model of mental disorder will help the diagnosis to be more objective, while diagnosis is currently usually based on questionnaires. Hence, exploration of reliable prediction models for neuroimaging data with a huge dataset, e.g., the UK Biobank dataset, will be of great importance in improving the understanding of brain function and help in the diagnosis of mental illness.

Third, an investigation into the directional connectivity of the brain, including Granger causality and effective connectivity, was performed in Chapter 5. Directional connectivity shows the direction and causality of the way one brain region has an effect on another, which helps in understanding asymmetries in the way these brain regions work hierarchically underlying certain processes, such as sensory information

processing in the brain. More directional connectivity measurements can be explored and tested with independent datasets.

Fourth, it is of great importance to explore the relationship between early life experiences, such as childhood trauma, the growing-up environment and parenting situation, with mental health status in later life. It is worth investigating whether this relationship is causal, and this will help to understand how mental disorders are developed and facilitate early diagnosis.

8.3 Summary

In summary, by exploring novel computational methods and modelling approaches to large-scale neuroimaging data, significant progress has been made in understanding the brain mechanism of impulsive behaviour and mental disorders. A new subtype of impulsivity was proposed that is reward-driven and related to the medial orbitofrontal cortex in Chapter 4. This proposal is based, for the first time, on a success prediction model of sensation-seeking from the brain's functional connectivity, which was further supported by another project investigating risk-taking from a dependent dataset (Chapter 6). These findings help to provide a more comprehensive understanding of impulsivity, which further benefits the diagnosis and treatment of addiction and other impulsivity-related mental disorders.

In addition, in Chapter 5, a comparison was conducted of traditional Granger causality and the newly developed method of measuring the brain's effective connectivity through the whole-brain connectivity network by implementing different machine learning prediction models. Generally, the GC feature provided slightly better prediction accuracy than the EC feature, indicating that the GC feature modelled the directional connectivity of the brain in this study better than the EC. A comparison of the efficiency of these five commonly used prediction models showed that elastic net regression provided better prediction accuracy than the other four algorithms in both EC and GC based models.

Chapter 7 highlighted, from a large-scale dataset, the long-lasting relationship between childhood traumatic events and mental health problems, including depression, anxiety, and self-harm, and related brain functional connectivity links in later life. This is the first study, to our knowledge, to explore the association between childhood traumatic events, brain function, mental health problems, and cognitive performance,

with a large sample. It provides insights into the neural mechanisms of the long-lasting relationship between childhood trauma and mental health status in later life, including brain areas involved in executive function, emotion, face processing and memory. In particular, the UK Biobank dataset, which includes neuroimaging data, genetic data, and a wide range of cognitive performance, mental health and physical assessments from over 500,000 participants, provides the opportunity to understand various behavioural measures and the underlying neuroimaging pathway. As in Chapters 6 and 7, significant associations in the underlying brain mechanism were revealed related to risk-taking and childhood trauma, and there certainly are more possibilities to explore in this dataset.

Appendix

Appendix - 1

The anatomical regions are defined in each hemisphere and their label in the automated anatomical labelling atlas AAL2 (Rolls et al., 2015). Column 4 provides a set of possible abbreviations for the anatomical descriptions.

NO.	ANATOMICAL DESCRIPTION	LABEL aal2.nii.gz	POSSIBLE ABBREVIATION
1,2	Precentral gyrus	Precentral	PreCG
3, 4	Superior frontal gyrus, dorsolateral	Frontal_Sup	SFG
5, 6	Middle frontal gyrus	Frontal_Mid	MFG
7, 8	Inferior frontal gyrus, opercular part	Frontal_Inf_Oper	IFGoperc
9, 10	Inferior frontal gyrus, triangular part	Frontal_Inf_Tri	IFGtriang
11, 12	IFG pars orbitalis,	Frontal_Inf_Orb	IFGorb
13, 14	Rolandic operculum	Rolandic_Oper	ROL
15, 16	Supplementary motor area	Supp_Motor_Area	SMA
17, 18	Olfactory cortex	Olfactory	OLF
19, 20	Superior frontal gyrus, medial	Frontal_Sup_Med	SFGmedial
21, 22	Superior frontal gyrus, medial orbital	Frontal_Med_Orb	PFCventmed
23, 24	Gyrus rectus	Rectus	REC
25, 26	Medial orbital gyrus	OFCmed	OFCmed
27, 28	Anterior orbital gyrus	OFCant	OFCant
29, 30	Posterior orbital gyrus	OFCpost	OFCpost
31, 32	Lateral orbital gyrus	OFClat	OFClat
33, 34	Insula	Insula	INS
35, 36	Anterior cingulate & paracingulate gyri	Cingulate_Ant	ACC
37, 38	Middle cingulate & paracingulate gyri	Cingulate_Mid	MCC
39, 40	Posterior cingulate gyrus	Cingulate_Post	PCC
41, 42	Hippocampus	Hippocampus	HIP
43, 44	Parahippocampal gyrus	ParaHippocampal	PHG
45, 46	Amygdala	Amygdala	AMYG
47, 48	Calcarine fissure and surrounding cortex	Calcarine	CAL
49, 50	Cuneus	Cuneus	CUN
51, 52	Lingual gyrus	Lingual	LING
53, 54	Superior occipital gyrus	Occipital_Sup	SOG
55, 56	Middle occipital gyrus	Occipital_Mid	MOG
57, 58	Inferior occipital gyrus	Occipital_Inf	IOG
59, 60	Fusiform gyrus	Fusiform	FFG
61, 62	Postcentral gyrus	Postcentral	PoCG
63, 64	Superior parietal gyrus	Parietal_Sup	SPG
65, 66	Inferior parietal gyrus, excluding supramarginal and angular gyri	Parietal_Inf	IPG
67, 68	SupraMarginal gyrus	SupraMarginal	SMG
69, 70	Angular gyrus	Angular	ANG
71, 72	Precuneus	Precuneus	PCUN
73, 74	Paracentral lobule	Paracentral_Lobule	PCL
75, 76	Caudate nucleus	Caudate	CAU
77, 78	Lenticular nucleus, Putamen	Putamen	PUT
79, 80	Lenticular nucleus, Pallidum	Pallidum	PAL
81, 82	Thalamus	Thalamus	THA
83, 84	Heschl's gyrus	Heschl	HES
85, 86	Superior temporal gyrus	Temporal_Sup	STG
87, 88	Temporal pole: superior temporal gyrus	Temporal_Pole_Sup	TPOsup
89, 90	Middle temporal gyrus	Temporal_Mid	MTG
91, 92	Temporal pole: middle temporal gyrus	Temporal_Pole_Mid	TPOmid
93, 94	Inferior temporal gyrus	Temporal_Inf	ITG

Appendix - 2

List of functional connectivity links (778 links) which were significantly different between the risk-taking group and the non-risk-taking group (p<0.001 FDR corrected) in the study described in chapter 6.

Region 1	Region 2	t value	p value
ParaHippocampal_R	Postcentral_R	7.31	2.8E-13
ParaHippocampal_R	Postcentral_L	7.11	1.2E-12
ParaHippocampal_R	Paracentral_Lobule_L	7.09	1.4E-12
Paracentral_Lobule_L	Temporal_Pole_Mid_L	6.86	7.2E-12
ParaHippocampal_L	Postcentral_R	6.85	7.6E-12
Paracentral_Lobule_R	Temporal_Pole_Mid_L	6.79	1.2E-11
Postcentral_L	Postcentral_R	6.64	3.2E-11
ParaHippocampal_L	Paracentral_Lobule_L	6.64	3.3E-11
ParaHippocampal_R	Paracentral_Lobule_R	6.61	4.1E-11
Paracentral_Lobule_L	Temporal_Pole_Mid_R	6.50	8.0E-11
Rolandic_Oper_L	ParaHippocampal_R	6.48	9.4E-11
Postcentral_R	Paracentral_Lobule_R	6.46	1.0E-10
ParaHippocampal_L	Occipital_Sup_L	6.44	1.2E-10
Paracentral_Lobule_R	Temporal_Pole_Mid_R	6.39	1.7E-10
Rolandic_Oper_R	ParaHippocampal_R	6.37	1.9E-10
Supp_Motor_Area_R	Frontal_Med_Orb_L	6.36	2.0E-10
ParaHippocampal_L	Postcentral_L	6.36	2.1E-10
Precentral_R	Paracentral_Lobule_R	6.35	2.1E-10
ParaHippocampal_L	Occipital_Sup_R	6.30	3.0E-10
Supp_Motor_Area_R	ParaHippocampal_L	6.26	3.8E-10
Supp_Motor_Area_R	ParaHippocampal_R	6.23	4.7E-10
ParaHippocampal_L	Paracentral_Lobule_R	6.22	5.0E-10
Postcentral_R	Temporal_Pole_Mid_L	6.22	5.1E-10
Parietal_Sup_R	Temporal_Pole_Mid_L	6.22	5.2E-10
Rolandic_Oper_R	ParaHippocampal_L	6.21	5.2E-10
ParaHippocampal_L	Fusiform_R	6.21	5.3E-10
ParaHippocampal_L	Lingual_R	6.20	5.7E-10
Rolandic_Oper_L	ParaHippocampal_L	6.18	6.4E-10
ParaHippocampal_L	Temporal_Sup_L	6.18	6.6E-10
Postcentral_L	Paracentral_Lobule_R	6.17	7.0E-10
ParaHippocampal_L	Cuneus_R	6.15	7.8E-10
Supp_Motor_Area_R	Temporal_Pole_Mid_L	6.15	7.9E-10
Postcentral_L	Temporal_Pole_Mid_L	6.15	8.0E-10
Hippocampus_R	Postcentral_R	6.14	8.3E-10
Hippocampus_R	Paracentral_Lobule_L	6.13	8.8E-10
Postcentral_L	Temporal_Pole_Mid_R	6.12	9.6E-10
Insula_R	ParaHippocampal_L	6.10	1.1E-09
Precentral_R	Temporal_Pole_Mid_L	6.08	1.2E-09
Occipital_Sup_R	Temporal_Pole_Mid_L	6.03	1.6E-09
ParaHippocampal_L	Parietal_Sup_R	6.03	1.7E-09

Insula_L	ParaHippocampal_L	6.03	1.7E-09
Postcentral_R	Temporal_Pole_Mid_R	6.01	1.9E-09
Occipital_Sup_L	Temporal_Pole_Mid_L	5.99	2.2E-09
ParaHippocampal_L	Fusiform_L	5.98	2.3E-09
Cuneus_R	Temporal_Pole_Mid_L	5.97	2.4E-09
Hippocampus_R	Paracentral_Lobule_R	5.95	2.8E-09
Precentral_R	Postcentral_L	5.95	2.8E-09
Precentral_R	ParaHippocampal_L	5.94	2.8E-09
Precentral_R	ParaHippocampal_R	5.90	3.7E-09
Fusiform_R	Temporal_Pole_Mid_L	5.89	3.9E-09
Frontal_Med_Orb_L	Postcentral_R	5.88	4.1E-09
ParaHippocampal_L	Heschl_R	5.87	4.5E-09
Precentral_R	Paracentral_Lobule_L	5.86	4.8E-09
Rectus_R	OFCpost_R	5.83	5.5E-09
Temporal_Sup_L	Temporal_Pole_Mid_L	5.83	5.8E-09
Fusiform_L	Temporal_Pole_Sup_R	5.82	6.0E-09
ParaHippocampal_L	Occipital_Inf_R	5.81	6.4E-09
Lingual_L	Temporal_Pole_Mid_L	5.81	6.5E-09
Cuneus_L	Postcentral_R	5.80	6.8E-09
Frontal_Sup_2_R	Frontal_Med_Orb_L	5.79	7.2E-09
Temporal_Pole_Mid_L	Temporal_Inf_R	5.77	8.0E-09
Cuneus_R	Postcentral_R	5.74	9.9E-09
ParaHippocampal_R	Temporal_Sup_L	5.73	1.0E-08
ParaHippocampal_R	Temporal_Pole_Sup_R	5.72	1.1E-08
Precentral_R	Temporal_Pole_Mid_R	5.71	1.1E-08
Fusiform_L	Temporal_Pole_Mid_L	5.71	1.2E-08
Rolandic_Oper_L	Temporal_Pole_Mid_L	5.70	1.2E-08
Precentral_R	Postcentral_R	5.65	1.6E-08
Lingual_R	Temporal_Pole_Mid_L	5.65	1.6E-08
Cuneus_L	Temporal_Pole_Mid_L	5.65	1.6E-08
ParaHippocampal_L	Lingual_L	5.64	1.7E-08
ParaHippocampal_L	Temporal_Sup_R	5.61	2.1E-08
Frontal_Sup_2_R	Temporal_Pole_Mid_L	5.60	2.1E-08
ParaHippocampal_L	SupraMarginal_R	5.59	2.4E-08
Occipital_Sup_R	Postcentral_R	5.57	2.5E-08
Occipital_Mid_R	Temporal_Pole_Mid_L	5.55	2.9E-08
ParaHippocampal_L	Cuneus_L	5.54	3.1E-08
Supp_Motor_Area_R	Temporal_Pole_Mid_R	5.53	3.3E-08
Temporal_Sup_L	Temporal_Pole_Sup_R	5.51	3.7E-08
Rolandic_Oper_L	Temporal_Pole_Mid_R	5.50	3.8E-08
Temporal_Sup_R	Temporal_Pole_Mid_L	5.50	3.8E-08
Insula_R	ParaHippocampal_R	5.50	3.9E-08
Frontal_Med_Orb_L	Paracentral_Lobule_L	5.49	4.0E-08
Postcentral_R	Paracentral_Lobule_L	5.48	4.4E-08
Temporal_Sup_R	Temporal_Pole_Sup_R	5.47	4.5E-08
ParaHippocampal_L	Occipital_Inf_L	5.46	4.7E-08
ParaHippocampal_R	Temporal_Sup_R	5.46	4.9E-08

Frontal_Med_Orb_L	OFCpost_R	5.46	4.9E-08
Temporal_Sup_L	Temporal_Pole_Mid_R	5.44	5.5E-08
ParaHippocampal_R	Temporal_Pole_Sup_L	5.43	5.6E-08
Supp_Motor_Area_R	Frontal_Med_Orb_R	5.43	5.7E-08
Precentral_L	ParaHippocampal_R	5.43	5.7E-08
Frontal_Med_Orb_R	OFCpost_R	5.43	5.8E-08
ParaHippocampal_L	Temporal_Inf_R	5.42	6.1E-08
Rectus_L	Postcentral_R	5.41	6.2E-08
Precuneus_R	Temporal_Pole_Sup_L	5.41	6.3E-08
Parietal_Sup_R	Temporal_Pole_Sup_L	5.41	6.3E-08
Frontal_Med_Orb_L	Parietal_Sup_R	5.39	7.1E-08
Precentral_R	Frontal_Med_Orb_L	5.38	7.4E-08
Temporal_Pole_Sup_R	Temporal_Inf_R	5.38	7.7E-08
ParaHippocampal_L	Parietal_Sup_L	5.37	8.1E-08
Precentral_L	Precentral_R	5.36	8.4E-08
ParaHippocampal_L	Heschl_L	5.34	9.4E-08
Temporal_Pole_Sup_R	Temporal_Mid_L	5.33	9.7E-08
Parietal_Sup_R	Temporal_Pole_Sup_R	5.33	9.7E-08
Cuneus_R	Paracentral_Lobule_R	5.33	9.8E-08
Rolandic_Oper_L	Rectus_R	5.33	9.8E-08
Hippocampus_R	Postcentral_L	5.33	1.0E-07
Supp_Motor_Area_L	Temporal_Pole_Sup_R	5.32	1.0E-07
Fusiform_L	Temporal_Pole_Sup_L	5.32	1.1E-07
ParaHippocampal_L	Occipital_Mid_R	5.31	1.1E-07
Rolandic_Oper_R	Temporal_Pole_Mid_L	5.30	1.2E-07
Occipital_Mid_L	Temporal_Pole_Mid_L	5.29	1.2E-07
Temporal_Sup_L	Temporal_Sup_R	5.29	1.3E-07
Frontal_Sup_2_R	Frontal_Med_Orb_R	5.28	1.3E-07
Cuneus_R	Temporal_Pole_Mid_R	5.27	1.4E-07
ParaHippocampal_R	Fusiform_R	5.27	1.4E-07
Insula_R	Parietal_Inf_L	5.26	1.5E-07
Supp_Motor_Area_R	Rectus_R	5.25	1.5E-07
Precentral_L	Temporal_Pole_Mid_R	5.24	1.6E-07
Frontal_Med_Orb_R	Postcentral_R	5.24	1.6E-07
Fusiform_R	Temporal_Pole_Sup_R	5.24	1.6E-07
Frontal_Med_Orb_L	Paracentral_Lobule_R	5.23	1.7E-07
ParaHippocampal_L	Occipital_Mid_L	5.23	1.7E-07
Rolandic_Oper_L	Temporal_Pole_Sup_R	5.21	1.9E-07
Fusiform_L	Postcentral_R	5.21	1.9E-07
Temporal_Pole_Sup_L	Temporal_Pole_Sup_R	5.20	2.0E-07
Rectus_R	Postcentral_R	5.20	2.0E-07
Fusiform_R	Temporal_Pole_Mid_R	5.19	2.1E-07
Supp_Motor_Area_R	Temporal_Pole_Sup_R	5.18	2.2E-07
Occipital_Sup_L	Temporal_Pole_Mid_R	5.17	2.3E-07
Heschl_L	Heschl_R	5.17	2.4E-07
Precuneus_R	Heschl_R	5.16	2.5E-07
Occipital_Sup_L	Postcentral_R	5.16	2.5E-07

Precentral_L	ParaHippocampal_L	5.16	2.5E-07
Frontal_Med_Orb_L	Postcentral_L	5.15	2.6E-07
Rolandic_Oper_R	Temporal_Pole_Mid_R	5.15	2.6E-07
Insula_L	ParaHippocampal_R	5.14	2.8E-07
Supp_Motor_Area_R	Hippocampus_R	5.14	2.8E-07
Insula_R	Precuneus_R	5.14	2.8E-07
Rolandic_Oper_R	Rectus_R	5.13	3.0E-07
Frontal_Med_Orb_R	Paracentral_Lobule_L	5.13	3.0E-07
Supp_Motor_Area_L	ParaHippocampal_R	5.12	3.1E-07
Precentral_L	Temporal_Pole_Mid_L	5.11	3.2E-07
Frontal_Sup_2_L	Frontal_Med_Orb_L	5.11	3.2E-07
Precentral_R	Rectus_R	5.09	3.5E-07
Temporal_Mid_R	Temporal_Pole_Mid_L	5.09	3.6E-07
Frontal_Med_Orb_L	Temporal_Inf_R	5.08	3.8E-07
Rolandic_Oper_L	Precuneus_R	5.08	3.9E-07
Precentral_R	Hippocampus_R	5.08	3.9E-07
Cuneus_L	Postcentral_L	5.08	3.9E-07
Rectus_R	Postcentral_L	5.07	3.9E-07
Parietal_Sup_L	Temporal_Pole_Mid_L	5.06	4.2E-07
ParaHippocampal_R	Heschl_R	5.06	4.3E-07
ParaHippocampal_L	Calcarine_R	5.05	4.3E-07
Parietal_Sup_L	Temporal_Pole_Sup_R	5.05	4.4E-07
OFCmed_R	Heschl_L	5.05	4.4E-07
Frontal_Med_Orb_L	Occipital_Sup_L	5.05	4.5E-07
Lingual_R	Temporal_Pole_Mid_R	5.05	4.5E-07
Frontal_Med_Orb_L	Cingulate_Ant_R	5.05	4.6E-07
OFCmed_L	Insula_R	5.04	4.6E-07
Temporal_Sup_R	Temporal_Pole_Sup_L	5.04	4.7E-07
Frontal_Sup_2_R	Cingulate_Post_L	5.04	4.7E-07
OFCpost_R	Angular_L	5.03	5.0E-07
ParaHippocampal_L	SupraMarginal_L	5.03	5.1E-07
Paracentral_Lobule_R	Temporal_Pole_Sup_R	5.03	5.1E-07
Supp_Motor_Area_R	OFClat_L	5.01	5.5E-07
Rectus_R	Insula_R	5.00	5.7E-07
OFCmed_R	Insula_R	5.00	5.7E-07
Frontal_Med_Orb_L	Occipital_Sup_R	5.00	5.8E-07
Occipital_Sup_R	Temporal_Pole_Mid_R	5.00	5.8E-07
Fusiform_R	Postcentral_R	5.00	5.9E-07
Temporal_Pole_Sup_L	Temporal_Mid_R	4.99	6.2E-07
Frontal_Med_Orb_L	Lingual_L	4.98	6.3E-07
Rectus_L	OFCpost_R	4.98	6.4E-07
Cuneus_R	Paracentral_Lobule_L	4.98	6.4E-07
Occipital_Sup_R	Paracentral_Lobule_R	4.98	6.5E-07
Postcentral_L	Paracentral_Lobule_L	4.97	6.7E-07
Precentral_L	Postcentral_R	4.97	6.7E-07
Cingulate_Mid_L	Heschl_R	4.97	6.8E-07
Paracentral_Lobule_L	Temporal_Pole_Sup_R	4.95	7.5E-07

Temporal_Sup_L	Temporal_Mid_L	4.95	7.5E-07
Calcarine_R	Temporal_Pole_Mid_L	4.95	7.6E-07
Frontal_Sup_2_R	Frontal_Sup_Medial_L	4.94	7.7E-07
Cingulate_Mid_L	ParaHippocampal_L	4.94	7.9E-07
Fusiform_L	Temporal_Pole_Mid_R	4.94	7.9E-07
Parietal_Inf_L	Heschl_R	4.93	8.2E-07
Fusiform_R	Temporal_Pole_Sup_L	4.93	8.2E-07
Cuneus_R	Postcentral_L	4.93	8.3E-07
Rectus_L	Postcentral_L	4.92	8.7E-07
ParaHippocampal_R	Occipital_Sup_R	4.92	8.8E-07
Temporal_Pole_Sup_L	Temporal_Inf_R	4.92	8.9E-07
Occipital_Mid_L	Postcentral_R	4.91	9.2E-07
OFCmed_R	Temporal_Pole_Sup_R	4.90	9.5E-07
Frontal_Med_Orb_L	Fusiform_L	4.90	9.7E-07
Precentral_L	Paracentral_Lobule_R	4.90	9.7E-07
Heschl_L	Temporal_Pole_Mid_R	4.90	9.8E-07
Cuneus_L	Temporal_Pole_Mid_R	4.89	1.0E-06
Temporal_Pole_Sup_R	Temporal_Mid_R	4.89	1.0E-06
Cuneus_L	Paracentral_Lobule_R	4.89	1.0E-06
ParaHippocampal_R	Lingual_R	4.88	1.0E-06
Paracentral_Lobule_R	Temporal_Pole_Sup_L	4.88	1.0E-06
Heschl_L	Temporal_Pole_Sup_R	4.88	1.1E-06
Occipital_Mid_R	Postcentral_R	4.88	1.1E-06
Rolandic_Oper_L	Frontal_Med_Orb_L	4.88	1.1E-06
ParaHippocampal_L	Calcarine_L	4.88	1.1E-06
Rolandic_Oper_L	Temporal_Sup_R	4.87	1.1E-06
Precuneus_R	Temporal_Pole_Sup_R	4.87	1.1E-06
Frontal_Med_Orb_L	Fusiform_R	4.87	1.1E-06
Temporal_Pole_Sup_R	Temporal_Pole_Mid_L	4.86	1.2E-06
Temporal_Sup_L	Temporal_Pole_Sup_L	4.86	1.2E-06
Rolandic_Oper_L	Temporal_Mid_R	4.85	1.2E-06
ParaHippocampal_L	Temporal_Pole_Sup_R	4.85	1.3E-06
OFCpost_L	Insula_R	4.84	1.3E-06
Cuneus_L	Temporal_Pole_Sup_L	4.84	1.3E-06
Rolandic_Oper_L	Temporal_Pole_Sup_L	4.82	1.5E-06
Supp_Motor_Area_L	Supp_Motor_Area_R	4.82	1.5E-06
Temporal_Pole_Mid_R	Temporal_Inf_R	4.81	1.5E-06
Supp_Motor_Area_R	Temporal_Pole_Sup_L	4.81	1.5E-06
Temporal_Sup_R	Temporal_Pole_Mid_R	4.81	1.5E-06
ParaHippocampal_R	Fusiform_L	4.81	1.5E-06
OFCpost_R	Cingulate_Post_L	4.81	1.5E-06
ParaHippocampal_R	Heschl_L	4.80	1.6E-06
Temporal_Pole_Sup_R	Temporal_Pole_Mid_R	4.80	1.6E-06
Precuneus_L	Heschl_R	4.79	1.7E-06
Supp_Motor_Area_R	Rectus_L	4.79	1.7E-06
Rectus_L	Paracentral_Lobule_L	4.79	1.7E-06
Insula_L	Temporal_Pole_Sup_R	4.79	1.7E-06

Parietal_Sup_R	Temporal_Pole_Mid_R	4.79	1.7E-06
Paracentral_Lobule_L	Paracentral_Lobule_R	4.79	1.7E-06
Calcarine_L	Temporal_Pole_Mid_L	4.79	1.7E-06
Frontal_Med_Orb_L	Cuneus_R	4.78	1.8E-06
Cuneus_R	Temporal_Pole_Sup_L	4.78	1.8E-06
Insula_L	Precuneus_R	4.78	1.8E-06
Cingulate_Ant_R	Cingulate_Post_L	4.77	1.8E-06
Supp_Motor_Area_R	Angular_L	4.77	1.8E-06
Precentral_R	Rectus_L	4.77	1.9E-06
Precuneus_R	Temporal_Pole_Mid_L	4.77	1.9E-06
Lingual_L	Temporal_Pole_Mid_R	4.77	1.9E-06
ParaHippocampal_L	ParaHippocampal_R	4.76	1.9E-06
Frontal_Sup_2_L	Frontal_Med_Orb_R	4.76	1.9E-06
Rectus_R	Heschl_L	4.76	2.0E-06
SupraMarginal_R	Temporal_Pole_Mid_L	4.75	2.0E-06
Rolandic_Oper_R	Temporal_Pole_Sup_R	4.75	2.0E-06
Frontal_Med_Orb_L	Heschl_R	4.75	2.1E-06
Rectus_R	Paracentral_Lobule_L	4.74	2.2E-06
Rolandic_Oper_L	Fusiform_L	4.74	2.2E-06
ParaHippocampal_R	Cuneus_R	4.74	2.2E-06
Frontal_Inf_Orb_2_L	Supp_Motor_Area_R	4.74	2.2E-06
Fusiform_L	Temporal_Sup_L	4.73	2.2E-06
Rolandic_Oper_R	Precuneus_R	4.73	2.3E-06
Fusiform_L	Paracentral_Lobule_R	4.73	2.3E-06
OFCmed_R	Temporal_Pole_Sup_L	4.72	2.4E-06
Rolandic_Oper_R	OFCmed_R	4.72	2.4E-06
SupraMarginal_L	Temporal_Pole_Sup_L	4.71	2.4E-06
Frontal_Med_Orb_L	Calcarine_L	4.71	2.4E-06
Rolandic_Oper_L	OFCmed_R	4.71	2.4E-06
Frontal_Med_Orb_R	Parietal_Sup_R	4.71	2.4E-06
OFCmed_R	OFCpost_R	4.71	2.5E-06
ParaHippocampal_R	SupraMarginal_L	4.71	2.5E-06
ParaHippocampal_R	Occipital_Sup_L	4.70	2.6E-06
Postcentral_L	Temporal_Pole_Sup_R	4.70	2.6E-06
Lingual_R	Postcentral_R	4.70	2.6E-06
Postcentral_R	Temporal_Pole_Sup_R	4.70	2.6E-06
Frontal_Med_Orb_L	Parietal_Sup_L	4.70	2.6E-06
Frontal_Med_Orb_R	Paracentral_Lobule_R	4.70	2.7E-06
Occipital_Sup_R	Postcentral_L	4.70	2.7E-06
Precentral_L	Frontal_Med_Orb_L	4.70	2.7E-06
Precuneus_R	Heschl_L	4.69	2.8E-06
OFCpost_L	OFCpost_R	4.68	2.8E-06
Precentral_L	Hippocampus_R	4.68	2.8E-06
Rolandic_Oper_L	Temporal_Mid_L	4.68	2.9E-06
Rolandic_Oper_L	Rectus_L	4.68	2.9E-06
Frontal_Inf_Tri_R	Cingulate_Post_L	4.66	3.1E-06
Rolandic_Oper_R	Frontal_Med_Orb_L	4.66	3.1E-06

Precuneus_R	Temporal_Sup_L	4.66	3.2E-06
Rectus_L	Paracentral_Lobule_R	4.66	3.2E-06
Frontal_Inf_Oper_R	Frontal_Med_Orb_L	4.66	3.2E-06
Cingulate_Mid_R	ParaHippocampal_L	4.66	3.2E-06
Heschl_L	Temporal_Pole_Mid_L	4.66	3.2E-06
Rolandic_Oper_R	Parietal_Inf_L	4.65	3.4E-06
ParaHippocampal_R	Parietal_Sup_R	4.64	3.4E-06
Frontal_Med_Orb_L	Insula_R	4.64	3.4E-06
Postcentral_L	Caudate_R	-4.64	3.5E-06
Frontal_Med_Orb_L	Cingulate_Mid_R	4.64	3.5E-06
Fusiform_L	Postcentral_L	4.64	3.5E-06
Frontal_Sup_2_R	Rectus_L	4.64	3.5E-06
Occipital_Sup_R	Paracentral_Lobule_L	4.64	3.5E-06
Frontal_Inf_Tri_R	Frontal_Med_Orb_L	4.64	3.5E-06
Rolandic_Oper_L	Parietal_Sup_R	4.64	3.6E-06
Frontal_Med_Orb_L	Calcarine_R	4.63	3.6E-06
Frontal_Med_Orb_R	Temporal_Inf_R	4.62	3.8E-06
Rectus_R	Temporal_Pole_Sup_R	4.62	3.8E-06
Precentral_L	Temporal_Pole_Sup_R	4.62	3.8E-06
Rectus_L	Temporal_Inf_R	4.62	3.9E-06
Rolandic_Oper_R	Heschl_R	4.62	4.0E-06
Insula_R	Cingulate_Post_L	4.61	4.0E-06
Cingulate_Post_L	SupraMarginal_R	4.61	4.0E-06
ParaHippocampal_R	Temporal_Inf_R	4.61	4.1E-06
ParaHippocampal_R	Occipital_Inf_R	4.60	4.2E-06
Cuneus_L	Temporal_Pole_Sup_R	4.60	4.3E-06
Rolandic_Oper_R	Temporal_Mid_L	4.59	4.4E-06
Rolandic_Oper_R	Rectus_L	4.59	4.4E-06
Lingual_R	Temporal_Pole_Sup_L	4.59	4.4E-06
SupraMarginal_L	Temporal_Pole_Sup_R	4.59	4.5E-06
Olfactory_L	Olfactory_R	4.59	4.5E-06
Lingual_R	Temporal_Pole_Sup_R	4.59	4.5E-06
OFCpost_L	Cingulate_Mid_R	4.59	4.5E-06
Insula_L	Parietal_Inf_L	4.58	4.6E-06
Rolandic_Oper_L	Precuneus_L	4.58	4.6E-06
Supp_Motor_Area_L	ParaHippocampal_L	4.58	4.6E-06
Insula_R	Precuneus_L	4.58	4.7E-06
Parietal_Inf_L	Temporal_Sup_L	4.58	4.8E-06
Frontal_Med_Orb_L	Lingual_R	4.57	4.8E-06
Rolandic_Oper_R	Temporal_Pole_Sup_L	4.57	4.8E-06
Temporal_Pole_Mid_L	Temporal_Pole_Mid_R	4.57	4.9E-06
Rolandic_Oper_L	Temporal_Inf_R	4.57	5.0E-06
Rolandic_Oper_R	Fusiform_L	4.57	5.0E-06
Heschl_R	Temporal_Pole_Sup_R	4.56	5.1E-06
Cuneus_R	Temporal_Pole_Sup_R	4.55	5.3E-06
Rolandic_Oper_R	OFCmed_L	4.55	5.3E-06
Fusiform_R	Paracentral_Lobule_R	4.55	5.4E-06

Lingual_L	Postcentral_R	4.55	5.4E-06
Hippocampus_R	Occipital_Sup_R	4.55	5.4E-06
OFCmed_L	Heschl_R	4.55	5.4E-06
Supp_Motor_Area_R	Temporal_Mid_L	4.54	5.5E-06
Frontal_Sup_Medial_R	Frontal_Med_Orb_R	4.54	5.6E-06
Fusiform_L	Temporal_Sup_R	4.54	5.7E-06
Precuneus_L	Temporal_Sup_L	4.54	5.7E-06
Cingulate_Post_L	Heschl_R	4.54	5.7E-06
Cuneus_L	Paracentral_Lobule_L	4.53	6.0E-06
Cingulate_Post_L	SupraMarginal_L	4.53	6.0E-06
Insula_R	Angular_R	4.53	6.0E-06
Occipital_Mid_R	Temporal_Pole_Sup_L	4.53	6.0E-06
OFCmed_L	Temporal_Pole_Sup_R	4.52	6.1E-06
OFCmed_R	Heschl_R	4.52	6.3E-06
Occipital_Inf_L	Postcentral_R	4.52	6.3E-06
Hippocampus_R	Occipital_Sup_L	4.51	6.4E-06
Frontal_Inf_Oper_R	ParaHippocampal_L	4.51	6.4E-06
Rectus_R	Temporal_Inf_R	4.51	6.6E-06
Frontal_Inf_Oper_R	Temporal_Pole_Mid_L	4.51	6.6E-06
Fusiform_R	Postcentral_L	4.51	6.7E-06
Occipital_Inf_L	Temporal_Pole_Mid_L	4.50	6.7E-06
Heschl_R	Temporal_Inf_L	4.50	6.8E-06
ParaHippocampal_R	Parietal_Sup_L	4.50	7.0E-06
Supp_Motor_Area_L	Frontal_Med_Orb_R	4.50	7.0E-06
Supp_Motor_Area_L	Rectus_R	4.50	7.0E-06
Insula_R	Cingulate_Mid_L	4.49	7.1E-06
Calcarine_R	Temporal_Pole_Mid_R	4.49	7.1E-06
Occipital_Mid_R	Postcentral_L	4.49	7.1E-06
Occipital_Sup_L	Paracentral_Lobule_R	4.49	7.3E-06
Precentral_L	Rectus_R	4.49	7.3E-06
Occipital_Inf_L	Temporal_Pole_Sup_R	4.48	7.3E-06
Parietal_Sup_R	Heschl_R	4.48	7.4E-06
Rectus_R	Temporal_Sup_L	4.48	7.5E-06
Cingulate_Mid_L	Heschl_L	4.48	7.5E-06
Rectus_R	Heschl_R	4.48	7.6E-06
Parietal_Sup_L	Temporal_Pole_Sup_L	4.48	7.7E-06
Frontal_Sup_Medial_L	Frontal_Sup_Medial_R	4.47	7.7E-06
Precentral_L	Paracentral_Lobule_L	4.47	7.9E-06
Rolandic_Oper_R	OFClat_L	4.47	7.9E-06
Cingulate_Mid_R	Heschl_R	4.47	7.9E-06
Temporal_Sup_R	Temporal_Mid_L	4.47	8.0E-06
Cingulate_Mid_L	Cingulate_Mid_R	4.46	8.3E-06
Insula_L	Cingulate_Mid_L	4.46	8.4E-06
Insula_L	Temporal_Pole_Sup_L	4.45	8.5E-06
Frontal_Inf_Orb_2_R	Rectus_L	4.45	8.7E-06
Parietal_Sup_L	Temporal_Pole_Mid_R	4.45	8.8E-06
Heschl_R	Temporal_Pole_Mid_R	4.44	8.8E-06

Supp_Motor_Area_R	OFCpost_L	4.44	8.9E-06
Frontal_Sup_Medial_L	OFCpost_R	4.44	9.0E-06
Frontal_Sup_Medial_L	Frontal_Med_Orb_R	4.44	9.1E-06
Rolandic_Oper_L	Heschl_R	4.44	9.1E-06
Occipital_Inf_R	Temporal_Pole_Mid_L	4.43	9.3E-06
Insula_R	Temporal_Pole_Mid_L	4.43	9.3E-06
Rolandic_Oper_L	Fusiform_R	4.43	9.3E-06
Lingual_R	Paracentral_Lobule_R	4.43	9.4E-06
Frontal_Med_Orb_R	Postcentral_L	4.43	9.4E-06
Rolandic_Oper_R	Temporal_Sup_R	4.43	9.6E-06
Fusiform_L	Heschl_R	4.42	9.8E-06
Frontal_Sup_Medial_R	OFCpost_R	4.42	9.8E-06
Rectus_R	Temporal_Sup_R	4.42	9.9E-06
Occipital_Mid_L	Temporal_Pole_Mid_R	4.42	9.9E-06
Heschl_L	Temporal_Sup_R	4.42	1.0E-05
OFCpost_L	Insula_L	4.41	1.0E-05
OFCpost_R	Temporal_Pole_Mid_L	4.41	1.0E-05
Thalamus_L	Thalamus_R	4.41	1.0E-05
Lingual_L	Temporal_Pole_Sup_L	4.41	1.0E-05
Frontal_Sup_Medial_R	Frontal_Med_Orb_L	4.41	1.0E-05
Frontal_Inf_Tri_R	Temporal_Pole_Mid_L	4.41	1.1E-05
Supp_Motor_Area_L	Frontal_Med_Orb_L	4.40	1.1E-05
Fusiform_L	Precuneus_L	4.40	1.1E-05
ParaHippocampal_R	Lingual_L	4.40	1.1E-05
Temporal_Pole_Sup_L	Temporal_Pole_Mid_R	4.40	1.1E-05
Supp_Motor_Area_L	Temporal_Pole_Mid_R	4.40	1.1E-05
Frontal_Med_Orb_L	Cuneus_L	4.40	1.1E-05
Rectus_L	Parietal_Sup_R	4.39	1.1E-05
Postcentral_L	Parietal_Sup_R	4.39	1.2E-05
Rectus_L	Amygdala_R	4.39	1.2E-05
Insula_R	Temporal_Pole_Sup_R	4.39	1.2E-05
Rolandic_Oper_L	OFCmed_L	4.39	1.2E-05
Occipital_Sup_R	Temporal_Pole_Sup_L	4.38	1.2E-05
Postcentral_R	Temporal_Pole_Sup_L	4.38	1.2E-05
Occipital_Mid_R	Temporal_Pole_Sup_R	4.38	1.2E-05
OFCpost_L	Precuneus_R	4.38	1.2E-05
Postcentral_L	Temporal_Pole_Sup_L	4.37	1.2E-05
Rolandic_Oper_L	Cuneus_L	4.37	1.3E-05
ParaHippocampal_R	Occipital_Inf_L	4.36	1.3E-05
Rolandic_Oper_L	Temporal_Sup_L	4.36	1.3E-05
ParaHippocampal_L	Temporal_Mid_R	4.36	1.3E-05
Heschl_R	Temporal_Pole_Mid_L	4.36	1.3E-05
Fusiform_R	Temporal_Sup_L	4.36	1.3E-05
Hippocampus_R	Parietal_Sup_R	4.36	1.3E-05
Frontal_Inf_Orb_2_R	Rectus_R	4.35	1.3E-05
Heschl_L	Temporal_Sup_L	4.35	1.4E-05
Temporal_Sup_L	Temporal_Inf_R	4.35	1.4E-05

SupraMarginal_L	Temporal_Pole_Mid_L	4.35	1.4E-05
Heschl_R	Temporal_Mid_L	4.35	1.4E-05
Frontal_Inf_Orb_2_R	Cingulate_Post_L	4.34	1.4E-05
Hippocampus_L	Postcentral_R	4.34	1.4E-05
Occipital_Mid_L	Temporal_Pole_Sup_R	4.34	1.4E-05
Frontal_Med_Orb_R	OFCpost_L	4.34	1.4E-05
ParaHippocampal_R	Temporal_Pole_Mid_L	4.34	1.4E-05
Frontal_Inf_Orb_2_R	Frontal_Med_Orb_L	4.34	1.5E-05
Frontal_Med_Orb_L	Insula_L	4.33	1.5E-05
Rectus_R	Fusiform_R	4.33	1.5E-05
Rolandic_Oper_R	OFCpost_L	4.33	1.5E-05
Heschl_R	Temporal_Sup_R	4.32	1.5E-05
Rectus_R	Temporal_Pole_Sup_L	4.32	1.5E-05
Precuneus_L	Temporal_Pole_Sup_R	4.32	1.6E-05
ParaHippocampal_R	Cuneus_L	4.32	1.6E-05
Fusiform_L	Precuneus_R	4.31	1.6E-05
Insula_L	Temporal_Pole_Mid_R	4.31	1.6E-05
Rolandic_Oper_R	Precuneus_L	4.31	1.6E-05
Frontal_Med_Orb_L	Occipital_Mid_L	4.31	1.7E-05
Precentral_R	Frontal_Med_Orb_R	4.31	1.7E-05
Heschl_R	Temporal_Sup_L	4.30	1.7E-05
Rectus_L	Fusiform_R	4.30	1.7E-05
Paracentral_Lobule_L	Temporal_Pole_Sup_L	4.30	1.7E-05
Hippocampus_L	Paracentral_Lobule_L	4.30	1.7E-05
Rolandic_Oper_R	Temporal_Mid_R	4.30	1.7E-05
Frontal_Med_Orb_L	SupraMarginal_R	4.29	1.8E-05
Frontal_Med_Orb_R	Parietal_Sup_L	4.29	1.8E-05
Insula_R	Cingulate_Mid_R	4.29	1.8E-05
SupraMarginal_R	Temporal_Pole_Sup_L	4.28	1.8E-05
Fusiform_L	Heschl_L	4.28	1.8E-05
OFCpost_L	Cingulate_Ant_R	4.28	1.8E-05
Parietal_Sup_L	Temporal_Sup_L	4.28	1.9E-05
Frontal_Sup_2_R	Temporal_Pole_Mid_R	4.28	1.9E-05
Precuneus_L	Temporal_Pole_Sup_L	4.28	1.9E-05
OFCpost_R	Angular_R	4.28	1.9E-05
Frontal_Inf_Tri_R	ParaHippocampal_L	4.28	1.9E-05
Precentral_R	Caudate_R	-4.26	2.0E-05
Rectus_R	OFCmed_R	4.26	2.0E-05
Postcentral_L	Caudate_L	-4.26	2.1E-05
Occipital_Sup_L	Temporal_Pole_Sup_L	4.26	2.1E-05
Temporal_Sup_L	Temporal_Mid_R	4.26	2.1E-05
Fusiform_L	Temporal_Mid_R	4.26	2.1E-05
Rolandic_Oper_L	Paracentral_Lobule_R	4.25	2.1E-05
Rectus_R	Insula_L	4.25	2.1E-05
ParaHippocampal_L	Temporal_Pole_Sup_L	4.25	2.2E-05
Frontal_Sup_2_R	Rectus_R	4.25	2.2E-05
Heschl_R	Temporal_Inf_R	4.25	2.2E-05

Occipital_Sup_L	Postcentral_L	4.25	2.2E-05
Rectus_L	Fusiform_L	4.24	2.2E-05
OFCpost_L	ParaHippocampal_R	4.24	2.2E-05
Olfactory_R	Cingulate_Ant_L	4.24	2.2E-05
OFCpost_L	Heschl_R	4.23	2.3E-05
Parietal_Sup_R	Temporal_Sup_L	4.23	2.3E-05
Rolandic_Oper_R	Parietal_Sup_R	4.23	2.3E-05
Fusiform_L	Paracentral_Lobule_L	4.23	2.4E-05
Rectus_R	Parietal_Sup_R	4.23	2.4E-05
Frontal_Inf_Orb_2_L	Precuneus_R	4.22	2.4E-05
OFCmed_L	Temporal_Pole_Sup_L	4.22	2.4E-05
Lingual_L	Temporal_Pole_Sup_R	4.22	2.4E-05
Rolandic_Oper_L	Frontal_Med_Orb_R	4.21	2.5E-05
Insula_R	Angular_L	4.21	2.5E-05
Frontal_Inf_Oper_R	Rectus_R	4.21	2.6E-05
Rectus_L	Insula_R	4.21	2.6E-05
Lingual_L	Paracentral_Lobule_R	4.21	2.6E-05
Rolandic_Oper_R	Frontal_Med_Orb_R	4.20	2.6E-05
Rectus_R	Paracentral_Lobule_R	4.20	2.7E-05
Frontal_Inf_Orb_2_R	Frontal_Med_Orb_R	4.20	2.7E-05
Postcentral_R	SupraMarginal_R	-4.20	2.7E-05
Cingulate_Mid_L	ParaHippocampal_R	4.19	2.7E-05
Cingulate_Mid_R	Cingulate_Post_L	4.19	2.7E-05
Cingulate_Mid_R	Heschl_L	4.19	2.8E-05
Temporal_Sup_L	Temporal_Inf_L	4.19	2.8E-05
Frontal_Med_Orb_L	Cingulate_Mid_L	4.19	2.8E-05
OFCmed_L	Temporal_Sup_R	4.19	2.8E-05
Fusiform_R	Paracentral_Lobule_L	4.19	2.8E-05
Hippocampus_R	ParaHippocampal_R	4.19	2.9E-05
OFClat_L	Postcentral_R	4.19	2.9E-05
Parietal_Sup_L	Heschl_R	4.18	2.9E-05
OFCpost_L	Temporal_Pole_Sup_R	4.18	2.9E-05
Occipital_Mid_R	Temporal_Pole_Mid_R	4.18	2.9E-05
Insula_L	Precuneus_L	4.18	3.0E-05
Rolandic_Oper_L	Parietal_Sup_L	4.18	3.0E-05
Occipital_Mid_L	Postcentral_L	4.17	3.0E-05
Rolandic_Oper_R	Temporal_Sup_L	4.17	3.1E-05
Postcentral_L	Putamen_L	-4.17	3.1E-05
Occipital_Sup_R	Temporal_Pole_Sup_R	4.17	3.1E-05
Rolandic_Oper_L	Parietal_Inf_L	4.17	3.1E-05
Frontal_Inf_Oper_R	Temporal_Pole_Mid_R	4.17	3.1E-05
OFCpost_L	Cingulate_Mid_L	4.16	3.2E-05
Frontal_Med_Orb_L	Temporal_Sup_L	4.16	3.2E-05
Insula_R	Temporal_Pole_Mid_R	4.16	3.2E-05
Cingulate_Mid_L	Temporal_Pole_Sup_R	4.16	3.3E-05
OFCmed_L	Cingulate_Mid_R	4.15	3.3E-05
Temporal_Pole_Sup_L	Temporal_Mid_L	4.15	3.3E-05

Frontal_Med_Orb_L	OFCant_R	4.15	3.3E-05
Insula_R	Temporal_Pole_Sup_L	4.15	3.3E-05
Frontal_Med_Orb_L	Occipital_Inf_R	4.15	3.3E-05
OFCmed_L	Temporal_Sup_L	4.15	3.3E-05
Frontal_Med_Orb_L	ParaHippocampal_R	4.15	3.3E-05
Rectus_L	OFCmed_L	4.15	3.3E-05
Supp_Motor_Area_L	Temporal_Sup_R	4.15	3.3E-05
Parietal_Inf_L	Temporal_Pole_Sup_R	4.15	3.3E-05
Cingulate_Mid_L	Precuneus_R	4.15	3.3E-05
ParaHippocampal_R	Occipital_Mid_L	4.15	3.3E-05
ParaHippocampal_R	SupraMarginal_R	4.15	3.4E-05
Rectus_L	Temporal_Sup_L	4.15	3.4E-05
Occipital_Mid_R	Paracentral_Lobule_R	4.14	3.4E-05
Cingulate_Mid_R	Temporal_Pole_Mid_L	4.14	3.4E-05
Angular_L	Temporal_Sup_L	4.14	3.5E-05
Temporal_Pole_Sup_L	Temporal_Pole_Mid_L	4.14	3.5E-05
OFClat_L	Insula_R	4.14	3.5E-05
Cingulate_Mid_R	Precuneus_R	4.14	3.5E-05
OFCmed_R	Insula_L	4.13	3.6E-05
Frontal_Inf_Tri_R	OFCpost_L	4.13	3.7E-05
Rolandic_Oper_R	Heschl_L	4.12	3.7E-05
Hippocampus_R	Amygdala_R	4.12	3.7E-05
Occipital_Sup_L	Temporal_Pole_Sup_R	4.12	3.8E-05
Occipital_Mid_L	Temporal_Pole_Sup_L	4.12	3.8E-05
Frontal_Med_Orb_L	Occipital_Mid_R	4.12	3.8E-05
Frontal_Sup_2_L	Temporal_Pole_Sup_R	4.12	3.9E-05
Heschl_L	Temporal_Pole_Sup_L	4.12	3.9E-05
ParaHippocampal_R	Amygdala_R	4.12	3.9E-05
Frontal_Med_Orb_R	OFCmed_R	4.12	3.9E-05
Rolandic_Oper_R	Parietal_Sup_L	4.11	3.9E-05
Rolandic_Oper_R	Temporal_Inf_R	4.11	3.9E-05
Frontal_Sup_2_R	Angular_L	4.11	3.9E-05
Cingulate_Mid_R	Temporal_Pole_Sup_L	4.11	4.0E-05
OFCpost_L	Heschl_L	4.11	4.0E-05
Frontal_Inf_Oper_R	Cingulate_Post_L	4.11	4.0E-05
OFCmed_L	Heschl_L	4.10	4.1E-05
Occipital_Mid_L	Paracentral_Lobule_R	4.10	4.1E-05
Calcarine_L	Temporal_Pole_Mid_R	4.10	4.1E-05
Rectus_R	Calcarine_R	4.10	4.2E-05
Frontal_Med_Orb_R	Heschl_R	4.10	4.2E-05
Rolandic_Oper_L	Rolandic_Oper_R	4.10	4.2E-05
Fusiform_R	Temporal_Sup_R	4.09	4.3E-05
Precuneus_L	Heschl_L	4.09	4.3E-05
Frontal_Inf_Orb_2_R	Temporal_Pole_Mid_L	4.09	4.3E-05
Frontal_Sup_2_R	OFCpost_L	4.09	4.4E-05
Postcentral_R	Caudate_R	-4.09	4.4E-05
Rolandic_Oper_L	OFCpost_L	4.09	4.4E-05

Rectus_L	ParaHippocampal_R	4.08	4.4E-05
SupraMarginal_R	Angular_L	4.08	4.5E-05
Parietal_Inf_L	Heschl_L	4.08	4.5E-05
Rectus_L	Temporal_Mid_R	4.08	4.5E-05
Frontal_Med_Orb_L	OFCmed_L	4.07	4.8E-05
Occipital_Inf_R	Temporal_Pole_Sup_R	4.07	4.8E-05
Heschl_L	Temporal_Mid_R	4.06	4.9E-05
ParaHippocampal_R	Temporal_Pole_Mid_R	4.06	4.9E-05
Heschl_L	Temporal_Mid_L	4.06	5.0E-05
Occipital_Mid_R	Paracentral_Lobule_L	4.06	5.0E-05
OFCmed_L	Temporal_Mid_R	4.06	5.0E-05
Insula_L	Cingulate_Mid_R	4.06	5.0E-05
Frontal_Inf_Tri_L	Supp_Motor_Area_R	4.05	5.0E-05
Frontal_Sup_2_L	Cingulate_Post_L	4.05	5.0E-05
Frontal_Sup_2_R	Temporal_Pole_Sup_R	4.05	5.1E-05
Frontal_Sup_Medial_L	Cingulate_Ant_R	4.05	5.1E-05
Rectus_R	OFCant_R	4.05	5.1E-05
Frontal_Med_Orb_R	Fusiform_R	4.05	5.2E-05
Rectus_L	Lingual_L	4.05	5.2E-05
Frontal_Med_Orb_L	Frontal_Med_Orb_R	4.04	5.3E-05
Insula_L	Cingulate_Post_L	4.04	5.3E-05
Rolandic_Oper_R	Fusiform_R	4.04	5.3E-05
OFCmed_R	ParaHippocampal_L	4.04	5.3E-05
Frontal_Inf_Tri_R	Temporal_Pole_Sup_L	4.04	5.4E-05
OFCmed_L	Cingulate_Mid_L	4.03	5.5E-05
Supp_Motor_Area_R	Cingulate_Post_L	4.03	5.6E-05
Supp_Motor_Area_L	Temporal_Pole_Sup_L	4.03	5.7E-05
Cingulate_Mid_R	ParaHippocampal_R	4.03	5.7E-05
Fusiform_R	Heschl_L	4.02	5.7E-05
Occipital_Sup_L	Paracentral_Lobule_L	4.02	5.7E-05
Cingulate_Mid_R	Temporal_Pole_Sup_R	4.02	5.8E-05
Occipital_Inf_R	Paracentral_Lobule_R	4.02	5.8E-05
Rectus_R	Cuneus_R	4.02	5.9E-05
Cingulate_Ant_R	Cingulate_Post_R	4.01	6.0E-05
Frontal_Inf_Tri_R	Frontal_Inf_Orb_2_L	4.01	6.1E-05
Rectus_R	Calcarine_L	4.01	6.1E-05
Cingulate_Post_L	Thalamus_R	4.01	6.1E-05
OFCpost_L	Precuneus_L	4.01	6.1E-05
OFCmed_R	Cingulate_Ant_L	4.01	6.2E-05
Precentral_R	Caudate_L	-4.01	6.2E-05
Rolandic_Oper_L	Angular_R	4.01	6.2E-05
OFCmed_R	Temporal_Sup_R	4.01	6.2E-05
Calcarine_R	Temporal_Pole_Sup_L	4.00	6.2E-05
SupraMarginal_L	Heschl_R	4.00	6.2E-05
Hippocampus_R	Parietal_Sup_L	4.00	6.4E-05
ParaHippocampal_R	Occipital_Mid_R	4.00	6.4E-05
Rolandic_Oper_L	Heschl_L	3.99	6.5E-05

Rectus_L	Temporal_Sup_R	3.99	6.6E-05
Cingulate_Ant_L	Cingulate_Ant_R	3.99	6.7E-05
Cingulate_Mid_L	Temporal_Pole_Sup_L	3.99	6.7E-05
Rectus_R	Lingual_R	3.99	6.7E-05
Frontal_Inf_Tri_R	Temporal_Pole_Mid_R	3.98	6.8E-05
Rectus_R	SupraMarginal_L	3.98	6.9E-05
Hippocampus_L	Hippocampus_R	3.98	6.9E-05
Frontal_Inf_Oper_R	OFCpost_L	3.98	6.9E-05
Amygdala_R	Paracentral_Lobule_L	3.98	7.0E-05
Parietal_Inf_L	Temporal_Sup_R	3.98	7.0E-05
Rectus_L	Occipital_Sup_L	3.98	7.0E-05
Cingulate_Ant_L	Precuneus_R	3.97	7.1E-05
Lingual_L	Postcentral_L	3.97	7.1E-05
Frontal_Inf_Tri_R	Temporal_Pole_Sup_R	3.97	7.2E-05
Fusiform_R	Precuneus_L	3.97	7.2E-05
Frontal_Med_Orb_R	Occipital_Sup_L	3.97	7.3E-05
Postcentral_L	Temporal_Mid_R	3.97	7.3E-05
Frontal_Med_Orb_R	Cingulate_Ant_R	3.97	7.4E-05
Frontal_Med_Orb_R	Temporal_Pole_Mid_L	3.96	7.6E-05
Fusiform_R	Heschl_R	3.96	7.6E-05
OFCmed_L	ParaHippocampal_L	3.95	7.7E-05
Lingual_R	Postcentral_L	3.95	7.7E-05
Frontal_Inf_Oper_R	Temporal_Pole_Sup_L	3.95	7.8E-05
Frontal_Med_Orb_R	Fusiform_L	3.95	7.8E-05
Insula_R	Heschl_R	3.95	7.9E-05
Frontal_Inf_Tri_R	Angular_L	3.94	8.2E-05
OFCmed_R	Temporal_Sup_L	3.94	8.3E-05
OFCmed_L	OFCpost_R	3.93	8.4E-05
Heschl_L	Temporal_Inf_R	3.93	8.6E-05
Fusiform_L	Temporal_Mid_L	3.93	8.6E-05
Postcentral_L	Thalamus_L	-3.93	8.6E-05
Frontal_Inf_Oper_R	Rectus_L	3.93	8.6E-05
Frontal_Sup_2_R	Temporal_Pole_Sup_L	3.93	8.7E-05
Insula_R	Parietal_Inf_R	3.92	8.7E-05
Olfactory_L	Frontal_Med_Orb_R	3.92	8.8E-05
Frontal_Inf_Oper_R	Temporal_Pole_Sup_R	3.92	8.9E-05
Rectus_L	Heschl_R	3.92	8.9E-05
Frontal_Med_Orb_L	Occipital_Inf_L	3.92	8.9E-05
Hippocampus_R	Amygdala_L	3.92	8.9E-05
Cingulate_Mid_R	Parietal_Inf_L	3.92	8.9E-05
Supp_Motor_Area_L	Heschl_R	3.92	8.9E-05
Occipital_Inf_L	Temporal_Pole_Sup_L	3.92	9.1E-05
Frontal_Inf_Orb_2_L	ParaHippocampal_R	3.91	9.1E-05
OFCpost_L	Temporal_Sup_L	3.91	9.1E-05
Precentral_L	Supp_Motor_Area_R	3.91	9.1E-05
Frontal_Med_Orb_R	Heschl_L	3.91	9.1E-05
Frontal_Inf_Orb_2_L	Temporal_Pole_Sup_R	3.91	9.2E-05

Frontal_Mid_2_R	Frontal_Med_Orb_L	3.91	9.2E-05
Frontal_Inf_Orb_2_R	Angular_L	3.91	9.3E-05
Precentral_R	Temporal_Pole_Sup_R	3.91	9.4E-05
Frontal_Med_Orb_L	SupraMarginal_L	3.91	9.4E-05
Rectus_R	Cuneus_L	3.91	9.4E-05
OFCmed_L	Precuneus_R	3.91	9.4E-05
ParaHippocampal_L	Precuneus_L	3.91	9.4E-05
Angular_R	Heschl_R	3.90	9.5E-05
OFClat_L	Temporal_Sup_L	3.90	9.5E-05
Insula_R	Temporal_Inf_L	3.90	9.7E-05
Rolandic_Oper_L	Angular_L	3.90	9.7E-05
Insula_R	Temporal_Mid_L	3.90	9.8E-05
OFCmed_L	Cingulate_Ant_L	3.89	9.9E-05
Rectus_L	Lingual_R	3.89	9.9E-05
OFClat_L	Heschl_R	3.89	9.9E-05
ParaHippocampal_L	Precuneus_R	3.89	1.0E-04
Hippocampus_R	Fusiform_R	3.89	1.0E-04
OFCpost_L	Parietal_Sup_R	3.89	1.0E-04
Supp_Motor_Area_R	Hippocampus_L	3.89	1.0E-04
Rectus_R	Parietal_Sup_L	3.89	1.0E-04
Insula_L	Heschl_R	3.89	1.0E-04
Frontal_Med_Orb_L	OFCpost_L	3.89	1.0E-04
Frontal_Med_Orb_L	Heschl_L	3.88	1.0E-04
Frontal_Inf_Oper_R	Frontal_Sup_Medial_L	3.88	1.0E-04
Parietal_Sup_L	Temporal_Sup_R	3.88	1.1E-04
Hippocampus_R	Cuneus_R	3.88	1.1E-04
OFCpost_L	SupraMarginal_R	3.87	1.1E-04
OFCmed_L	Insula_L	3.87	1.1E-04
Frontal_Inf_Oper_R	Frontal_Inf_Orb_2_L	3.87	1.1E-04
ParaHippocampal_L	Putamen_R	3.87	1.1E-04
Occipital_Inf_R	Precuneus_R	3.87	1.1E-04
OFCpost_L	Cuneus_L	3.87	1.1E-04
Precuneus_R	Temporal_Pole_Mid_R	3.87	1.1E-04
Precentral_L	Caudate_R	-3.86	1.1E-04
Rectus_L	Cingulate_Mid_R	3.86	1.1E-04
SupraMarginal_R	Temporal_Pole_Sup_R	3.86	1.1E-04
Frontal_Med_Orb_R	Occipital_Sup_R	3.86	1.1E-04
Occipital_Inf_R	Postcentral_R	3.86	1.1E-04
Cingulate_Post_R	SupraMarginal_R	3.86	1.1E-04
ParaHippocampal_R	Amygdala_L	3.86	1.1E-04
Occipital_Inf_L	Temporal_Pole_Mid_R	3.86	1.2E-04
Lingual_L	Paracentral_Lobule_L	3.85	1.2E-04
Supp_Motor_Area_R	Angular_R	3.85	1.2E-04
Frontal_Med_Orb_R	Rectus_L	3.85	1.2E-04
Rectus_R	SupraMarginal_R	3.85	1.2E-04
Rolandic_Oper_R	Temporal_Inf_L	3.85	1.2E-04
Supp_Motor_Area_L	Heschl_L	3.85	1.2E-04

Rolandic_Oper_R	Cuneus_L	3.84	1.2E-04
Hippocampus_L	Postcentral_L	3.84	1.2E-04
OFCpost_R	Temporal_Pole_Mid_R	3.84	1.2E-04
ParaHippocampal_R	Calcarine_R	3.84	1.2E-04
Cingulate_Ant_L	SupraMarginal_R	3.84	1.2E-04
Heschl_R	Temporal_Mid_R	3.84	1.2E-04
Rolandic_Oper_L	OFClat_L	3.84	1.2E-04
OFCant_R	Temporal_Pole_Sup_R	3.84	1.2E-04
Temporal_Mid_L	Temporal_Mid_R	3.84	1.2E-04
Frontal_Inf_Tri_R	Frontal_Med_Orb_R	3.83	1.3E-04
Frontal_Med_Orb_L	OFCmed_R	3.83	1.3E-04
Insula_L	Temporal_Mid_R	3.83	1.3E-04
Frontal_Sup_2_R	OFClat_L	3.83	1.3E-04
Occipital_Inf_R	Temporal_Pole_Sup_L	3.83	1.3E-04
Supp_Motor_Area_R	OFCmed_L	3.83	1.3E-04
Rectus_L	Cuneus_L	3.83	1.3E-04
Insula_L	Fusiform_L	3.83	1.3E-04
Occipital_Inf_L	Paracentral_Lobule_R	3.83	1.3E-04
Rolandic_Oper_R	Angular_R	3.83	1.3E-04
OFCmed_R	Cingulate_Mid_L	3.83	1.3E-04
OFCmed_R	SupraMarginal_R	3.83	1.3E-04
Heschl_R	Temporal_Pole_Sup_L	3.83	1.3E-04
Rectus_R	Occipital_Sup_L	3.83	1.3E-04
Rolandic_Oper_R	Angular_L	3.83	1.3E-04
Frontal_Med_Orb_R	Occipital_Inf_R	3.82	1.3E-04
Olfactory_L	OFCmed_L	3.82	1.3E-04
Precentral_L	Temporal_Pole_Sup_L	3.82	1.4E-04
Rectus_R	Temporal_Pole_Mid_L	3.82	1.4E-04
Hippocampus_R	Temporal_Inf_R	3.82	1.4E-04
Rolandic_Oper_L	Temporal_Inf_L	3.82	1.4E-04
Frontal_Med_Orb_R	Insula_R	3.82	1.4E-04
Frontal_Inf_Orb_2_L	Cingulate_Mid_R	3.81	1.4E-04
SupraMarginal_L	Temporal_Pole_Mid_R	3.81	1.4E-04
Postcentral_R	Temporal_Mid_R	3.81	1.4E-04
Parietal_Sup_R	Heschl_L	3.81	1.4E-04
Frontal_Sup_Medial_R	Angular_L	3.81	1.4E-04
Rectus_R	Cingulate_Mid_R	3.81	1.4E-04
Angular_L	Heschl_R	3.81	1.4E-04
Frontal_Inf_Orb_2_L	Precuneus_L	3.81	1.4E-04
OFCmed_L	Postcentral_L	3.80	1.4E-04
Postcentral_R	Temporal_Sup_R	3.80	1.4E-04
Precentral_L	Thalamus_L	-3.80	1.4E-04
Frontal_Inf_Orb_2_L	Cingulate_Mid_L	3.80	1.4E-04
OFCmed_L	OFCpost_L	3.80	1.4E-04
Insula_L	Angular_R	3.80	1.4E-04
OFCpost_L	Temporal_Sup_R	3.80	1.5E-04
Rolandic_Oper_L	Hippocampus_R	3.80	1.5E-04

Precentral_R	Thalamus_L	-3.80	1.5E-04
Frontal_Med_Orb_R	Temporal_Pole_Sup_R	3.80	1.5E-04
Hippocampus_L	Occipital_Sup_R	3.79	1.5E-04
Temporal_Mid_R	Temporal_Pole_Mid_R	3.79	1.5E-04
Hippocampus_R	Occipital_Mid_R	3.78	1.5E-04
Insula_R	Fusiform_L	3.78	1.5E-04
Frontal_Inf_Orb_2_R	OFCpost_L	3.78	1.6E-04
Rectus_L	Cingulate_Ant_R	3.78	1.6E-04
Postcentral_R	Temporal_Mid_L	3.78	1.6E-04
SupraMarginal_L	Angular_L	3.78	1.6E-04
OFClat_L	SupraMarginal_R	3.78	1.6E-04
Occipital_Inf_R	Temporal_Pole_Mid_R	3.78	1.6E-04
Lingual_R	Paracentral_Lobule_L	3.77	1.6E-04
Rectus_R	Temporal_Mid_R	3.77	1.6E-04
Frontal_Med_Orb_L	Cingulate_Ant_L	3.77	1.6E-04
Olfactory_R	Frontal_Med_Orb_L	3.77	1.6E-04
Frontal_Inf_Tri_R	Cingulate_Post_R	3.77	1.6E-04
Frontal_Inf_Orb_2_L	Insula_R	3.77	1.7E-04
Supp_Motor_Area_L	Precuneus_R	3.77	1.7E-04
Occipital_Inf_L	Postcentral_L	3.77	1.7E-04
Frontal_Inf_Orb_2_L	OFCpost_R	3.77	1.7E-04
OFCpost_L	Temporal_Mid_R	3.76	1.7E-04
Temporal_Pole_Sup_R	Temporal_Inf_L	3.76	1.7E-04
Precentral_L	Postcentral_L	3.76	1.7E-04
OFClat_L	SupraMarginal_L	3.76	1.7E-04
Cuneus_L	Temporal_Sup_L	3.76	1.7E-04
Frontal_Inf_Orb_2_L	SupraMarginal_R	3.76	1.7E-04
Rectus_L	Cuneus_R	3.76	1.7E-04
Insula_R	Temporal_Mid_R	3.76	1.7E-04
OFCmed_R	ParaHippocampal_R	3.76	1.7E-04
Rectus_R	Fusiform_L	3.76	1.7E-04
Precentral_L	Rectus_L	3.76	1.7E-04
OFClat_L	Temporal_Sup_R	3.75	1.8E-04

Appendix - 3

The anatomical regions are defined in each hemisphere using the Shen atlas, with appropriate names provided for each Shen atlas region by finding the corresponding part in the AAL2 atlas. Note: _L indicates left hemisphere; _R indicates right hemisphere; The AAL2 names provided were obtained by mapping the MNI coordinates of each Shen atlas area to the corresponding AAL2 atlas area.

No.	Region name	Anatomical description	No.	Region name	Anatomical description
1	OFCpost_R	Posterior orbitofrontal gyrus	126	Frontal_Mid_2_R	Middle frontal gyrus
2	OFCpost_L	Posterior orbitofrontal gyrus	127	Frontal_Sup_Medial_R	Superior frontal gyrus, medial
3	OFCant_R	Anterior orbitofrontal gyrus	128	Cuneus_R	Cuneus
4	OFCant_L	Anterior orbitofrontal gyrus	129	ParaHippocampal_R	Parahippocampal gyrus
5	OFCmed_R	Medial orbitofrontal gyrus	130	Cingulate_Post_R	Posterior cingulate gyrus
6	OFCmed_L	Medial orbitofrontal gyrus	131	Lingual_R	Lingual gyrus
7	Rectus_R	Gyrus rectus	132	Frontal_Mid_2_R	Middle frontal gyrus
8	Rectus_L	Gyrus rectus	133	Cingulate_Mid_R	Middle cingulate & paracingulate gyri
9	Olfactory_R	Olfactory cortex	134	Precentral_R	Precentral gyrus
10	Olfactory_L	Olfactory cortex	135	Frontal_Mid_2_L	Middle frontal gyrus
11	OFClat_R	Lateral orbitofrontal gyrus	136	Frontal_Inf_Tri_L	Inferior frontal gyrus, triangular part
12	OFClat_L	Lateral orbitofrontal gyrus	137	Frontal_Inf_Oper_L	Inferior frontal gyrus, opercular part
13	Frontal_Inf_Orb_2_R	Inferior Frontal Gyrus, orbital part	138	Precuneus_L	Precuneus
14	Frontal_Inf_Orb_2_L	Inferior Frontal Gyrus, orbital part	139	Temporal_Inf_L	Inferior temporal gyrus
15	Precentral_R	Precentral gyrus	140	Postcentral_L	Postcentral gyrus
16	Frontal_Sup_2_R	Superior frontal gyrus, dorsolateral	141	Putamen_L	Lenticular Putamen nucleus,
17	Frontal_Med_Orb_R	Superior frontal gyrus, medial orbital (or ventromedial prefrontal cortex)	142	Caudate_L	Caudate nucleus
18	Postcentral_R	Postcentral gyrus	143	Cingulate_Mid_L	Middle cingulate & paracingulate gyri
19	SupraMarginal_R	Supramarginal gyrus	144	Occipital_Mid_L	Middle occipital gyrus
20	OFClat2	Lateral orbitofrontal cortex	145	Postcentral_L	Postcentral gyrus
21	Precentral_R	Precentral gyrus	146	Thalamus_L	Thalamus
22	Postcentral_R	Postcentral gyrus	147	Calcarine_L	Calcarine fissure and surrounding cortex
23	Frontal_Mid_2_R	Middle frontal gyrus	148	Postcentral_L	Postcentral gyrus
24	Temporal_Inf_R	Inferior temporal gyrus	149	Parietal_Inf_L	Inferior parietal gyrus, excluding supramarginal and angular gyri
25	Thalamus_R	Thalamus	150	Cingulate_Ant_L	Anterior cingulate & paracingulate gyri
26	Lingual_R	Lingual gyrus	151	Insula_L	Insula
27	Calcarine_R	Calcarine fissure and surrounding cortex	152	Frontal_Mid_2_L	Middle frontal gyrus
28	Heschl_R	Heschl's gyrus	153	Calcarine_L	Calcarine fissure and surrounding cortex
29	Precuneus_R	Precuneus	154	Parietal_Inf_L	Inferior parietal gyrus, excluding supramarginal and angular gyri

30	SupraMarginal_R	Supramarginal gyrus	155	Thalamus_L	Thalamus
31	Temporal_Sup_R	Superior temporal gyrus	156	Lingual_L	Lingual gyrus
32	Temporal_Inf_R	Inferior temporal gyrus	157	Insula_L	Insula
33	Frontal_Inf_Tri_R	Inferior frontal gyrus, triangular part	158	Precuneus_L	Precuneus
34	Precuneus_R	Precuneus	159	Supp_Motor_Area_L	Supplementary motor area
35	Temporal_Mid_R	Middle temporal gyrus	160	Cingulate_Mid_L	Middle cingulate & paracingulate gyri
36	Angular_R	Angular gyrus	161	Cingulate_Mid_L	Middle cingulate & paracingulate gyri
37	Caudate_R	Caudate nucleus	162	Precentral_L	Precentral gyrus
38	Temporal_Pole_Mid_R	Temporal pole: middle temporal gyrus	163	Fusiform_L	Fusiform gyrus
39	Cingulate_Mid_R	Middle cingulate & paracingulate gyri	164	Frontal_Mid_2_L	Middle frontal gyrus
40	Postcentral_R	Postcentral gyrus	165	Cingulate_Ant_L	Anterior cingulate & paracingulate gyri
41	Parietal_Sup_R	Superior parietal gyrus	166	Temporal_Pole_Mid_L	Temporal pole: middle temporal gyrus
42	Postcentral_R	Postcentral gyrus	167	Cingulate_Ant_L	Anterior cingulate & paracingulate gyri
43	Temporal_Mid_R	Middle temporal gyrus	168	Temporal_Sup_L	Superior temporal gyrus
44	Postcentral_R	Postcentral gyrus	169	Calcarine_L	Calcarine fissure and surrounding cortex
45	Temporal_Inf_R	Inferior temporal gyrus	170	Occipital_Mid_L	Middle occipital gyrus
46	Cuneus_R	Cuneus	171	Precuneus_L	Precuneus
47	Frontal_Sup_Medial_R	Superior frontal gyrus, medial	172	Supp_Motor_Area_L	Supplementary motor area
48	Occipital_Mid_R	Middle occipital gyrus	173	Temporal_Pole_Sup_L	Temporal pole: superior temporal gyrus
49	Occipital_Sup_R	Superior occipital gyrus	174	Cuneus_L	Cuneus
50	Precuneus_R	Precuneus	175	Hippocampus_L	Hippocampus
51	ParaHippocampal_R	Parahippocampal gyrus	176	Angular_L	Angular gyrus
52	Insula_R	Insula	177	Frontal_Mid_Orb_R (or OFClat)	Lateral orbital gyrus
53	Temporal_Sup_R	Superior temporal gyrus	178	Angular_L	Angular gyrus
54	Precuneus_R	Precuneus	179	SupraMarginal_L	Supramarginal gyrus
55	Frontal_Sup_Medial_R	Superior frontal gyrus, medial	180	Precentral_L	Precentral gyrus
56	Cingulate_Post_R	Posterior cingulate cortex (retrosplenial)	181	Temporal_Inf_L	Inferior temporal gyrus
57	Calcarine_R	Calcarine fissure and surrounding cortex	182	Hippocampus_L	Hippocampus
58	Postcentral_R	Postcentral gyrus	183	Frontal_Sup_2_L	Superior frontal gyrus, dorsolateral
59	Temporal_Mid_R	Middle temporal gyrus	184	Temporal_Inf_L	Inferior temporal gyrus
60	Caudate_R	Caudate nucleus	185	Frontal_Sup_2_L	Superior frontal gyrus, dorsolateral
61	Calcarine_R	Calcarine fissure and surrounding cortex	186	Cingulate_Post_L	Posterior cingulate gyrus
62	Cingulate_Ant_R	Anterior cingulate & paracingulate gyri	187	Lingual_L	Lingual gyrus
63	Cingulate_Mid_R	Middle cingulate & paracingulate gyri	188	Precentral_L	Precentral gyrus
64	Temporal_Sup_R	Superior temporal gyrus	189	Insula_L	Insula
65	Postcentral_R	Postcentral gyrus	190	Lingual_L	Lingual gyrus

66	Hippocampus_R	Hippocampus	191	Temporal_Mid_L	Middle temporal gyrus
67	Supp_Motor_Area_R	Supplementary motor area	192	Temporal_Mid_L	Middle temporal gyrus
68	Parietal_Sup_R	Superior parietal gyrus	193	Fusiform_L	Fusiform gyrus
69	Temporal_Mid_R	Middle temporal gyrus	194	Occipital_Mid_L	Middle occipital gyrus
70	Frontal_Mid_2_R	Middle frontal gyrus	195	Frontal_Inf_Tri_L	Inferior frontal gyrus, triangular part
71	Frontal_Sup_2_R	Superior frontal gyrus, dorsolateral	196	Insula_L	Insula
72	Frontal_Med_Orb_R	Superior frontal gyrus,medial orbital (or ventromedial prefrontal cortex)	197	Fusiform_L	Fusiform gyrus
73	Frontal_Mid_2_R	Middle frontal gyrus	198	Temporal_Sup_L	Superior temporal gyrus
74	Cingulate_Ant_R	Anterior cingulate & paracingulate gyri	199	Parietal_Inf_L	Inferior parietal gyrus, excluding supramarginal and angular gyri
75	Temporal_Pole_Mid_R	Temporal pole: middle temporal gyrus	200	Occipital_Mid_L	Middle occipital gyrus
76	Cingulate_Mid_R	Middle cingulate & paracingulate gyri	201	Cuneus_L	Cuneus
77	Frontal_Mid_2_R	Middle frontal gyrus	202	Precuneus_L	Precuneus
78	Fusiform_R	Fusiform gyrus	203	Frontal_Sup_Medial_L	Superior frontal gyrus, medial
79	Temporal_Sup_R	Superior temporal gyrus	204	Frontal_Mid_2_L	Middle frontal gyrus
80	Hippocampus_R	Hippocampus	205	Lingual_L	Lingual gyrus
81	Temporal_Pole_Sup_R	Temporal pole: superior temporal gyrus	206	Frontal_Sup_2_L	Superior frontal gyrus, dorsolateral
82	Parietal_Sup_R	Superior parietal gyrus	207	Temporal_Mid_L	Middle temporal gyrus
83	Cingulate_Ant_R	Anterior cingulate & paracingulate gyri	208	Cingulate_Mid_L	Middle cingulate & paracingulate gyri
84	Insula_R	Insula	209	Parietal_Sup_L	Superior parietal gyrus
85	Temporal_Sup_R	Superior temporal gyrus	210	Hippocampus_L	Hippocampus
86	Cuneus_R	Cuneus	211	Temporal_Mid_L	Middle temporal gyrus
87	Frontal_Sup_2_R	Superior frontal gyrus, dorsolateral	212	Fusiform_L	Fusiform gyrus
88	Fusiform_R	Fusiform gyrus	213	Lingual_L	Lingual gyrus
89	Frontal_Mid_2_R	Middle frontal gyrus	214	Temporal_Sup_L	Superior temporal gyrus
90	Temporal_Mid_R	Middle temporal gyrus	215	Temporal_Inf_L	Inferior temporal gyrus
91	Temporal_Inf_R	Inferior temporal gyrus	216	Parietal_Sup_L	Superior parietal gyrus
92	Insula_R	Insula	217	SupraMarginal_L	Supramarginal gyrus
93	Cingulate_Mid_R	Middle cingulate & paracingulate gyri	218	Precentral_L	Precentral gyrus
94	Insula_R	Insula	219	Temporal_Inf_L	Inferior temporal gyrus
95	Parietal_Inf_R	Inferior parietal gyrus, excluding supramarginal and angular gyri	220	Temporal_Pole_Sup_L	Temporal pole: superior temporal gyrus
96	Temporal_Mid_R	Middle temporal gyrus	221	SupraMarginal_L	Supramarginal gyrus
97	Lingual_R	Lingual gyrus	222	Insula_L	Insula
98	Fusiform_R	Fusiform gyrus	223	Occipital_Inf_L	Inferior occipital gyrus
99	Putamen_R	Lenticular nucleus, Putamen	224	Frontal_Sup_Medial_L	Superior frontal gyrus, medial
100	Insula_R	Insula	225	Precuneus_L	Precuneus
101	Parietal_Inf_R	Inferior parietal gyrus, excluding supramarginal and angular gyri	226	Occipital_Mid_L	Middle occipital gyrus
102	Frontal_Sup_2_R	Superior frontal gyrus, dorsolateral	227	Frontal_Mid_2_L	Middle frontal gyrus
103	Occipital_Inf_R	Inferior occipital gyrus	228	Paracentral_Lobule _L	Paracentral lobule

104	Frontal_Inf_Tri_R	Inferior frontal gyrus, triangular part	229	Postcentral_L	Postcentral gyrus
105	Supp_Motor_Area_R	Supplementary motor area	230	Precuneus_L	Precuneus
106	Occipital_Sup_R	Superior occipital gyrus	231	Occipital_Inf_L	Inferior occipital gyrus
107	Frontal_Inf_Tri_R	Inferior frontal gyrus, triangular part	232	Cingulate_Mid_L	Middle cingulate & paracingulate gyri
108	Fusiform_R	Fusiform gyrus	233	Frontal_Mid_2_L	Middle frontal gyrus
109	Fusiform_R	Fusiform gyrus	234	Thalamus_L	Thalamus
110	Frontal_Inf_Oper_R	Inferior frontal gyrus, opercular part	235	Postcentral_L	Postcentral gyrus
111	Fusiform_R	Fusiform gyrus	236	Caudate_L	Caudate nucleus
112	Fusiform_R	Fusiform gyrus	237	Cingulate_Mid_L	Middle cingulate & paracingulate gyri
113	Caudate_R	Caudate nucleus	238	Temporal_Pole_Mid_L	Temporal pole: middle temporal gyrus
114	Precentral_R	Precentral gyrus	239	Hippocampus_L	Hippocampus
115	Lingual_R	Lingual gyrus	240	Frontal_Sup_Medial_L	Superior frontal gyrus, medial
116	Thalamus_R	Thalamus	241	Temporal_Sup_L	Superior temporal gyrus
117	Frontal_Med_Orb_R	Superior frontal gyrus, medial orbital (or ventromedial prefrontal cortex)	242	Insula_L	Insula
118	Occipital_Mid_R	Middle occipital gyrus	243	Calcarine_L	Calcarine fissure and surrounding cortex
119	Occipital_Mid_R	Middle occipital gyrus	244	Cingulate_Ant_L	Anterior cingulate & paracingulate gyri
120	Temporal_Mid_R	Middle temporal gyrus	245	Caudate_L	Caudate nucleus
121	Temporal_Pole_Mid_R	Temporal pole: middle temporal gyrus	246	Frontal_Med_Orb_L	Superior frontal gyrus, medial orbital (or ventromedial prefrontal cortex)
122	Frontal_Inf_Oper_R	Inferior frontal gyrus, opercular part	247	Occipital_Mid_L	Middle occipital gyrus
123	Parietal_Inf_R	Inferior parietal gyrus, excluding supramarginal and angular gyri	248	Frontal_Inf_Tri_L	Inferior frontal gyrus, triangular part
124	Calcarine_R	Calcarine fissure and surrounding cortex	249	Supp_Motor_Area_ L	Supplementary motor area
125	Putamen_R	Lenticular nucleus, Putamen	250	Postcentral_L	Postcentral gyrus

Appendix - 4

A full list of functional connectivity links which were significantly correlated with childhood traumatic experience score (p<0.01 FDR corrected) in the study is described in chapter 7.

Region 1	Region 2	r value	p value
Angular_L	Temporal_Inf_L	-0.040	1.9E-06
Angular_R	Precentral_L	-0.045	1.0E-07
Angular_R	Temporal_Inf_L	-0.045	1.2E-07
Angular_R	Temporal_Mid_R	-0.038	8.3E-06
Angular_R	Frontal_Inf_Tri_L	-0.037	1.2E-05
Angular_R	Precentral_L	-0.036	1.8E-05
Angular_R	Temporal_Mid_L	-0.034	7.5E-05
Calcarine_R	Frontal_Inf_Tri_L	-0.035	2.9E-05
Calcarine_R	Precentral_L	-0.035	3.9E-05
Calcarine_R	Temporal_Inf_L	-0.034	4.8E-05
Cingulate_Mid_L	SupraMarginal_L	-0.034	5.1E-05
Cuneus_L	Temporal_Inf_L	-0.037	1.5E-05
Cuneus_L	Cingulate_Mid_L	-0.034	6.8E-05
Cuneus_R	Frontal_Inf_Tri_L	-0.038	5.6E-06
Cuneus_R	Temporal_Inf_L	-0.036	1.6E-05
Cuneus_R	Precentral_L	-0.035	3.1E-05
Cuneus_R	Frontal_Inf_Tri_L	-0.034	6.4E-05
Frontal_Inf_Tri_L	Rectus_L	-0.038	7.7E-06
Frontal_Inf_Tri_L	Rectus_R	-0.034	5.3E-05
Frontal_Inf_Tri_L	Fusiform_L	-0.034	5.4E-05
Frontal_Med_Orb_L	Rectus_L	-0.035	2.9E-05
Frontal_Mid_2_L	Postcentral_L	-0.034	5.8E-05
Frontal_Mid_2_R	Precentral_L	-0.038	6.6E-06
Frontal_Mid_2_R	Precuneus_R	-0.037	1.0E-05
Frontal_Mid_2_R	Precentral_L	-0.037	1.1E-05
Frontal_Mid_2_R	Frontal_Inf_Tri_R	-0.036	1.7E-05
Frontal_Mid_2_R	Precuneus_L	-0.036	2.4E-05
Frontal_Mid_2_R	Parietal_Sup_R	-0.035	2.8E-05
Frontal_Mid_2_R	Occipital_Inf_L	-0.035	3.9E-05
Frontal_Mid_2_R	Lingual_R	-0.034	4.6E-05
Frontal_Mid_2_R	Fusiform_R	-0.034	4.7E-05
Frontal_Mid_2_R	Fusiform_L	-0.034	4.8E-05
Frontal_Mid_2_R	Fusiform_R	-0.034	4.9E-05
Frontal_Sup_2_L	Fusiform_L	-0.035	2.7E-05
Frontal_Sup_2_L	Occipital_Inf_L	-0.035	3.5E-05
Frontal_Sup_2_L	Precentral_L	-0.034	5.4E-05
Frontal_Sup_2_L	Precentral_L	-0.034	5.6E-05
Frontal_Sup_2_R	Precentral_L	-0.042	8.9E-07
Frontal_Sup_2_R	Postcentral_L	-0.039	4.3E-06
Frontal_Sup_2_R	Parietal_Inf_L	-0.039	4.3E-06
Frontal_Sup_2_R	Fusiform_R	-0.037	9.8E-06

Frontal_Sup_2_R	Precentral_L	-0.037	1.3E-05
Frontal_Sup_2_R	Parietal_Inf_L	-0.037	1.5E-05
Frontal_Sup_2_R	Fusiform_L	-0.037	1.6E-05
Frontal_Sup_2_R	Frontal_Inf_Tri_L	-0.036	1.9E-05
Frontal_Sup_2_R	SupraMarginal_R	-0.036	2.1E-05
Frontal_Sup_2_R	Frontal_Inf_Tri_L	-0.036	2.2E-05
Frontal_Sup_2_R	Precentral_R	-0.035	2.7E-05
Frontal_Sup_2_R	Frontal_Inf_Tri_L	-0.035	3.2E-05
Frontal_Sup_2_R	Postcentral_R	-0.035	3.4E-05
Frontal_Sup_2_R	Fusiform_R	-0.035	3.5E-05
Frontal_Sup_2_R	Fusiform_R	-0.035	4.1E-05
Frontal_Sup_2_R	Occipital_Inf_L	-0.035	4.3E-05
Frontal_Sup_2_R	Frontal_Inf_Tri_L	-0.034	5.2E-05
Frontal_Sup_2_R	Precentral_L	-0.034	5.8E-05
Frontal_Sup_2_R	shen_roi_126	-0.034	6.6E-05
Frontal_Sup_2_R	Lingual_R	-0.034	6.7E-05
Frontal_Sup_2_R	OFCant_L	-0.034	7.0E-05
Frontal_Sup_2_R	Parietal_Inf_L	-0.034	7.1E-05
Frontal_Sup_2_R	Fusiform_R	-0.034	7.2E-05
Frontal_Sup_2_R	Lingual_R	-0.034	7.4E-05
Frontal_Sup_Medial_R	Temporal_Mid_L	-0.039	4.3E-06
Frontal_Sup_Medial_R	Frontal_Inf_Tri_L	-0.037	1.3E-05
Frontal_Sup_Medial_R	Precentral_L	-0.036	2.7E-05
Frontal_Sup_Medial_R	Parietal_Inf_L	-0.035	3.2E-05
Frontal_Sup_Medial_R	Frontal_Inf_Tri_L	-0.034	5.2E-05
Frontal_Sup_Medial_R	Temporal_Inf_L	-0.034	7.4E-05
Fusiform_R	Precentral_L	-0.037	1.1E-05
Fusiform_R	Precentral_L	-0.036	1.8E-05
Fusiform_R	Frontal_Inf_Tri_L	-0.036	1.9E-05
Fusiform_R	Precentral_L	-0.036	2.1E-05
Fusiform_R	Frontal_Sup_2_L	-0.036	2.4E-05
Fusiform_R	Parietal_Inf_L	-0.035	2.7E-05
Fusiform_R	Precentral_L	-0.035	3.2E-05
Fusiform_R	Frontal_Mid_2_L	-0.035	4.4E-05
Hippocampus_R	Temporal_Mid_L	-0.036	2.6E-05
Lingual_R	Temporal_Inf_L	-0.043	2.8E-07
Lingual_R	Frontal_Inf_Tri_L	-0.039	4.2E-06
Lingual_R	Precentral_L	-0.037	1.4E-05
Lingual_R	Cingulate_Mid_L	-0.036	2.4E-05
Lingual_R	Temporal_Mid_L	-0.036	2.5E-05
Lingual_R	Precentral_L	-0.035	2.8E-05
Lingual_R	Precentral_L	-0.035	3.2E-05
Lingual_R	Precuneus_L	-0.035	3.4E-05
Lingual_R	Precentral_L	-0.035	3.6E-05
Lingual_R	Temporal_Inf_L	-0.034	5.8E-05
Lingual_R	Frontal_Inf_Tri_L	-0.034	7.0E-05
Lingual_R	Precentral_L	-0.034	7.3E-05

OFCmed_L	OFCant_R	-0.036	2.5E-05
OFCmed_L	OFClat_R	-0.035	4.2E-05
Occipital_Mid_R	Precentral_L	-0.037	1.1E-05
Occipital_Sup_R	Precentral_L	-0.036	2.0E-05
ParaHippocampal_R	Precentral_L	-0.038	5.4E-06
ParaHippocampal_R	Temporal_Mid_L	-0.038	7.0E-06
ParaHippocampal_R	Temporal_Inf_L	-0.035	2.7E-05
ParaHippocampal_R	Precentral_L	-0.034	4.7E-05
ParaHippocampal_R	Precuneus_L	-0.034	7.0E-05
Parietal_Sup_R	Temporal_Inf_R	-0.037	1.2E-05
Parietal_Sup_R	Angular_R	-0.034	4.8E-05
Parietal_Sup_R	Temporal_Mid_R	-0.034	5.5E-05
Postcentral_L	Temporal_Mid_L	-0.036	1.9E-05
Postcentral_L	Temporal_Sup_L	-0.035	3.0E-05
Postcentral_L	Temporal_Inf_L	-0.034	6.1E-05
Postcentral_R	Temporal_Inf_R	-0.036	1.8E-05
Postcentral_R	Rolandic_Oper_L	-0.035	4.3E-05
Precentral_L	Precuneus_L	-0.038	5.8E-06
Precentral_L	Fusiform_L	-0.038	7.7E-06
Precentral_L	Fusiform_L	-0.036	2.3E-05
Precentral_L	Temporal_Pole_Mid_L	-0.035	3.9E-05
Precentral_L	Precuneus_L	-0.035	4.4E-05
Precentral_L	Precuneus_L	-0.034	6.0E-05
Precentral_R	SupraMarginal_L	-0.037	1.0E-05
Precentral_R	Temporal_Mid_R	-0.034	7.1E-05
Precuneus_L	Rectus_L	-0.039	5.3E-06
Precuneus_R	Temporal_Inf_L	-0.042	5.1E-07
Precuneus_R	Precentral_L	-0.041	9.5E-07
Precuneus_R	Precentral_L	-0.041	1.1E-06
Precuneus_R	Precentral_L	-0.041	1.1E-06
Precuneus_R	Temporal_Inf_L	-0.039	3.9E-06
Precuneus_R	Cingulate_Mid_L	-0.037	1.0E-05
Precuneus_R	Frontal_Inf_Tri_L	-0.037	1.1E-05
Precuneus_R	Precentral_L	-0.037	1.2E-05
Precuneus_R	Frontal_Inf_Tri_L	-0.035	2.9E-05
Precuneus_R	Temporal_Mid_L	-0.035	3.3E-05
Precuneus_R	Temporal_Mid_L	-0.035	3.9E-05
Precuneus_R	Frontal_Inf_Tri_L	-0.035	4.2E-05
Precuneus_R	Precuneus_L	-0.035	4.5E-05
Precuneus_R	Precentral_L	-0.034	5.1E-05
Precuneus_R	Angular_L	-0.034	5.3E-05
Precuneus_R	Cingulate_Mid_L	-0.034	5.7E-05
Precuneus_R	Temporal_Mid_L	-0.034	6.2E-05
Precuneus_R	Rectus_L	-0.034	6.6E-05
Precuneus_R	Frontal_Mid_2_L	-0.034	7.0E-05
Rolandic_Oper_R	Temporal_Inf_R	-0.039	5.0E-06
Supp_Motor_Area_L	Rolandic_Oper_L	-0.036	1.7E-05

Supp_Motor_Area_L	SupraMarginal_L	-0.035	3.4E-05
Supp_Motor_Area_R	SupraMarginal_L	-0.035	2.8E-05
Supp_Motor_Area_R	SupraMarginal_L	-0.035	4.1E-05
SupraMarginal_R	Temporal_Inf_R	-0.041	1.2E-06
Temporal_Inf_L	ParaHippocampal_L	-0.038	5.7E-06
Temporal_Inf_L	Rectus_L	-0.037	1.2E-05
Temporal_Inf_L	Precuneus_L	-0.036	2.5E-05
Temporal_Inf_L	OFCmed_L	-0.035	4.1E-05
Temporal_Inf_R	Temporal_Inf_L	-0.046	4.9E-08
Temporal_Inf_R	Temporal_Mid_L	-0.044	2.4E-07
Temporal_Inf_R	Postcentral_L	-0.043	3.4E-07
Temporal_Inf_R	Parietal_Inf_L	-0.041	1.1E-06
Temporal_Inf_R	Parietal_Inf_L	-0.041	1.3E-06
Temporal_Inf_R	Frontal_Inf_Tri_L	-0.041	1.4E-06
Temporal_Inf_R	Parietal_Sup_L	-0.040	2.4E-06
Temporal_Inf_R	Frontal_Inf_Tri_L	-0.040	2.6E-06
Temporal_Inf_R	SupraMarginal_L	-0.040	2.8E-06
Temporal_Inf_R	Precentral_L	-0.039	3.5E-06
Temporal_Inf_R	Postcentral_L	-0.039	5.1E-06
Temporal_Inf_R	Parietal_Inf_L	-0.039	5.3E-06
Temporal_Inf_R	Temporal_Mid_R	-0.038	5.4E-06
Temporal_Inf_R	Temporal_Sup_R	-0.038	5.4E-06
Temporal_Inf_R	Temporal_Mid_L	-0.038	6.8E-06
Temporal_Inf_R	Rolandic_Oper_L	-0.037	9.4E-06
Temporal_Inf_R	Temporal_Sup_L	-0.037	9.9E-06
Temporal_Inf_R	Temporal_Inf_R	-0.037	1.2E-05
Temporal_Inf_R	Frontal_Sup_2_L	-0.037	1.3E-05
Temporal_Inf_R	Rolandic_Oper_R	-0.037	1.4E-05
Temporal_Inf_R	Precentral_L	-0.037	1.5E-05
Temporal_Inf_R	Fusiform_L	-0.036	2.0E-05
Temporal_Inf_R	Fusiform_R	-0.036	2.7E-05
Temporal_Inf_R	Temporal_Mid_R	-0.035	2.9E-05
Temporal_Inf_R	Precentral_L	-0.034	4.8E-05
Temporal_Inf_R	Temporal_Sup_L	-0.034	5.1E-05
Temporal_Inf_R	Frontal_Inf_Tri_L	-0.034	5.4E-05
Temporal_Inf_R	Postcentral_L	-0.034	5.8E-05
Temporal_Inf_R	Temporal_Inf_R	-0.034	6.1E-05
Temporal_Inf_R	Frontal_Sup_2_L	-0.034	6.3E-05
Temporal_Inf_R	Precuneus_L	-0.034	6.5E-05
Temporal_Mid_L	Temporal_Inf_L	-0.039	5.1E-06
Temporal_Mid_L	Temporal_Mid_L	-0.036	1.8E-05
Temporal_Mid_L	Fusiform_L	-0.034	7.3E-05
Temporal_Mid_R	Temporal_Inf_L	-0.041	1.3E-06
Temporal_Mid_R	Frontal_Inf_Tri_L	-0.039	3.7E-06
Temporal_Mid_R	Precentral_L	-0.039	4.6E-06
Temporal_Mid_R	Temporal_Mid_L	-0.037	1.3E-05
Temporal_Mid_R	Postcentral_L	-0.035	3.8E-05

Temporal_Mid_R	Fusiform_R	-0.035	3.9E-05
Temporal_Mid_R	Cuneus_R	-0.034	5.5E-05
Temporal_Mid_R	Temporal_Mid_R	-0.034	5.9E-05
Temporal_Mid_R	Temporal_Inf_R	-0.034	6.0E-05
Temporal_Mid_R	Hippocampus_R	-0.034	6.3E-05
Temporal_Mid_R	Hippocampus_R	-0.034	6.8E-05
Temporal_Pole_Mid_L	Temporal_Inf_L	-0.034	4.9E-05
Temporal_Pole_Mid_R	Temporal_Inf_L	-0.034	7.2E-05
Temporal_Pole_Sup_L	Temporal_Inf_L	-0.039	4.2E-06
Temporal_Pole_Sup_R	Temporal_Inf_L	-0.036	2.0E-05
Temporal_Sup_R	Temporal_Inf_R	-0.036	2.4E-05
Temporal_Sup_R	Calcarine_R	-0.034	6.8E-05

Appendix - 5

Example code of t-test analysis between two groups of data that utilises covariates of no interest with FDR correction of the result.

```
for i=1:size(fc_data_hc,3)
    DependentVariable = gretna_fishertrans([fc_data_hc(:,:,i);...
     fc_data_con(:,:,i)]);
    GroupLabel = [zeros(size(fc_data_hc,1),1);...
     ones(size(fc_data_con,1),1)];
     Covariate = [cov_all_hc; cov_all_con];
    [T_value(i,:), P_value(i,:)] = ttest2_cov_improve...
    (DependentVariable, GroupLabel, Covariate);
    %% two sample t-test with removing the effect of covariates
     Cohens_d(i,:) = 2*T_value(i,:)/sqrt(length(GroupLabel)-2);
end
bon_threshold = 0.05/length(ssjnum(P_value));
%% Bonferroni correction
fdr_threshold = gretna_FDR(ssjnum(P_value),0.001);
%% FDR correction
[Significant_links, Significant_nodes] =extract_edges_multi_ttest...
(P_value, T_value, fdr_threshold, 'aal2');
%% Extract significant links and nodes
```

Appendix - 6

Example code of elastic net prediction model with cross-validation.

a) Feature selection

```
cval = nan(size(fc_train,2),size(fc_train,1));
pval = nan(size(fc_train,2),size(fc_train,1));
pheno_select = Subscale_all_train;
for j=1:size(fc_train,1)
     fc_select = gretna_fishertrans(squeeze(fc_train(j,:,:)))';
     [cval(:,j), pval(:,j)] = partialcorr(pheno_select, fc_select,...
      cov_all_train,'row','complete');
end
```

b) Optimize parameters

```
for alpha=0.01:0.1:1
       for gama=0.01:0.1:1
             [model,info]=lasso(fc_prediction,subscales_train,'Alpha',...
            alpha,'Lambda',gama);
            for i=1:size(fc_test_selected,2)
                Predicted_Scores(i) =sum(model.*fc_test_selected(:,i));
            end
            [r(count11),p(count11)]=corr(Predicted_Scores',score_test);
            result(count11,:)={r(count11),p(count11),edgeNames,model,...
            info.MSE,Predicted_Scores,alpha,gama};
            count11=count11+1;
       end
   end
```

Appendix - 7

Example code of calculation of effective connectivity of the whole brain

a) Calculation of the empirical FC value in the current time point (FC0) and FC value at one time point later (FC1)

```
% calculate FC0 and FC1
if 1
    FC0_emp = zeros(n_sub,N,N);
    FC1_emp = zeros(n_sub,N,N);
    n_T = size(tc_all,1);
    ts = tc_all;
    for i_sub = 1:size(tc_all,3)
        for i=1:N
            if mod(i,2)==1
                ii = floor((i+1)/2);
            else
                ii = 95 - floor((i+1)/2);
            end
            for j=1:N               if mod(j,2)==1
                    jj = floor((j+1)/2);
                else
                    jj = 95 - floor((j+1)/2);
                end
                FC0_emp(i_sub,ii,jj) = dot(ts(1:n_T-1,i,i_sub),...
              ts(1:n_T-1,j,i_sub)) / (n_T-2.);
                FC1_emp(i_sub,ii,jj) = dot(ts(1:n_T-1,i,i_sub),...
              ts(2:n_T,j,i_sub)) / (n_T-2.);
            end
        end
    end
```

b) Optimize the effective connectivity values to best predict the empirical FC values.

```
% optimization
sprintf('*opt*')
for i_sub = 1:n_sub
    % initial parameters
    EC = zeros(N); %initial conectivity
    Sigma = eye(N)*noise_level^2; % initial noise
    %best distance between model and empirical data
    best_dist = 1e10;
    best_Pearson = 0;
    %objective FC matrices (empirical)
    FC0_obj = squeeze(FC0_emp(i_sub,:,:));
    FC1_obj = squeeze(FC1_emp(i_sub,:,:));
    %record model parameters and outputs
    dist_FC_hist = zeros(n_opt,1)*NaN;
    Pearson_FC_hist = zeros(n_opt,1)*NaN;
    stop_opt = 0;
    i_opt = 1;
    while ~stop_opt
        %calculate Jacobian of dynamical system
        J = -eye(N)/tau_x(i_sub)+EC;
        %calculate FC0 and FCtau for model
        FC0 = lyap(J,Sigma);
        FC1 = FC0*expm(J'); %%%was a dot() before de * between these two
        %calculate error between model and empirical data for FC0 and FC_tau
(matrix distance)
        err_FC0 = sqrt(sum((FC0(:)-FC0_obj(:)).^2)/sum((FC0_obj(:)).^2));
        err_FCtau = sqrt(sum((FC1(:)-FC1_obj(:)).^2)/sum((FC1_obj(:)).^2));
        dist_FC_hist(i_opt) = 0.5*(err_FC0+err_FCtau);
        %calculate Pearson corr between model and empirical data for FC0 and
FC_tau
        Pearson_FC_hist(i_opt) = 0.5*(corr(FC0(:),FC0_obj(:))...
       +corr(FC1(:),FC1_obj(:)));
      %%%reshape (adash)   #####

        % best fit given matrix distance best for FC0/FC1 between model and
empirical data
        if dist_FC_hist(i_opt) < best_dist
            best_dist = dist_FC_hist(i_opt);
```

```
%Jacobian update with weighted FC updates depending on respective
error
        Delta_FC0 = FC0_obj-FC0;
        Delta_FCtau = FC1_obj-FC1;
        Delta_J = transpose(pinv(FC0)*(Delta_FC0+Delta_FCtau*expm(-
J')));
        %update conectivity and noise
        EC = EC + epsilon_EC * Delta_J;
        EC(EC>max_val_EC) = max_val_EC;
        EC(EC<min_val_EC) = min_val_EC;
        EC(not(mask_EC)) = 0;


        Sigma = Sigma + epsilon_Sigma * Delta_FC0;
        Sigma(Sigma<min_val_Sigma) = min_val_Sigma;
        Sigma(not(mask_Sigma)) = 0;


        %check if end optimization: if FC error becomes too large
        if i_opt<n_opt-1
            stop_opt = i_opt>20 && (dist_FC_hist(i_opt)>1.5);
        else
            stop_opt = 1;
        end
        if ~stop_opt
            i_opt = i_opt+1;
        else
            sprintf('stop at step %d; best FC
dist %d',i_opt,best_dist)
        end
    end
end
```

Reference

Abler B, Walter H, Erk S, Kammerer H, Spitzer M (2006) Prediction error as a linear function of reward probability is coded in human nucleus accumbens. NeuroImage 31:790-795.

Achenbach TM, Rescorla L (2003) Manual for the ASEBA adult forms & profiles. Burlington: University of Vermont: Research Center for Children, Youth and Families.

Ainslie G (1975) Specious reward: a behavioral theory of impulsiveness and impulse control. Psychol Bull 82:463-496.

Akaike H (1974) A new look at the statistical model identification. IEEE transactions on automatic control 19:716-723.

Alfaro-Almagro F et al. (2018) Image processing and Quality Control for the first 10,000 brain imaging datasets from UK Biobank. Neuroimage 166:400-424.

Arbabshirani MR, Plis S, Sui J, Calhoun VD (2017) Single subject prediction of brain disorders in neuroimaging: Promises and pitfalls. NeuroImage 145:137-165.

Aron AR, Poldrack RA (2006) Cortical and subcortical contributions to Stop signal response inhibition: role of the subthalamic nucleus. J Neurosci 26:2424-2433.

Baldwin JR, Reuben A, Newbury JB, Danese A (2019) Agreement Between Prospective and Retrospective Measures of Childhood Maltreatment: A Systematic Review and Meta-analysis. JAMA Psychiatry 76:584-593.

Ballard K, Knutson B (2009) Dissociable neural representations of future reward magnitude and delay during temporal discounting. Neuroimage 45:143-150.

Bardo MT, Donohew RL, Harrington NG (1996) Psychobiology of novelty seeking and drug seeking behavior. Behav Brain Res 77:23-43.

Bari A, Robbins TW (2013) Inhibition and impulsivity: behavioral and neural basis of response control. Prog Neurobiol 108:44-79.

Basu A, McLaughlin KA, Misra S, Koenen KC (2017) Childhood Maltreatment and Health Impact: The Examples of Cardiovascular Disease and Type 2 Diabetes Mellitus in Adults. Clin Psychol (New York) 24:125-139.

Benjamini Y, Hochberg Y (1995) Controlling the false discovery rate: a practical and powerful approach to multiple testing. Journal of the royal statistical society Series B (Methodological) 57:289-300.

Bentler PM (1990) Comparative fit indexes in structural models. Psychol Bull 107:238-246.

Berridge KC, Kringelbach ML (2015) Pleasure systems in the brain. Neuron 86:646-664.

Bhui K, Bhugra D (2002) Explanatory models for mental distress: implications for clinical practice and research. Br J Psychiatry 181:6-7.

Biswal B, Yetkin FZ, Haughton VM, Hyde JS (1995) Functional connectivity in the motor cortex of resting human brain using echo-planar MRI. Magn Reson Med 34:537-541.

Bjork JM, Pardini DA (2015) Who are those "risk-taking adolescents"? Individual differences in developmental neuroimaging research. Dev Cogn Neurosci 11:56-64.

Blais A-R, Weber EU (2006) A domain-specific risk-taking (DOSPERT) scale for adult populations. Judgement and decision making 1:33-47.

Blankenstein NE, Peper JS, Crone EA, van Duijvenvoorde ACK (2017) Neural Mechanisms Underlying Risk and Ambiguity Attitudes. J Cogn Neurosci 29:1845-1859.

Blinowska KJ, Kus R, Kaminski M (2004) Granger causality and information flow in multivariate processes. Phys Rev E Stat Nonlin Soft Matter Phys 70:050902.

Bolsinger J, Seifritz E, Kleim B, Manoliu A (2018) Neuroimaging Correlates of Resilience to Traumatic Events-A Comprehensive Review. Front Psychiatry 9:693.

Braams BR, Peper JS, van der Heide D, Peters S, Crone EA (2016) Nucleus accumbens response to rewards and testosterone levels are related to alcohol use in adolescents and young adults. Dev Cogn Neurosci 17:83-93.

Bradley MM, Codispoti M, Cuthbert BN, Lang PJ (2001) Emotion and motivation I: defensive and appetitive reactions in picture processing. Emotion 1:276-298.

Browne MW, Cudeck R (1992) Alternative ways of assessing model fit. Sociological methods & research 21:230-258.

Caballero-Gaudes C, Reynolds RC (2017) Methods for cleaning the BOLD fMRI signal. NeuroImage 154:128-149.

Cai H, Zhu J, Yu Y (2020) Robust prediction of individual personality from brain functional connectome. Soc Cogn Affect Neurosci 15:359-369.

Cai W, Ryali S, Chen T, Li CS, Menon V (2014) Dissociable roles of right inferior frontal cortex and anterior insula in inhibitory control: evidence from intrinsic and task-related functional parcellation, connectivity, and response profile analyses across multiple datasets. J Neurosci 34:14652-14667.

Cavanna AE, Trimble MR (2006) The precuneus: a review of its functional anatomy and behavioural correlates. Brain 129:564-583.

Chase HW, Fournier JC, Bertocci MA, Greenberg T, Aslam H, Stiffler R, Lockovich J, Graur S, Bebko G, Forbes EE, Phillips ML (2017) A pathway linking reward circuitry, impulsive sensation-seeking and risky decision-making in young adults: identifying neural markers for new interventions. Transl Psychiatry 7:e1096.

Cheng W, Rolls ET, Gu H, Zhang J, Feng J (2015) Autism: reduced connectivity between cortical areas involved in face expression, theory of mind, and the sense of self. Brain 138:1382-1393.

Cheng W, Rolls ET, Zhang J, Sheng W, Ma L, Wan L, Luo Q, Feng J (2017) Functional connectivity decreases in autism in emotion, self, and face circuits identified by Knowledge-based Enrichment Analysis. Neuroimage 148:169-178.

Cheng W, Rolls ET, Qiu J, Yang D, Ruan H, Wei D, Zhao L, Meng J, Xie P, Feng J (2018) Functional Connectivity of the Precuneus in Unmedicated Patients With Depression. Biol Psychiatry Cogn Neurosci Neuroimaging 3:1040-1049.

Cheng W, Rolls ET, Qiu J, Liu W, Tang Y, Huang CC, Wang X, Zhang J, Lin W, Zheng L, Pu J, Tsai SJ, Yang AC, Lin CP, Wang F, Xie P, Feng J (2016) Medial reward and lateral non-reward orbitofrontal cortex circuits change in opposite directions in depression. Brain 139:3296-3309.

Cheng W, Rolls ET, Robbins TW, Gong W, Liu Z, Lv W, Du J, Wen H, Ma L, Quinlan EB, Garavan H, Artiges E, Papadopoulos Orfanos D, Smolka MN, Schumann G, Kendrick K, Feng J (2019a) Decreased brain connectivity in smoking contrasts with increased connectivity in drinking. Elife 8.

Cheng W, Rolls ET, Robbins TW, Gong W, Liu Z, Lv W, Du J, Wen H, Ma L, Quinlan EB, Garavan H, Artiges E, Papadopoulos Orfanos D, Smolka MN, Schumann G, Kendrick K, Feng J (2019b) Decreased brain connectivity in smoking contrasts with increased connectivity in drinking. Elife 8:e40765.

Cieslik EC, Zilles K, Caspers S, Roski C, Kellermann TS, Jakobs O, Langner R, Laird AR, Fox PT, Eickhoff SB (2013) Is there "one" DLPFC in cognitive action control? Evidence for heterogeneity from co-activation-based parcellation. Cereb Cortex 23:2677-2689.

Colclough GL, Smith SM, Nichols TE, Winkler AM, Sotiropoulos SN, Glasser MF, Van Essen DC, Woolrich MW (2017) The heritability of multi-modal connectivity in human brain activity. Elife 6.

Collins HR, Corbly CR, Liu X, Kelly TH, Lynam D, Joseph JE (2012) Too little, too late or too much, too early? Differential hemodynamics of response inhibition in high and low sensation seekers. Brain Res 1481:1-12.

Collishaw S, Pickles A, Messer J, Rutter M, Shearer C, Maughan B (2007) Resilience to adult psychopathology following childhood maltreatment: evidence from a community sample. Child Abuse Negl 31:211-229.
Copeland WE, Shanahan L, Hinesley J, Chan RF, Aberg KA, Fairbank JA, van den Oord E, Costello EJ (2018) Association of Childhood Trauma Exposure With Adult Psychiatric Disorders and Functional Outcomes. JAMA Netw Open 1:e184493.
Cox RW (1996) AFNI: software for analysis and visualization of functional magnetic resonance neuroimages. Comput Biomed Res 29:162-173.
Cristofori I, Cohen-Zimerman S, Grafman J (2019) Executive functions. Handb Clin Neurol 163:197-219.
Critchley H, Daly E, Phillips M, Brammer M, Bullmore E, Williams S, Van Amelsvoort T, Robertson D, David A, Murphy D (2000) Explicit and implicit neural mechanisms for processing of social information from facial expressions: a functional magnetic resonance imaging study. Hum Brain Mapp 9:93-105.
Cservenka A, Herting MM, Seghete KL, Hudson KA, Nagel BJ (2013) High and low sensation seeking adolescents show distinct patterns of brain activity during reward processing. NeuroImage 66:184-193.
Cui Z, Gong G (2018) The effect of machine learning regression algorithms and sample size on individualized behavioral prediction with functional connectivity features. NeuroImage 178:622-637.
Dai Z, Yan C, Wang Z, Wang J, Xia M, Li K, He Y (2012) Discriminative analysis of early Alzheimer's disease using multi-modal imaging and multi-level characterization with multi-classifier (M3). NeuroImage 59:2187-2195.
Dalley JW, Robbins TW (2017) Fractionating impulsivity: neuropsychiatric implications. Nat Rev Neurosci 18:158-171.
de Vos F, Koini M, Schouten TM, Seiler S, van der Grond J, Lechner A, Schmidt R, de Rooij M, Rombouts S (2018) A comprehensive analysis of resting state fMRI measures to classify individual patients with Alzheimer's disease. NeuroImage 167:62-72.
Deng W et al. (2019) Separate neural systems for behavioral change and for emotional responses to failure during behavioral inhibition. Hum Brain Mapp 38:3527-3537.
Dixon ML (2015) Cognitive control, emotional value, and the lateral prefrontal cortex. Front Psychol 6:758.
Dodds CM, Morein-Zamir S, Robbins TW (2011) Dissociating inhibition, attention, and response control in the frontoparietal network using functional magnetic resonance imaging. Cereb Cortex 21:1155-1165.
Dosenbach NU, Nardos B, Cohen AL, Fair DA, Power JD, Church JA, Nelson SM, Wig GS, Vogel AC, Lessov-Schlaggar CN, Barnes KA, Dubis JW, Feczko E, Coalson RS, Pruett JR, Jr., Barch DM, Petersen SE, Schlaggar BL (2010) Prediction of individual brain maturity using fMRI. Science 329:1358-1361.
Drysdale AT et al. (2017) Erratum: Resting-state connectivity biomarkers define neurophysiological subtypes of depression. Nat Med 23:264.
Du J, Rolls ET, Gong W, Cao M, Vatansever D, Zhang J, Cheng W, Feng J (2021) Association between parental age, brain structure, and behavioral and cognitive problems in children. Mol Psychiatry:in revision.
Eickhoff SB, Milham M, Vanderwal T (2020) Towards clinical applications of movie fMRI. Neuroimage 217:116860.
Erus G, Battapady H, Satterthwaite TD, Hakonarson H, Gur RE, Davatzikos C, Gur RC (2015) Imaging patterns of brain development and their relationship to cognition. Cereb Cortex 25:1676-1684.
Evenden JL (1999) Varieties of impulsivity. Psychopharmacology (Berl) 146:348-361.

Feng C, Yuan J, Geng H, Gu R, Zhou H, Wu X, Luo Y (2018) Individualized prediction of trait narcissism from whole-brain resting-state functional connectivity. Hum Brain Mapp.
Feng R, Rolls ET, Cheng W, Feng J (2020) Hypertension is associated with reduced hippocampal connectivity and impaired memory. EBioMedicine 61:103082.
Fink M (1999) Delirious mania. Bipolar Disord 1:54-60.
Finn ES, Shen X, Scheinost D, Rosenberg MD, Huang J, Chun MM, Papademetris X, Constable RT (2015) Functional connectome fingerprinting: identifying individuals using patterns of brain connectivity. Nat Neurosci 18:1664-1671.
Fisher RA (1992) Statistical methods for research workers. In: Breakthroughs in statistics, pp 66-70: Springer.
Fox MD, Zhang D, Snyder AZ, Raichle ME (2009) The global signal and observed anticorrelated resting state brain networks. Journal of neurophysiology 101:3270-3283.
Franco M, Vivo JM (2019) Cluster Analysis of Microarray Data. Methods Mol Biol 1986:153-183.
Freton M, Lemogne C, Bergouignan L, Delaveau P, Lehericy S, Fossati P (2014) The eye of the self: precuneus volume and visual perspective during autobiographical memory retrieval. Brain Struct Funct 219:959-968.
Friedman J, Hastie T, Tibshirani R (2010) Regularization Paths for Generalized Linear Models via Coordinate Descent. J Stat Softw 33:1-22.
Friston K (2009) Causal modelling and brain connectivity in functional magnetic resonance imaging. PLoS Biol 7:e33.
Friston KJ, Mechelli A, Turner R, Price CJ (2000) Nonlinear responses in fMRI: the Balloon model, Volterra kernels, and other hemodynamics. Neuroimage 12:466-477.
Friston KJ, Kahan J, Biswal B, Razi A (2014) A DCM for resting state fMRI. Neuroimage 94:396-407.
Friston KJ, Williams S, Howard R, Frackowiak RS, Turner R (1996) Movement-related effects in fMRI time-series. Magn Reson Med 35:346-355.
Frodl T, Reinhold E, Koutsouleris N, Donohoe G, Bondy B, Reiser M, Moller HJ, Meisenzahl EM (2010) Childhood stress, serotonin transporter gene and brain structures in major depression. Neuropsychopharmacology 35:1383-1390.
Gheorghe DA, Li C, Gallacher J, Bauermeister S (2021) Associations of perceived adverse lifetime experiences with brain structure in UK Biobank participants. J Child Psychol Psychiatry 62:822-830.
Gianotti LR, Knoch D, Faber PL, Lehmann D, Pascual-Marqui RD, Diezi C, Schoch C, Eisenegger C, Fehr E (2009) Tonic activity level in the right prefrontal cortex predicts individuals' risk taking. Psychol Sci 20:33-38.
Gibson LE, Alloy LB, Ellman LM (2016) Trauma and the psychosis spectrum: A review of symptom specificity and explanatory mechanisms. Clin Psychol Rev 49:92-105.
Gilson M, Moreno-Bote R, Ponce-Alvarez A, Ritter P, Deco G (2016) Estimation of Directed Effective Connectivity from fMRI Functional Connectivity Hints at Asymmetries of Cortical Connectome. PLoS Comput Biol 12:e1004762.
Gilson M, Deco G, Friston KJ, Hagmann P, Mantini D, Betti V, Romani GL, Corbetta M (2018) Effective connectivity inferred from fMRI transition dynamics during movie viewing points to a balanced reconfiguration of cortical interactions. Neuroimage 180:534-546.
Golchert J, Smallwood J, Jefferies E, Liem F, Huntenburg JM, Falkiewicz M, Lauckner ME, Oligschlager S, Villringer A, Margulies DS (2017) In need of constraint: Understanding the role of the cingulate cortex in the impulsive mind. NeuroImage 146:804-813.
Gong W, Rolls ET, Du J, Feng J, Cheng W (2021) Brain structure is linked to the association between family environment and behavioral problems in children in the ABCD study. Nature Communications 12:3769.

Gotts SJ, Saad ZS, Jo HJ, Wallace GL, Cox RW, Martin A (2013) The perils of global signal regression for group comparisons: a case study of Autism Spectrum Disorders. Front Hum Neurosci 7:356.

Grabenhorst F, Rolls ET (2011) Value, pleasure and choice in the ventral prefrontal cortex. Trends Cogn Sci 15:56-67.

Granger CW (1969) Investigating causal relations by econometric models and cross-spectral methods. Econometrica: journal of the Econometric Society:424-438.

Green JG, McLaughlin KA, Berglund PA, Gruber MJ, Sampson NA, Zaslavsky AM, Kessler RC (2010) Childhood adversities and adult psychiatric disorders in the national comorbidity survey replication I: associations with first onset of DSM-IV disorders. Arch Gen Psychiatry 67:113-123.

Green L, Myerson J (2013) How many impulsivities? A discounting perspective. J Exp Anal Behav 99:3-13.

Gregorios-Pippas L, Tobler PN, Schultz W (2009) Short-term temporal discounting of reward value in human ventral striatum. Journal of neurophysiology 101:1507-1523.

Greve DN, Fischl B (2009) Accurate and robust brain image alignment using boundary-based registration. NeuroImage 48:63-72.

Griffanti L, Salimi-Khorshidi G, Beckmann CF, Auerbach EJ, Douaud G, Sexton CE, Zsoldos E, Ebmeier KP, Filippini N, Mackay CE, Moeller S, Xu J, Yacoub E, Baselli G, Ugurbil K, Miller KL, Smith SM (2014) ICA-based artefact removal and accelerated fMRI acquisition for improved resting state network imaging. Neuroimage 95:232-247.

Grill-Spector K, Weiner KS, Gomez J, Stigliani A, Natu VS (2018) The functional neuroanatomy of face perception: from brain measurements to deep neural networks. Interface Focus 8:20180013.

Hamilton JP, Chen G, Thomason ME, Schwartz ME, Gotlib IH (2011) Investigating neural primacy in Major Depressive Disorder: multivariate Granger causality analysis of resting-state fMRI time-series data. Mol Psychiatry 16:763-772.

Hammen C (2005) Stress and depression. Annu Rev Clin Psychol 1:293-319.

Hanson JL, Chung MK, Avants BB, Rudolph KD, Shirtcliff EA, Gee JC, Davidson RJ, Pollak SD (2012) Structural variations in prefrontal cortex mediate the relationship between early childhood stress and spatial working memory. J Neurosci 32:7917-7925.

Harris N, Newby J, Klein RG (2015) Competitiveness facets and sensation seeking as predictors of problem gambling among a sample of university student gamblers. J Gambl Stud 31:385-396.

Hasselmo ME, Rolls ET, Baylis GC (1989) The role of expression and identity in the face-selective responses of neurons in the temporal visual cortex of the monkey. Behav Brain Res 32:203-218.

Haynes JD (2015) A Primer on Pattern-Based Approaches to fMRI: Principles, Pitfalls, and Perspectives. Neuron 87:257-270.

Hein G, Knight RT (2008) Superior temporal sulcus--It's my area: or is it? J Cogn Neurosci 20:2125-2136.

Hoyle RH, Fejfar MC, Miller JD (2000) Personality and sexual risk taking: a quantitative review. J Pers 68:1203-1231.

Huettel SA, Stowe CJ, Gordon EM, Warner BT, Platt ML (2006) Neural signatures of economic preferences for risk and ambiguity. Neuron 49:765-775.

Humphreys KL, LeMoult J, Wear JG, Piersiak HA, Lee A, Gotlib IH (2020) Child maltreatment and depression: A meta-analysis of studies using the Childhood Trauma Questionnaire. Child Abuse Negl 102:104361.

Itahashi T, Kosibaty N, Hashimoto RI, Aoki YY (2021) Prediction of life satisfaction from resting-state functional connectome. Brain Behav 11:e2331.

Jenkinson M, Beckmann CF, Behrens TE, Woolrich MW, Smith SM (2012) Fsl. NeuroImage 62:782-790.
Jonah BA (1997) Sensation seeking and risky driving: a review and synthesis of the literature. Accid Anal Prev 29:651-665.
Joseph JE, Liu X, Jiang Y, Lynam D, Kelly TH (2009) Neural correlates of emotional reactivity in sensation seeking. Psychol Sci 20:215-223.
Julian LJ (2011) Measures of anxiety: State-Trait Anxiety Inventory (STAI), Beck Anxiety Inventory (BAI), and Hospital Anxiety and Depression Scale-Anxiety (HADS-A). Arthritis Care Res (Hoboken) 63 Suppl 11:S467-472.
Kafashan M, Palanca BJA, Ching S (2018) Dimensionality reduction impedes the extraction of dynamic functional connectivity states from fMRI recordings of resting wakefulness. J Neurosci Methods 293:151-161.
Kandel BM, Wang DJ, Gee JC, Avants BB (2015) Eigenanatomy: sparse dimensionality reduction for multi-modal medical image analysis. Methods 73:43-53.
Kendler KS, Karkowski LM, Prescott CA (1999) Causal relationship between stressful life events and the onset of major depression. Am J Psychiatry 156:837-841.
Kessler RC (1997) The effects of stressful life events on depression. Annu Rev Psychol 48:191-214.
Kessler RC, Davis CG, Kendler KS (1997) Childhood adversity and adult psychiatric disorder in the US National Comorbidity Survey. Psychol Med 27:1101-1119.
Kim SG (2018) Biophysics of BOLD fMRI investigated with animal models. J Magn Reson 292:82-89.
Koch W, Teipel S, Mueller S, Benninghoff J, Wagner M, Bokde AL, Hampel H, Coates U, Reiser M, Meindl T (2012) Diagnostic power of default mode network resting state fMRI in the detection of Alzheimer's disease. Neurobiol Aging 33:466-478.
Koob GF, Volkow ND (2010) Neurocircuitry of addiction. Neuropsychopharmacology 35:217-238.
Krstajic D, Buturovic LJ, Leahy DE, Thomas S (2014) Cross-validation pitfalls when selecting and assessing regression and classification models. J Cheminform 6:10.
Kruschwitz JD, Simmons AN, Flagan T, Paulus MP (2012) Nothing to lose: processing blindness to potential losses drives thrill and adventure seekers. Neuroimage 59:2850-2859.
Kus R, Kaminski M, Blinowska KJ (2004) Determination of EEG activity propagation: pair-wise versus multichannel estimate. IEEE Trans Biomed Eng 51:1501-1510.
Levy BJ, Wagner AD (2011) Cognitive control and right ventrolateral prefrontal cortex: reflexive reorienting, motor inhibition, and action updating. Ann N Y Acad Sci 1224:40-62.
Linhartova P, Latalova A, Kosa B, Kasparek T, Schmahl C, Paret C (2019) fMRI neurofeedback in emotion regulation: A literature review. Neuroimage 193:75-92.
Liu Z, Zhang J, Xie X, Rolls ET, Sun J, Zhang K, Jiao Z, Chen Q, Zhang J, Qiu J, Feng J (2018a) Neural and genetic determinants of creativity. NeuroImage 174:164-176.
Liu Z, Zhang J, Zhang K, Zhang J, Li X, Cheng W, Li M, Zhao L, Deng W, Guo W, Ma X, Wang Q, Matthews PM, Feng J, Li T (2018b) Distinguishable brain networks relate disease susceptibility to symptom expression in schizophrenia. Hum Brain Mapp 39:3503-3515.
Logan GD, Van Zandt T, Verbruggen F, Wagenmakers EJ (2014) On the ability to inhibit thought and action: general and special theories of an act of control. Psychol Rev 121:66-95.
Lu S, Xu R, Cao J, Yin Y, Gao W, Wang D, Wei Z, Hu S, Huang M, Li L, Xu Y (2019) The left dorsolateral prefrontal cortex volume is reduced in adults reporting childhood trauma independent of depression diagnosis. J Psychiatr Res 112:12-17.
Luo Q, Lu W, Cheng W, Valdes-Sosa PA, Wen X, Ding M, Feng J (2013) Spatio-temporal Granger causality: a new framework. Neuroimage 79:241-263.

Luo Q et al. (2019) Association of a Schizophrenia-Risk Nonsynonymous Variant With Putamen Volume in Adolescents: A Voxelwise and Genome-Wide Association Study. JAMA Psychiatry.

Lynam DR, Smith GT, Whiteside SP, Cyders MA (2006) The UPPS-P: Assessing five personality pathways to impulsive behavior. West Lafayette, IN: Purdue University.

Macoveanu J, Fisher PM, Haahr ME, Frokjaer VG, Knudsen GM, Siebner HR (2014) Effects of selective serotonin reuptake inhibition on neural activity related to risky decisions and monetary rewards in healthy males. Neuroimage 99:434-442.

MacPherson L, Magidson JF, Reynolds EK, Kahler CW, Lejuez CW (2010) Changes in sensation seeking and risk-taking propensity predict increases in alcohol use among early adolescents. Alcohol Clin Exp Res 34:1400-1408.

Markov NT et al. (2014) A weighted and directed interareal connectivity matrix for macaque cerebral cortex. Cereb Cortex 24:17-36.

Marreiros AC, Kiebel SJ, Friston KJ (2008) Dynamic causal modelling for fMRI: a two-state model. NeuroImage 39:269-278.

Marusak HA, Thomason ME, Peters C, Zundel C, Elrahal F, Rabinak CA (2016) You say 'prefrontal cortex' and I say 'anterior cingulate': meta-analysis of spatial overlap in amygdala-to-prefrontal connectivity and internalizing symptomology. Transl Psychiatry 6:e944.

McCrimmon AW, Smith AD (2013) Review of the Wechsler abbreviated scale of intelligence, (WASI-II). In: Sage Publications Sage CA: Los Angeles, CA.

McDonald RP (1990) Structural equations with latent variables. Journal of the American Statistical Association 85:1175-1177.

McLaughlin KA, Sheridan MA, Lambert HK (2014) Childhood adversity and neural development: deprivation and threat as distinct dimensions of early experience. Neurosci Biobehav Rev 47:578-591.

McLaughlin KA, Conron KJ, Koenen KC, Gilman SE (2010) Childhood adversity, adult stressful life events, and risk of past-year psychiatric disorder: a test of the stress sensitization hypothesis in a population-based sample of adults. Psychol Med 40:1647-1658.

McLaughlin KA et al. (2017) Childhood adversities and post-traumatic stress disorder: evidence for stress sensitisation in the World Mental Health Surveys. Br J Psychiatry 211:280-288.

Miller KL et al. (2016) Multimodal population brain imaging in the UK Biobank prospective epidemiological study. Nat Neurosci 19:1523-1536.

Mitra A, Snyder AZ, Tagliazucchi E, Laufs H, Raichle ME (2015) Propagated infra-slow intrinsic brain activity reorganizes across wake and slow wave sleep. Elife 4.

Mizuhara H, Yamaguchi Y (2007) Human cortical circuits for central executive function emerge by theta phase synchronization. Neuroimage 36:232-244.

Morey RA, Haswell CC, Hooper SR, De Bellis MD (2016) Amygdala, Hippocampus, and Ventral Medial Prefrontal Cortex Volumes Differ in Maltreated Youth with and without Chronic Posttraumatic Stress Disorder. Neuropsychopharmacology 41:791-801.

Morris LS, Kundu P, Baek K, Irvine MA, Mechelmans DJ, Wood J, Harrison NA, Robbins TW, Bullmore ET, Voon V (2016) Jumping the Gun: Mapping Neural Correlates of Waiting Impulsivity and Relevance Across Alcohol Misuse. Biol Psychiatry 79:499-507.

Nanni V, Uher R, Danese A (2012) Childhood maltreatment predicts unfavorable course of illness and treatment outcome in depression: a meta-analysis. Am J Psychiatry 169:141-151.

Navarro Schroder T, Haak KV, Zaragoza Jimenez NI, Beckmann CF, Doeller CF (2015) Functional topography of the human entorhinal cortex. Elife 4.

Nieder A, Dehaene S (2009) Representation of number in the brain. Annu Rev Neurosci 32:185-208.

Nooner KB et al. (2012) The NKI-Rockland Sample: A Model for Accelerating the Pace of Discovery Science in Psychiatry. Front Neurosci 6:152.
Norman KA, Polyn SM, Detre GJ, Haxby JV (2006) Beyond mind-reading: multi-voxel pattern analysis of fMRI data. Trends Cogn Sci 10:424-430.
O'Doherty J, Kringelbach ML, Rolls ET, Hornak J, Andrews C (2001) Abstract reward and punishment representations in the human orbitofrontal cortex. Nat Neurosci 4:95-102.
Orru G, Pettersson-Yeo W, Marquand AF, Sartori G, Mechelli A (2012) Using Support Vector Machine to identify imaging biomarkers of neurological and psychiatric disease: a critical review. Neurosci Biobehav Rev 36:1140-1152.
Park HJ, Friston K (2013) Structural and functional brain networks: from connections to cognition. Science 342:1238411.
Patel AX, Kundu P, Rubinov M, Jones PS, Vertes PE, Ersche KD, Suckling J, Bullmore ET (2014) A wavelet method for modeling and despiking motion artifacts from resting-state fMRI time series. NeuroImage 95:287-304.
Peng D, Liddle EB, Iwabuchi SJ, Zhang C, Wu Z, Liu J, Jiang K, Xu L, Liddle PF, Palaniyappan L, Fang Y (2015) Dissociated large-scale functional connectivity networks of the precuneus in medication-naive first-episode depression. Psychiatry Res 232:250-256.
Penny WD, Friston KJ, Ashburner JT, Kiebel SJ, Nichols TE (2011) Statistical parametric mapping: the analysis of functional brain images: Elsevier.
Perosa V, Priester A, Ziegler G, Cardenas-Blanco A, Dobisch L, Spallazzi M, Assmann A, Maass A, Speck O, Oltmer J, Heinze HJ, Schreiber S, Duzel E (2020) Hippocampal vascular reserve associated with cognitive performance and hippocampal volume. Brain 143:622-634.
Petkus AJ, Lenze EJ, Butters MA, Twamley EW, Wetherell JL (2018) Childhood Trauma Is Associated With Poorer Cognitive Performance in Older Adults. J Clin Psychiatry 79.
Qu Y, Galvan A, Fuligni AJ, Lieberman MD, Telzer EH (2015) Longitudinal Changes in Prefrontal Cortex Activation Underlie Declines in Adolescent Risk Taking. J Neurosci 35:11308-11314.
Rae CL, Hughes LE, Anderson MC, Rowe JB (2015) The prefrontal cortex achieves inhibitory control by facilitating subcortical motor pathway connectivity. J Neurosci 35:786-794.
Raggetti G, Ceravolo MG, Fattobene L, Di Dio C (2017) Neural Correlates of Direct Access Trading in a Real Stock Market: An fMRI Investigation. Front Neurosci 11:536.
Rao LL, Zhou Y, Zheng D, Yang LQ, Li S (2018) Genetic Contribution to Variation in Risk Taking: A Functional MRI Twin Study of the Balloon Analogue Risk Task. Psychol Sci 29:1679-1691.
Raposo SM, Mackenzie CS, Henriksen CA, Afifi TO (2014) Time does not heal all wounds: older adults who experienced childhood adversities have higher odds of mood, anxiety, and personality disorders. Am J Geriatr Psychiatry 22:1241-1250.
Raymond C, Marin MF, Majeur D, Lupien S (2018) Early child adversity and psychopathology in adulthood: HPA axis and cognitive dysregulations as potential mechanisms. Prog Neuropsychopharmacol Biol Psychiatry 85:152-160.
Razi A, Seghier ML, Zhou Y, McColgan P, Zeidman P, Park HJ, Sporns O, Rees G, Friston KJ (2017) Large-scale DCMs for resting-state fMRI. Netw Neurosci 1:222-241.
Ren Z, Daker RJ, Shi L, Sun J, Beaty RE, Wu X, Chen Q, Yang W, Lyons IM, Green AE, Qiu J (2021) Connectome-Based Predictive Modeling of Creativity Anxiety. Neuroimage 225:117469.
Rizzolatti G (2014) Confounding the origin and function of mirror neurons. Behav Brain Sci 37:218-219.
Rizzolatti G, Craighero L (2004) The mirror-neuron system. Annu Rev Neurosci 27:169-192.

Robbins TW (2002) The 5-choice serial reaction time task: behavioural pharmacology and functional neurochemistry. Psychopharmacology (Berl) 163:362-380.
Roebroeck A, Formisano E, Goebel R (2005) Mapping directed influence over the brain using Granger causality and fMRI. Neuroimage 25:230-242.
Rolls ET (2014a) Emotion and decision making explained: Oxford University Press.
Rolls ET (2014b) Emotion and Decision-Making Explained. Oxford: Oxford University Press.
Rolls ET (2016) Cerebral cortex: principles of operation: Oxford University Press.
Rolls ET (2017a) The roles of the orbitofrontal cortex via the habenula in non-reward and depression, and in the responses of serotonin and dopamine neurons. Neurosci Biobehav Rev 75:331-334.
Rolls ET (2017b) The orbitofrontal cortex and emotion in health and disease, including depression. Neuropsychologia doi: 10.1016/j.neuropsychologia.2017.1009.1021.
Rolls ET (2018a) The storage and recall of memories in the hippocampo-cortical system. Cell Tissue Res 373:577-604.
Rolls ET (2018b) The brain, emotion, and depression: Oxford University Press.
Rolls ET (2019a) The orbitofrontal cortex and emotion in health and disease, including depression. Neuropsychologia 128:14-43.
Rolls ET (2019b) The Orbitofrontal Cortex. Oxford: Oxford University Press.
Rolls ET (2021) Brain Computations: What and How. Oxford: Oxford University Press.
Rolls ET, McCabe C, Redoute J (2008) Expected value, reward outcome, and temporal difference error representations in a probabilistic decision task. Cereb Cortex 18:652-663.
Rolls ET, Joliot M, Tzourio-Mazoyer N (2015) Implementation of a new parcellation of the orbitofrontal cortex in the automated anatomical labeling atlas. Neuroimage 122:1-5.
Rolls ET, Cheng W, Feng J (2020a) The orbitofrontal cortex: reward, emotion and depression. Brain Commun 2:fcaa196.
Rolls ET, Wan Z, Cheng W, Feng J (2022) Risk-taking in humans and the medial orbitofrontal cortex reward system. Neuroimage 249:118893.
Rolls ET, Cheng W, Gilson M, Gong W, Deco G, Lo CZ, Yang AC, Tsai SJ, Liu ME, Lin CP, Feng J (2020b) Beyond the disconnectivity hypothesis of schizophrenia. Cereb Cortex 30:1213-1233.
Rolls ET, Cheng W, Gilson M, Qiu J, Hu Z, Ruan H, Li Y, Huang CC, Yang AC, Tsai SJ, Zhang X, Zhuang K, Lin CP, Deco G, Xie P, Feng J (2018) Effective Connectivity in Depression. Biol Psychiatry Cogn Neurosci Neuroimaging 3:187-197.
Rosenberg MD, Finn ES, Scheinost D, Papademetris X, Shen X, Constable RT, Chun MM (2016) A neuromarker of sustained attention from whole-brain functional connectivity. Nat Neurosci 19:165-171.
Rosseel Y (2012) Lavaan: An R package for structural equation modeling and more. Version 0.5–12 (BETA). Journal of statistical software 48:1-36.
Ruedl G, Abart M, Ledochowski L, Burtscher M, Kopp M (2012) Self reported risk taking and risk compensation in skiers and snowboarders are associated with sensation seeking. Accid Anal Prev 48:292-296.
Rushworth MF, Kolling N, Sallet J, Mars RB (2012) Valuation and decision-making in frontal cortex: one or many serial or parallel systems? Curr Opin Neurobiol 22:946-955.
Rushworth MF, Noonan MP, Boorman ED, Walton ME, Behrens TE (2011) Frontal cortex and reward-guided learning and decision-making. Neuron 70:1054-1069.
Saad ZS, Gotts SJ, Murphy K, Chen G, Jo HJ, Martin A, Cox RW (2012) Trouble at rest: how correlation patterns and group differences become distorted after global signal regression. Brain Connect 2:25-32.

Salimi-Khorshidi G, Douaud G, Beckmann CF, Glasser MF, Griffanti L, Smith SM (2014) Automatic denoising of functional MRI data: combining independent component analysis and hierarchical fusion of classifiers. Neuroimage 90:449-468.
Sargent JD, Tanski S, Stoolmiller M, Hanewinkel R (2010) Using sensation seeking to target adolescents for substance use interventions. Addiction 105:506-514.
Schirmer A, Adolphs R (2017) Emotion Perception from Face, Voice, and Touch: Comparisons and Convergence. Trends Cogn Sci 21:216-228.
Scholvinck ML, Maier A, Ye FQ, Duyn JH, Leopold DA (2010) Neural basis of global resting-state fMRI activity. Proc Natl Acad Sci U S A 107:10238-10243.
Schonberg T, Fox CR, Poldrack RA (2011) Mind the gap: bridging economic and naturalistic risk-taking with cognitive neuroscience. Trends Cogn Sci 15:11-19.
Schreiner MW, Klimes-Dougan B, Cullen KR (2019) Neural Correlates of Suicidality in Adolescents with Major Depression: Resting-State Functional Connectivity of the Precuneus and Posterior Cingulate Cortex. Suicide Life Threat Behav 49:899-913.
Schrouff J, Rosa MJ, Rondina JM, Marquand AF, Chu C, Ashburner J, Phillips C, Richiardi J, Mourao-Miranda J (2013) PRoNTo: pattern recognition for neuroimaging toolbox. Neuroinformatics 11:319-337.
Schultz W (2015) Neuronal Reward and Decision Signals: From Theories to Data. Physiol Rev 95:853-951.
Shallice T, Cipolotti L (2018) The Prefrontal Cortex and Neurological Impairments of Active Thought. Annu Rev Psychol 69:157-180.
Shen X, Tokoglu F, Papademetris X, Constable RT (2013) Groupwise whole-brain parcellation from resting-state fMRI data for network node identification. Neuroimage 82:403-415.
Sheridan MA, McLaughlin KA (2014) Dimensions of early experience and neural development: deprivation and threat. Trends Cogn Sci 18:580-585.
Shi Y, Liu W, Liu R, Zeng Y, Wu L, Huang S, Cai G, Yang J, Wu W (2019) Investigation of the emotional network in depression after stroke: A study of multivariate Granger causality analysis of fMRI data. J Affect Disord 249:35-44.
Shonkoff JP, Garner AS, Committee on Psychosocial Aspects of C, Family H, Committee on Early Childhood A, Dependent C, Section on D, Behavioral P (2012) The lifelong effects of early childhood adversity and toxic stress. Pediatrics 129:e232-246.
Siegel JS, Ramsey LE, Snyder AZ, Metcalf NV, Chacko RV, Weinberger K, Baldassarre A, Hacker CD, Shulman GL, Corbetta M (2016) Disruptions of network connectivity predict impairment in multiple behavioral domains after stroke. Proc Natl Acad Sci U S A 113:E4367-4376.
Smith BD, Davidson RA, Perlstein W, Gonzalez F (1990) Sensation-seeking: electrodermal and behavioral effects of stimulus content and intensity. Int J Psychophysiol 9:179-188.
Smith SM, Nichols TE, Vidaurre D, Winkler AM, Behrens TE, Glasser MF, Ugurbil K, Barch DM, Van Essen DC, Miller KL (2015) A positive-negative mode of population covariation links brain connectivity, demographics and behavior. Nat Neurosci 18:1565-1567.
Smith SM et al. (2013) Resting-state fMRI in the Human Connectome Project. Neuroimage 80:144-168.
Smitha KA, Akhil Raja K, Arun KM, Rajesh PG, Thomas B, Kapilamoorthy TR, Kesavadas C (2017) Resting state fMRI: A review on methods in resting state connectivity analysis and resting state networks. Neuroradiol J 30:305-317.
Steinberg L (2008) A Social Neuroscience Perspective on Adolescent Risk-Taking. Dev Rev 28:78-106.
Strother SC (2006) Evaluating fMRI preprocessing pipelines. IEEE Eng Med Biol Mag 25:27-41.
Suglia SF et al. (2018) Childhood and Adolescent Adversity and Cardiometabolic Outcomes: A Scientific Statement From the American Heart Association. Circulation 137:e15-e28.

Susser E, Widom CS (2012) Still searching for lost truths about the bitter sorrows of childhood. Schizophr Bull 38:672-675.
Teicher MH, Samson JA (2016) Annual Research Review: Enduring neurobiological effects of childhood abuse and neglect. J Child Psychol Psychiatry 57:241-266.
Telzer EH, Jorgensen NA, Prinstein MJ, Lindquist KA (2021) Neurobiological Sensitivity to Social Rewards and Punishments Moderates Link Between Peer Norms and Adolescent Risk Taking. Child Dev 92:731-745.
Tottenham N (2015) Social scaffolding of human amygdala-mPFCcircuit development. Soc Neurosci 10:489-499.
Trotta A, Murray RM, Fisher HL (2015) The impact of childhood adversity on the persistence of psychotic symptoms: a systematic review and meta-analysis. Psychol Med 45:2481-2498.
Turova T, Rolls ET (2019) Analysis of Biased Competition and Cooperation for Attention in the Cerebral Cortex. Front Comput Neurosci 13:51.
van Dam DS, van der Ven E, Velthorst E, Selten JP, Morgan C, de Haan L (2012) Childhood bullying and the association with psychosis in non-clinical and clinical samples: a review and meta-analysis. Psychol Med 42:2463-2474.
Van Essen DC, Smith SM, Barch DM, Behrens TE, Yacoub E, Ugurbil K, Consortium WU-MH (2013) The WU-Minn Human Connectome Project: an overview. Neuroimage 80:62-79.
Van Essen DC et al. (2012) The Human Connectome Project: a data acquisition perspective. Neuroimage 62:2222-2231.
Varese F, Smeets F, Drukker M, Lieverse R, Lataster T, Viechtbauer W, Read J, van Os J, Bentall RP (2012) Childhood adversities increase the risk of psychosis: a meta-analysis of patient-control, prospective- and cross-sectional cohort studies. Schizophr Bull 38:661-671.
Velikonja T, Velthorst E, Zinberg J, Cannon TD, Cornblatt BA, Perkins DO, Cadenhead KS, Tsuang MT, Addington J, Woods SW, McGlashan T, Mathalon DH, Stone W, Keshavan M, Seidman L, Bearden CE (2021) Childhood trauma and cognitive functioning in individuals at clinical high risk (CHR) for psychosis. Dev Psychopathol 33:53-64.
Vidaurre D, Abeysuriya R, Becker R, Quinn AJ, Alfaro-Almagro F, Smith SM, Woolrich MW (2018) Discovering dynamic brain networks from big data in rest and task. Neuroimage 180:646-656.
Voon V, Irvine MA, Derbyshire K, Worbe Y, Lange I, Abbott S, Morein-Zamir S, Dudley R, Caprioli D, Harrison NA, Wood J, Dalley JW, Bullmore ET, Grant JE, Robbins TW (2014) Measuring "waiting" impulsivity in substance addictions and binge eating disorder in a novel analogue of rodent serial reaction time task. Biol Psychiatry 75:148-155.
Wan Z, Rolls ET, Cheng W, Feng J (2020) Sensation-seeking is related to functional connectivities of the medial orbitofrontal cortex with the anterior cingulate cortex. Neuroimage 215:116845.
Wang H, Rolls ET, Du X, Du J, Yang D, Li J, Li F, Cheng W, Feng J (2020) Severe nausea and vomiting in pregnancy: psychiatric and cognitive problems, and brain structure in children. BMC Med 18:228.
Wang L, Uhrig L, Jarraya B, Dehaene S (2015) Representation of numerical and sequential patterns in macaque and human brains. Curr Biol 25:1966-1974.
Wang L, Zhang J, Zhang Y, Yan R, Liu H, Qiu M (2016) Conditional Granger Causality Analysis of Effective Connectivity during Motor Imagery and Motor Execution in Stroke Patients. Biomed Res Int 2016:3870863.
Wang X, Ren Y, Zhang W (2017) Depression Disorder Classification of fMRI Data Using Sparse Low-Rank Functional Brain Network and Graph-Based Features. Comput Math Methods Med 2017:3609821.

Wee CY, Yang S, Yap PT, Shen D, Alzheimer's Disease Neuroimaging I (2016) Sparse temporally dynamic resting-state functional connectivity networks for early MCI identification. Brain Imaging Behav 10:342-356.

Whelan R et al. (2012) Adolescent impulsivity phenotypes characterized by distinct brain networks. Nat Neurosci 15:920-925.

Whiteside SP, Lynam DR (2001) The five factor model and impulsivity: Using a structural model of personality to understand impulsivity. Personality and individual differences 30:669-689.

Whittle S, Yap MB, Yucel M, Sheeber L, Simmons JG, Pantelis C, Allen NB (2009) Maternal responses to adolescent positive affect are associated with adolescents' reward neuroanatomy. Soc Cogn Affect Neurosci 4:247-256.

Wilkinson RG (1997) Socioeconomic determinants of health. Health inequalities: relative or absolute material standards? BMJ 314:591-595.

Yang GJ, Murray JD, Repovs G, Cole MW, Savic A, Glasser MF, Pittenger C, Krystal JH, Wang XJ, Pearlson GD, Glahn DC, Anticevic A (2014) Altered global brain signal in schizophrenia. Proc Natl Acad Sci U S A 111:7438-7443.

Yaple Z, Arsalidou M (2018) N-back Working Memory Task: Meta-analysis of Normative fMRI Studies With Children. Child Dev 89:2010-2022.

Yeo BT, Krienen FM, Sepulcre J, Sabuncu MR, Lashkari D, Hollinshead M, Roffman JL, Smoller JW, Zollei L, Polimeni JR, Fischl B, Liu H, Buckner RL (2011) The organization of the human cerebral cortex estimated by intrinsic functional connectivity. J Neurophysiol 106:1125-1165.

Yokota S, Takeuchi H, Hashimoto T, Hashizume H, Asano K, Asano M, Sassa Y, Taki Y, Kawashima R (2015) Individual differences in cognitive performance and brain structure in typically developing children. Dev Cogn Neurosci 14:1-7.

Yu M, Linn KA, Shinohara RT, Oathes DJ, Cook PA, Duprat R, Moore TM, Oquendo MA, Phillips ML, McInnis M, Fava M, Trivedi MH, McGrath P, Parsey R, Weissman MM, Sheline YI (2019) Childhood trauma history is linked to abnormal brain connectivity in major depression. Proc Natl Acad Sci U S A 116:8582-8590.

Zheng Y, Li Q, Tian M, Nan W, Yang G, Liang J, Liu X (2017) Deficits in voluntary pursuit and inhibition of risk taking in sensation seeking. Hum Brain Mapp 38:6019-6028.

Zou H, Hastie T (2005) Regularization and variable selection via the elastic net. Journal of the Royal Statistical Society: Series B (Statistical Methodology) 67:301-320.

Zovetti N, Rossetti MG, Perlini C, Maggioni E, Bontempi P, Bellani M, Brambilla P (2020) Default mode network activity in bipolar disorder. Epidemiol Psychiatr Sci 29:e166.

Zuckerman M (1994) Behavioral expressions and biosocial bases of sensation seeking: Cambridge University Press.

Zuckerman M, Como P (1983) Sensation seeking and arousal systems. Personality and Individual Differences 4:381-386.

Zuckerman M, Kuhlman DM (2000) Personality and risk-taking: common biosocial factors. J Pers 68:999-1029.